

QUALITATIVE STUDY ON THE POTENTIAL OF LACTIC AND GLUCONIC
ACIDS FOR ACIDIZING OPERATIONS

by

Luai Alhamad

© Copyright by Luai Alhamad, 2020
All Rights Reserved

A thesis submitted to the Faculty and the Board of Trustees of the Colorado School of Mines in partial fulfillment of the requirements for the degree of Doctor of Philosophy (Petroleum Engineering).

Golden, Colorado

Date: _____

Signed: _____
Luai Alhamad

Signed: _____
Dr. Jennifer L. Miskimins
Thesis Advisor

Golden, Colorado

Date: _____

Signed: _____
Dr. Jennifer L. Miskimins
Associate Professor and Interim Head
Department of Petroleum Engineering

ABSTRACT

Organic acids are commonly used to replace hydrochloric acid (HCl) in high temperature reservoir applications, as they are less corrosive and weaker than HCl. However, organic acids are weaker than HCl and have shown some problems due to acid reaction product solubility. One such organic acid, lactic acid, produces calcium lactate when it reacts with calcite, which has a low solubility in water. Nevertheless, reaction product solubility can be improved by up to five times when gluconate ions coexist with lactate and calcium ions. The objective of this research is to evaluate lactic and gluconic acid mixtures in terms of dissolving calcite, reaction products, corrosion, wettability and generating dominant wormholes.

Lactic and gluconic acids were mixed together using both deionized water and seawater to conduct calcite solubility tests. Corrosion tests, between 4 and 12 hours, were also run under reservoir conditions. Zeta potential measurements were performed to determine alterations in rock wettability. A formation response test (FRT) apparatus was used to perform different coreflood tests using different combinations of injection rates, total acid concentrations, and temperatures. These tests were accompanied with analytical results from inductively coupled plasma (ICP) and ion chromatography (IC) to measure calcium, iron and sulfate ions in solution.

The results showed that mixing lactic and gluconic acids at a 1:1 molar ratio provided the optimal results as no precipitation occurred at total acids strengths of 10 wt% to 33 wt%. Seawater usage caused calcium sulfate precipitation; therefore, three scale inhibitors were evaluated to determine mitigation rates. Acid calcite dissolving results were satisfactory when calcite was exposed to a 1:1 and 2:1 molar ratio of crushed core-to-acid ratios, as at least 50% of the crushed

core was dissolved. However, the two-acid mixture showed a corrosion rate that was higher than the acceptable rates at 200 and 300°F where a trace of iron lactate precipitated at 300°F. Five gpt from a sulfur-based corrosion inhibitor was enough to mitigate the corrosion rate to allow for twelve hours of protection.

Wettability alteration was noticeable due to the spent acid and the used additives interaction with calcite particles. The zeta potential study showed the importance of following the common practice of including a mutual solvent in the treatment to lower the negative impact of acids and additives.

Coreflood tests showed that the lactic and gluconic acid mixture penetrated the tested core with minimal acid pore volume without any face dissolution or salt precipitation on the core faces. However, maintaining the optimum total acid concentration, injection rate, and temperature was important to deliver the optimum results. These parameters had a direct effect on the produced dissolution pattern and the minimum required pore volume to breakthrough.

This research presents a set of diverse experimental data to confirm lactic acid accompanied by gluconic acid can penetrate carbonate formation without any by-product precipitation. The two organic acids are less corrosive and less hazardous than HCl and can provide a safe operation environment, while decreasing replacement and maintenance costs.

TABLE OF CONTENTS

ABSTRACT.....	iii
LIST OF FIGURES	ix
LIST OF TABLES.....	xvii
NOMENCLATURE	xviii
ACKNOWLEDGMENTS	xxiii
DEDICATION.....	xxv
CHAPTER 1 INTRODUCTION.....	1
1.1 Research Motivation.....	2
1.2 Problem Statement.....	4
1.3 Research Objectives.....	5
1.4 Tested Materials and Fluids.....	5
1.5 Thesis Overview	6
CHAPTER 2 LITERATURE REVIEW.....	7
2.1 Reservoir Stimulation	7
2.1.1 Skin Effect	9
2.1.2 Acid Stimulation and Dissolution Patterns.....	12
2.1.3 Manipulating Skin Effect and Damage Distance.....	14
2.2 Acid Used in Matrix Acidizing.....	17
2.2.1 HCl Applications and Limitations	17
2.2.2 Organic Acids	20
2.3 Lactic and Gluconic Acids.....	21
2.3.1 Lactic Acid Manufacturing and Production.....	25

2.3.2 Gluconic Acid Manufacturing and Production	27
2.4 Presence of Sulfate Ions in Acidic Solutions	27
2.5 Corrosion.....	29
2.5.1 Corrosion Inhibition in Acidizing Operations	31
2.5.2 Corrosion Inhibitors for HCl and Organic Acids.....	31
2.6 Wettability Alteration	32
CHAPTER 3 TESTING PROTOCOLS	35
3.1 Solubility Test.....	35
3.1.1 Test Principle	35
3.1.2 Test Apparatus	36
3.1.3 Test Procedure	36
3.1.4 Calculation Example	39
3.2 Solubility Test using Synthetic Seawater	40
3.2.1 Seawater Preparation.....	40
3.2.2 Scale Inhibitors Preparation.....	41
3.3 Corrosion Test.....	42
3.3.1 Test Principle	42
3.3.2 Test Apparatus	43
3.3.3 Test Procedure	43
3.4 Wettability Test.....	45
3.4.1 Test Principle	45
3.4.2 Test Apparatus	46
3.4.3 Test Procedure	46
3.5 Coreflooding Test	47
3.5.1 Test Principle	47

3.5.2 Test Apparatus	49
3.5.3 Test Procedure	49
3.6 Experimental Repeatability and Reproducibility	51
CHAPTER 4 SOLUBILITY TEST: RESULTS AND DISCUSSION	53
4.1 Solubility Test of Acids Prepared Using Deionized Water	53
4.1.1 Lactic Acid Reaction With Calcium Carbonate.....	53
4.1.2 Lactic and Gluconic Acids Reaction With Calcium Carbonate.....	58
4.1.3 Total Acid Concentration and Temperature Effects on the LA:GA Acid Mixture Dissolving Capacity.....	62
4.1.4 Crushed Core Amount Effects on the Acid Mixture Dissolving Capacity	65
4.2 Solubility Test of Acids Prepared Using Synthetic Seawater.....	66
4.2.1 Dissolving Capacity of Acid Mixtures Prepared by Seawater.....	67
4.2.2 Scale Inhibitor Effects on Mitigating Sulfate Ions Bonding With Calcium Ions	71
CHAPTER 5 CORROSION TEST: RESULTS AND DISCUSSION.....	75
5.1 Corrosion Testing Without a Corrosion Inhibitor.....	75
5.1.1 Corrosion Testing Using 9 wt% Lactic Acid and 9 wt% of Gluconic Acid	76
5.1.2 Corrosion Testing Using 14 wt% and 27 wt% LA:GA Acid Mixtures at 1:1 Molar Ratio.....	83
5.1.3 Corrosion Testing Using 15 wt% Hydrochloric Acid.....	88
5.2 Corrosion Testing With a Corrosion Inhibitor.....	89
CHAPTER 6 WETTABILITY TEST: RESULTS AND DISCUSSION.....	94
6.1 Zeta Potential and Tested Rock Wettability	94
6.2 Zeta Potential Measurements After Six Hours	96
6.3 Zeta Potential Measurements After Ten Days	103
CHAPTER 7 COREFLOOD TEST: RESULTS AND DISCUSSION	107
7.1 Injection Rate Effects.....	108

7.2 Total Acid Concentration Effects	112
7.3 Test Temperature Effects	115
7.4 Seawater Usage Effects.....	118
7.5 CT Scans of a Core Flood by a 20 wt% Acid Mixture	119
CHAPTER 8 FIELD IMPLICATIONS: APPLICATION AND DISCUSSION	122
8.1 Application.....	122
8.1.1 Matrix Acidizing Wormhole Sensitivity to Different Parameters	122
8.1.2 Acid Fracturing	129
8.2 Hydrochloric Acid and Organic Acid Mixture in Acidizing Operations.....	135
8.2.1 Acid Reactivity	135
8.2.2 Acid Corrosiveness	137
8.2.3 Emulsion and Sludging Tendency	139
8.2.4 Additives and Wettability	139
8.2.5 Economical Analysis	143
8.3 Research Contribution	146
CHAPTER 9 CONCLUSIONS AND RECOMMENDATIONS	149
9.1 Conclusions.....	149
9.2 Recommendations.....	154
REFERENCES	156

LIST OF FIGURES

Figure 1.1	Coreflooded cores that represent face dissolution (A) and a dominant wormhole (B) (He et al. 2011; Akanni and Nasr-El-Din 2016).....	4
Figure 2.1	Skin factor effect on IPR curve. It shows the importance of restoring skin factor to lower values as doing so increases the flow rate at a specific bottomhole flowing pressure (From Economides and Boney 2000).	8
Figure 2.2	Additional pressure drop in the flow convergence region due to near wellbore alteration and damages (From Petrowiki 2015).....	9
Figure 2.3	Two region zones caused by positive skin factor: damaged (r_s) and undamaged (r_e) (From Economides and Boney 2000).	11
Figure 2.4	Schematic of common dissolution patterns. Maintaining the optimum injection rate can lead to dominant wormhole pattern (From Economides and Boney 2000).	14
Figure 2.5	Skin factor effect on steady state flow rate. It shows that reducing the skin factor by damage removal can be very beneficial in conventional formations while it is less so in tight formations.	15
Figure 2.6	Damage distance effect on reducing the skin factor. The skin factor can be highly reduced when formation damage within 0 to 20 ft of the wellbore is removed.	16
Figure 2.7	A carbonate core that was coreflooded using HCl at high temperature. The high reactivity and dissolving power caused a face dissolution to this core (From Akanni and Nasr-El-Din 2016).....	18
Figure 2.8	Chemical structures for (a) gluconic acid, (b) lactic acid and (c) calcium lactate gluconate.	24
Figure 2.9	Uses and demands of lactic acid among different industries (From Komesu et al. 2017).	26
Figure 2.10	Anodic and cathodic sites corrosion on metal surface (From Brondel et al. 1994).	30
Figure 2.11	Zones affected by matrix acidizing due to spent acid invasion into the treated formation (From Saneifar et al. 2010).	33
Figure 2.12	Wettability contact angle.	33

Figure 3.1	Schematics of solubility test apparatus. PARR 4760 test vessel schematic is shown on the left side, Mtops heating mantle schematic is shown in the middle, and a photo of the test vessel is shown on the right side.	36
Figure 3.2	Comparable tubular coupons that exhibited different pitting rates caused by acid expose (From Smith et al. 1978).....	45
Figure 3.3	A photo of the Zetasizer Nano series used to measure the Zeta potential.	47
Figure 3.4	A schematic of the Chandler 6100 FRT.	51
Figure 4.1	Sampling tubes from 12 wt% lactic acid reaction with crushed core at 70°F and 1,000 psi. White precipitation started to appear before 24 hours of conducting the test.	54
Figure 4.2	Calcium ion concentrations versus time for the reaction of 12 wt% lactic acid with crushed core at 70°F and 1,000 psi.	55
Figure 4.3	Sampling tubes from 9 wt% lactic acid reaction with crushed core at 70°F and 1,000 psi. White precipitation started to appear before 24 hours of conducting the test.	56
Figure 4.4	Calcium ion concentrations versus time for the reaction of 9 wt% and 12 wt% lactic acid with crushed core at 70°F and 1,000 psi.....	57
Figure 4.5	XRD spectrum of the collected solids that confirmed calcium lactate precipitation.	58
Figure 4.6	Sampling tubes from 14 wt% of (1:1) lactic and gluconic acid reactions with crushed core at 70°F and 1,000 psi.	59
Figure 4.7	Calcium ion concentrations versus time for the reaction of 9 wt% lactic acid and 14 wt% (1:1) of lactic and gluconic acids with crushed core at 70°F and 1,000 psi.....	60
Figure 4.8	Sampling tubes from 1 M (2:1) of lactic and gluconic acid reactions with crushed core at 200°F and 1,000 psi. Calcium lactate precipitation can be seen deposited after a few days of conducting the test.	61
Figure 4.9	Solubility tests of (1:1), (2:1) and (3:1) molar ratios of lactic and gluconic acids with a total acid strength of 1 M at 200°F and 1,000 psi.....	62
Figure 4.10	Solubility tests of different total acid strength of (1:1) lactic and gluconic acids at room conditions.	63
Figure 4.11	Calcium ion concentrations versus time for the reaction of 27 wt% of (1:1) lactic and gluconic acids with crushed core at 70, 200, and 300°F and 1,000 psi.	64

Figure 4.12	Solubility test of 27 wt% (1:1) lactic and gluconic acids at different temperatures using 1,000 psi of nitrogen pressure.	64
Figure 4.13	Solubility test of 27 wt% and 33 wt% using 2:1 crushed core-to-acid molarity ratio at 200°F and 1,000 psi.	65
Figure 4.14	Calcium ion concentrations versus time for the reaction of 27 wt% and 33 wt% 2:1 crushed core-to-acid molarity ratio at 200°F and 1,000 psi.	66
Figure 4.15	XRD spectrum of the collected solids from solubility tests of acids prepared with synthetic seawater that confirmed calcium sulfate precipitation.	68
Figure 4.16	Sampling tubes from acids prepared with synthetic seawater that were reacted with crushed core at room conditions. Calcium sulfate precipitation started to appear after a few days of conducting the test.	68
Figure 4.17	Sulfate ion concentrations of 15 wt% HCl and 27 wt% of (1:1) LA:GA acid mixture prepared by seawater that were tested at room conditions.	69
Figure 4.18	Solubility test of 27 wt% (1:1) lactic and gluconic acids prepared by synthetic seawater at different temperatures.	70
Figure 4.19	Solubility test results of different total acid strengths of (1:1) lactic and gluconic acids prepared by synthetic seawater at room conditions.	71
Figure 4.20	Sulfate ions levels within 14 & 27 wt% LA:GA acid solutions when 5 & 10 ppm of scale inhibitors were used with the solutions that contained 4,000 ppm of sulfate ions.	72
Figure 4.21	Sulfate ions levels within 14 & 27 wt% LA:GA acid solutions when 5 & 10 ppm of scale inhibitors were used with the solutions that contained 6,000 ppm of sulfate ions.	72
Figure 4.22	Sulfate ions levels within 14 & 27 wt% LA:GA acid solutions when 5 & 10 ppm of scale inhibitors were used with the solutions that contained 12,000 ppm of sulfate ions.	73
Figure 5.1	Tested steel coupon before and after soaking it at 200°F and 1,000 psi using 9 wt% lactic acid solution for 4 hours.	77
Figure 5.2	Tested steel coupon before and after soaking it at 300°F and 1,000 psi using 9 wt% lactic acid solution for 4 hours.	77
Figure 5.3	Iron ion concentrations in solution for 9 wt% lactic acid solution that was tested at 200 and 300°F at 1,000 psi for 4 hours.	78

Figure 5.4	Sampling tubes of 9 wt% lactic acid solution that was tested at 200°F (on the left) and 300°F (on the right) at 1,000 psi for 4 hours. Iron lactate precipitation started to deposit after two hours of conducting the test at 300°F.....	78
Figure 5.5	Spectrum of the collected solids that confirmed iron lactate precipitation.....	79
Figure 5.6	Tested steel coupon before and after soaking it at 200°F and 1,000 psi using 9 wt% gluconic acid solution for 4 hours.	80
Figure 5.7	Tested steel coupon before and after soaking it at 200°F and 1,000 psi using 9 wt% gluconic acid solution for 4 hours.	81
Figure 5.8	Iron ion concentrations in solution for 9 wt% gluconic acid solution that was tested at 200 and 300°F at 1,000 psi for 4 hours.....	82
Figure 5.9	Sampling tubes of 9 wt% gluconic acid solution that was tested at 200°F (on the left) and 300°F (on the right) at 1,000 psi for 4 hours. The increase in temperature caused a change in the solution color.	82
Figure 5.10	Sampling tubes of 14 wt% LA:GA acid mixture solution that was tested at 200°F (on the left) and 300°F (on the right) at 1,000 psi for 4 hours.....	84
Figure 5.11	Iron ion concentrations in solution for 14 wt% LA:GA acid mixture solution that was tested at 200 and 300°F at 1,000 psi for 4 hours.	84
Figure 5.12	Tested steel coupon before and after soaking it at 200°F and 1,000 psi using 14 wt% LA:GA acid mixture solution for 4 hours.	85
Figure 5.13	Tested steel coupon before and after soaking it at 300°F and 1,000 psi using 14 wt% LA:GA acid mixture solution for 4 hours.	85
Figure 5.14	Tested steel coupon before and after soaking it at 300°F and 1,000 psi using 27 wt% LA:GA acid mixture solution for 4 hours.	86
Figure 5.15	Sampling tubes of 27 wt% LA:GA acid mixture solution that was tested at 300°F and 1,000 psi for 4 hours.	87
Figure 5.16	Iron ion concentrations in solution for 27 wt% LA:GA acid mixture solution that was tested at 300°F and 1,000 psi for 4 hours.	87
Figure 5.17	Tested steel coupon before and after soaking it at 300°F and 1,000 psi using 15 wt% HCl acid solution for three hours.	89
Figure 5.18	Tested steel coupon before and after soaking it at 200°F and 1,000 psi using 14 wt% LA:GA acid mixture solution for 4 hours with 5 gpt of corrosion inhibitor.	90

Figure 5.19	Tested steel coupon before and after soaking it at 300°F and 1,000 psi using 14 wt% LA:GA acid mixture solution for 4 hours with 5 gpt of corrosion inhibitor.	91
Figure 5.20	Tested steel coupon before and after soaking it at 200°F and 1,000 psi using 27 wt% LA:GA acid mixture solution for 4 hours with 5 gpt of corrosion inhibitor.	92
Figure 5.21	Tested steel coupon before and after soaking it at 300°F and 1,000 psi using 27 wt% LA:GA acid mixture solution for 4 hours with 5 gpt of corrosion inhibitor.	92
Figure 5.22	Tested steel coupon before and after soaking it at 300°F and 1,000 psi using 27 wt% LA:GA acid mixture solution for 12 hours with 5 gpt of corrosion inhibitor.	93
Figure 5.23	Corrosion ratings of the 15 wt% HCl tested for 3 hours, the 27 wt% LA:GA acid mixture without corrosion inhibitor tested for 4 hours, and the 27 wt% LA:GA acid mixture with 5 gpt of corrosion inhibitor tested for 12 hours.	93
Figure 6.1	Illustration of potential difference as a function of distance from the charged surface of a particle suspended in a dispersion medium (From Taqvi and Bassioni 2019).	95
Figure 6.2	Zeta potential values of deionized water and seawater solutions after six hours of particle suspension at room temperature.	98
Figure 6.3	Zeta potential values of deionized water and 14 wt% LA:GA acid mixture with and without a corrosion inhibitor after six hours of particle suspension at room temperature.	100
Figure 6.4	Zeta potential values of seawater with 4,000 ppm of sulfate and 14 wt% acid mixtures prepared with the same seawater with scale inhibitors.	101
Figure 6.5	The chemical structure of scale inhibitor A.	101
Figure 6.6	The chemical structure of scale inhibitor B.	102
Figure 6.7	The chemical structure of scale inhibitor C.	102
Figure 6.8	Zeta potential values of seawater with 4,000 ppm of sulfate and 14 wt% LA:GA acid mixtures prepared with the same seawater with scale inhibitors and a corrosion inhibitor.	103
Figure 6.9	Zeta potential values of deionized water and seawater solutions after six hours and ten days of particle suspension at room temperature.	105

Figure 6.10	Zeta potential values of deionized water and 14 wt% LA:GA acid mixture with and with a corrosion inhibitor after six hours and ten days of particle suspension at room temperature.	106
Figure 6.11	Zeta potential values comparison of 14 wt% inhibited LA:GA acid mixture prepared by seawater with and without a corrosion inhibitor.	106
Figure 7.1	Schematic of common dissolution patterns. Maintaining the optimum injection rate can lead to dominant wormhole pattern (From Economides and Boney 2000).	109
Figure 7.2	Test 1 core inlet face before and after treatment showing face dissolution due to low injection rate.	110
Figure 7.3	Pressure drop across a tested core at 200°F using 2 cm ³ /min of 20 wt% (1:1) LA:GA acid mixture.	111
Figure 7.4	Pressure drop across a tested core at 200°F using 3 cm ³ /min of 20 wt% (1:1) LA:GA acid mixture.	111
Figure 7.5	Pressure drop across a tested core at 200°F using 4 cm ³ /min of 20 wt% (1:1) LA:GA acid mixture.	112
Figure 7.6	Pressure drop across a tested core at 200°F using 3 cm ³ /min of 14 wt% (1:1) LA:GA acid mixture.	113
Figure 7.7	Pressure drop across a tested core at 200°F using 3 cm ³ /min of 20 wt% (1:1) LA:GA acid mixture.	114
Figure 7.8	Pressure drop across a tested core at 200°F using 3 cm ³ /min of 27 wt% (1:1) LA:GA acid mixture.	114
Figure 7.9	Pressure drop across a tested core at 150°F using 3 cm ³ /min of 20 wt% (1:1) LA:GA acid mixture.	116
Figure 7.10	Pressure drop across a tested core at 200°F using 3 cm ³ /min of 20 wt% (1:1) LA:GA acid mixture.	116
Figure 7.11	Pressure drop across a tested core at 300°F using 3 cm ³ /min of 20 wt% (1:1) LA:GA acid mixture.	117
Figure 7.12	The inlet faces of cores tested at 200°F (left) and 300°F (right), where it can be seen the difference in the main propagated wormhole size.	118
Figure 7.13	Pressure drop across a tested core at 200°F using 3 cm ³ /min of 20 wt% (1:1) LA:GA acid mixture prepared by seawater.	119

Figure 7.14	CT scans of a low permeability Indiana Limestone core before being treated with 20 wt% acid mixture using 3 cm ³ /min at 200°F. Each scan is approximately 1/4" into the core moving from the injection end to the other side, top left to bottom right.....	120
Figure 7.15	CT scans of a low permeability Indiana Limestone core treated with 20 wt% acid mixture using 3 cm ³ /min at 200°F. Each scan is approximately 1/4" into the core moving from the injection end to the other side, top left to bottom right.	121
Figure 8.1	Temperature effect on the required pore volumes to breakthrough using a flow rate of 3 cm ³ /min and a total LA:GA acid concentration of 20 wt%.....	126
Figure 8.2	Total LA:GA acid concentration effect on the required pore volumes to breakthrough using a flow rate 3 cm ³ /min and a temperature of 200°F.	126
Figure 8.3	Dolomite cores treated with 3.4% HCl using different injection rates and test temperatures. This figure illustrates the effect of test temperature on the optimum injection rate to break through the tested cores (From Hill and Schechter 2000).	127
Figure 8.4	Injection rate effect on the required pore volumes to breakthrough using an acid mixture of 20 wt% at 200°F.....	128
Figure 8.5	The inlet and side faces of a core tested using a high flow rate of 4 cm ³ /min. Multiple inlet and exit holes (circled in red) indicate that a ramified dissolution pattern was created.....	128
Figure 8.6	The acid penetration differences between HCl in limestone and dolomite formations. This difference also illustrates the effect of acid reactivity on the acid penetration distance, as it is lower in dolomite formations (From Elbel and Britt 2000).....	131
Figure 8.7	Calcium ion concentrations versus time for the reaction of 9 wt% lactic acid and 14 wt% (1:1) of lactic and gluconic acids with crushed core at 70°F and 1,000 psi.....	133
Figure 8.8	Example of different cores treated with 15% HCl. The figure shows that 15% HCl usually needs one pore volume or less to breakthrough a limestone core (From Wang et al. 1993).....	134
Figure 8.9	CT scans of a low permeability Indiana Limestone core treated with 20 wt% LA:GA acid mixture using 3 cm ³ /min at 200°F. Each scan is approximately 1/4" into the core moving from the injection end to the other side, top left to bottom right.	135
Figure 8.10	Corrosion rates per hour of 15 wt% HCl solution, 14 wt% LA:GA acid mixture, and 27 wt% LA:GA acid mixture. The tests were run at 300°F. The 14 wt%	

	LA:GA acid mixture provides an 61% reduction in corrosion rate over the 15 wt% HCl solution.....	138
Figure 8.11	Calcium ion concentrations versus time for the reaction of 9 wt% lactic acid and 14 wt% (1:1) of lactic and gluconic acids with crushed core at 70°F and 1,000 psi.....	140
Figure 8.12	Iron ion concentrations in solution for 9 wt% lactic acid solution that was tested at 200 and 300°F at 1,000 psi for 4 hours.....	141
Figure 8.13	Zeta potential values of deionized water (DW) and 14 wt% acid mixture with and with a corrosion inhibitor after 6 hours and 10 days of particles suspension at room temperature.	142

LIST OF TABLES

Table 2.1	Limitations for Controlling Leak-off Rate Methods (Blauch et al. 2003).....	19
Table 2.2	Achievable Protection Time for HCl at Different Temperatures Compared to The Achievable Corrosion Protection for Acetic Acid Time (Robert and Crowe 2000).	19
Table 2.3	Solubility of Salts Produced From Common Organic Acid Reactions With Calcium Carbonate.	21
Table 2.4	Physical and Chemical Properties of Lactic Acid (Martinez et al. 2013).....	22
Table 2.5	Physical and Chemical Properties of Gluconic Acid (Ramachandran et al. 2006).	25
Table 2.6	Scale Inhibitors Used in This Research and Their Chemistry Base.	29
Table 2.7	Sulfur-Based Corrosion Inhibitor Chemical Composition.	32
Table 3.1	Typical Composition for Arabian Gulf Seawater (Ahmed et al. 2017).....	41
Table 3.2	Acceptable Ranges of Corrosion Rate Based on Temperature Ranges.	44
Table 4.1	Solubility Comparison Between Acid Solutions Prepared With Deionized Water (DW) and Seawater (SW) at Room Conditions.....	67
Table 5.1	Corrosion Rates of the Tested Solutions at 200 and 300°F.	75
Table 6.1	The Twelve Different Solutions Tested Using Zeta Potential at Room Temperature.	97
Table 7.1	Coreflood Tests Along with Pore Volumes Needed to Breakthrough The Tested Cores.	108
Table 8.1	Economical Comparison Between Different Kind of Acids. The Main Acid is Based on Lactic and Gluconic Acids While the Other Three are Based on HCl.	145

NOMENCLATURE

A	= core area, cm ²
A _T	= critical pore size area
B	= formation volume factor, reservoir volume/ surface volume
CaCl ₂	= calcium chloride
CaL ₂	= calcium lactate
CaSO ₄	= calcium sulfate
Ca ²⁺	= calcium ion
C ₃ H ₆ O ₃	= lactic acid chemical formula
C ₆ H ₁₂ O ₇	= gluconate ion chemical formula
CH ₃ CH(OH)CO ₂ ⁻	= lactate ion chemical formula
CO ₂	= carbon dioxide
CaCO ₃	= calcium carbonate
CI	= corrosion inhibitor
CT	= computed tomography
C _{HCl}	= acid concentration
C _o	= acid concentration
C _{weak acid}	= weak acid concentration
C _m	= molarity, mole/mL
C _p	= acid concentration, frac
d _{5 wt% KCL}	= density of 5 wt% KCl brine, g/cm ³

d_a	= density of acid at the desired concentration, g/mL
d_a	= density of the acid at the desired concentration, g/mL
d_s	= acid stock density, g/mL
D_t	= dielectric constant of the suspending solution at temperature t
DW	= deionized water
E_f	= reaction rate constant
EM	= electrophoretic mobility at temperature t
FRT	= formation response tester
FTIR	= Fourier Transform Infra-Red
GA	= gluconic acid
gpt	= gallon per thousand
h	= net formation thickness
HCl	= hydrochloric acid
HF	= hydrofluoric acid
H^+	= hydrogen ion
H_2O	= chemical formula of water
HCO_3^-	= bicarbonate
H_2CO_3	= carbonic acid
IC	= ion chromatography
ICP	= inductively coupled plasma
IPR	= inflow performance rate
K_a	= dissociation constant
K_d	= dissociation constant of weak acids

k	= permeability, md
k_s	= damaged zone permeability, md
L	= core length, cm
L^-	= lactate ion
LA	= lactic acid
M_{acid}	= acid molar mass, g/mole
M_{CaCO_3}	= crushed core molar mass, g/mole
md	= millidarcy
Na_2SO_4	= sodium sulfate
$n_{\text{acid solution}}$	= number of moles within acid solution, moles
OH^-	= hydroxide ion
pK_a	= dissociation logarithmic constant
PLA	= polylactic acid
ppm	= part per million
PV	= core pore volume, cm^3
p_s	= outer boundary pressure, psi
$p_{\text{wf,d}}$	= flowing bottom hole pressure in damaged case, psi
$p_{\text{wf,id}}$	= flowing bottom hole pressure in ideal case, psi
q	= flow rate at surface, STB/D
q_i	= Injection rate, cm^3/min
r_e	= drainage radius, ft
r_{HCl}	= reaction rate of HCl
r_s	= damaged zone radius, ft

r_w	= wellbore radius, ft
s	= skin factor, dimensionless
SI	= scale inhibitor
SI-A	= scale inhibitor A
SI-B	= scale inhibitor B
SI-C	= scale inhibitor B
SO_4^{2-}	= sulfate ion
SW	= seawater
u	= injection rate
$V_{\text{acid stock}}$	= volume amount taken from an acid stock, mL
V_f	= solution final volume, mL
ν_t	= viscosity of the suspending solution at temperature t
V	= core volume, cm^3
W_0	= crushed core weight before test, gram
W_1	= unreacted crushed core weight after test, gram
W_{CaCO_3}	= weight of crushed core used in the test, gram
X_a	= desired acid concentration, frac
X_s	= acid stock initial concentration, frac
XRD	= X-ray diffraction
Δp_s	= altered zone additional pressure drops, psi
ΔP	= differential pressure across the tested core, psi
α	= magnitude of the reaction
μ	= viscosity, cp

ξ = zeta potential, mV

ϕ = core porosity, frac

ACKNOWLEDGMENTS

First and foremost, I would like to thank God for giving me the strength, health, ability, and knowledge to pursue my Doctor of Philosophy in petroleum engineering. This journey would not be possible without His blessings.

I want to thank my wife, Alaa, for her full support and endurance during every step of this long journey. I would not be able to reach this step of my degree process without her. Thanks to my biggest source of strength and inspiration, my parents, Ahmed and Huda. Thanks for everything you did for me. I am nothing without you.

Special thanks to my advisor Dr. Jennifer Miskimins for her enormous support in the past three years. She has always been there for me during difficult times to inspire me in passing the research challenges. She has given me all the needed supervision to complete my research without deviating away from the main objectives. I remember many stressful times where I had different issues with my experiments. Her kindness and inspirational words were the support I needed to pass these times. Thank you, Dr. Miskimins, for being my advisor. You are a fantastic person who I was lucky to work with.

I would like to thank my committee members Dr. Stephen Sonnenberg, Dr. Mansur Ermila, Dr. Michael Heeley, and Dr. Yilin Fan. Thank you all for offering and providing support for me. The success of this journey would not be possible without your useful feedback from the research proposal defense to the thesis defense. I also would like to thank Dr. Azra Tutuncu, who passed away this year. Dr. Tutuncu is in my heart, and I will always remember her. She is an amazing soul, and her legacy will not be forgotten.

I would like to thank the Department of Petroleum Engineering faculty here at Colorado School of Mines for their continuous help. My gratitude to Denise Winn-Bower for her support and assistance in all matters. She is the soul of the graduate program. Thanks to my friends in the FAST Consortium, and thanks go to FAST members as well for their useful feedback. I would also like to thank my sponsor employer Saudi Aramco for granting me the opportunity to pursue my education in petroleum engineering. Lastly, my appreciation and thanks go to Halliburton Company for the support and help to obtain the needed corrosion inhibitor for this research.

This dissertation is dedicated to my beloved parents

Ahmed and Huda;

To my beloved wife

Alaa;

To my children, sisters, and brother.

Thank you all for giving me the support to reach this achievement.

CHAPTER 1

INTRODUCTION

Reservoir stimulation was introduced in the oil and gas industry to improve well productivity or injectivity by enhancing reservoir and wellbore connectivity. This improvement can delay the need for artificial lift or can unlock production in new formations. Along with that, reservoir stimulation can manipulate inflow performance rate (IPR) curves, specifically the inflow curve, to redeem old production wells that have developed a substantial amount of skin damage with time (Economides and Boney 2000).

Reservoir stimulation includes two main methods: acid stimulation and hydraulic fracturing. The focus of this study is on the first, which includes three types of treatments: acid washing, matrix acidizing, and acid fracturing. Hydrochloric acid (HCl) is considered the most commonly used acid and has been used since the late 1800's (Buijse et al. 2004; Mahmoud et al. 2011). However, the strong dissolution level, high corrosion rate, and poor etching pattern, specifically at high reservoir temperature, motivated the industry and academia to retard HCl using emulsified acid, gelled acid, or surfactants. Unfortunately, all these methods have their limitations (Blauch et al. 2003; Nasr-El-Din et al. 2007, 2009).

Organic acids, including formic acid, acetic acid, and citric acid, have been implemented in the industry as stimulation acids, iron control agents, and formation damage removal agents (Robert and Crowe 2000). In stimulation operations, formic and acetic acids have been utilized to overcome the corrosion and the dissolution rate challenges associated with HCl. Along with that, citric acid was introduced in capsule forms to generate acid under in-situ conditions and has been

used as an iron control agent (Crowe and Minor 1985; Elkatatny and Nasr-El-Din 2012; Zhang et al. 2016). However, due to potential damage from reaction product salts and the nature of the reaction, these acids could not achieve the desired stimulation efficiency (Nasr-El-Din et al. 2007).

Formic and acetic acids produce calcium formate and calcium acetate when they react with calcite with which they have a solubility of 166 g/L and 300 g/L in water, respectively (Rabie et al. 2015). Citric acid produces calcium citrate which has a significant low solubility of 0.85 g/L in water (Nasr-El-Din et al. 2007).

Lactic acid is an α -hydroxy carboxylic acid that has served the oil and gas operations as an iron control agent and as a component in drilling fluid filter cake (Elkatatny and Nasr-El-Din 2012). Lactic acid produces calcium lactate salt when it reacts with calcite. However, this salt has good solubility in water in comparison with other organic acids when it is combined with gluconic acid as it produces calcium lactate gluconate which has a solubility of 400 g/L compared to 79 g/L in water for calcium lactate.

This research was performed to provide a better understanding about lactic acid performance in stimulating carbonate formations along with potential associated damages from lactic acid and gluconic acid interactions with calcite particles, limestone cores, and steel wellbore pipe coupons. Multiple tests were done under different temperatures and pressure to achieve the research goals and to provide guidelines to use lactic acid in an optimum practice for onshore and offshore carbonate acidizing operations.

1.1 Research Motivation

Numerous studies have been conducted on organic acid performance in carbonate and sandstone acidizing operations with much less focus on lactic acid. Reaction product solubility is

one of the main reasons to avoid using most of the available organic acids due to probable formation damage. If these reaction products were left inside stimulated formations, permeability and flow impairment could arise, and reservoir productivity could ultimately decrease.

Mixing gluconic acid with lactic acid produces a salt that has much better solubility in water than calcium lactate. This salt, called calcium lactate gluconate, has a solubility of 400 g/L compared to 79 g/L in water of calcium lactate. The idea was first approached by Gerstner and Ladenburg (2002), who reported an increase of 33% of calcium lactate salt solubility with the combination of sodium gluconate. Phadungath and Metzger (2011) applied this novel approach in the food industry to avoid calcium lactate precipitation that appears on the surface of cheese after six months of aging.

HCl is exceptionally reactive and corrosive in high-temperature applications, which causes severe corrosion and pitting on downhole tubulars. Maintenance, replacements, and workover operations due to corrosion damages along with safety hazards, urged researchers to find less corrosive alternative fluids (Buijse et al. 2004; Nasr-El-Din et al. 2007; Rabie et al. 2015). Lactic and gluconic acids are environmentally friendly products that do not impose substantial risks during field operations. Both acids are less corrosive than HCl, which could ultimately be a significant step toward protecting downhole tubulars.

HCl has a high dissolving power at high temperature and can compromise the acidizing goals by creating face dissolution patterns instead of dominant wormhole patterns. On the other hand, lactic and gluconic acids are retarded acids, which make them much weaker acids than HCl. Weak acids react slowly which keep acid reactions focused on one pathway with tip penetration, which forms an entirely dominant wormhole instead of a face dissolution as compared in Figure 1.1.



Figure 1.1 Coreflooded cores that represent face dissolution (A) and a dominant wormhole (B) (He et al. 2011; Akanni and Nasr-El-Din 2016).

1.2 Problem Statement

In this research, lactic and gluconic acid performance on carbonate acidizing operations was addressed by four main tests, including solubility, corrosion, wettability, and coreflood tests. These tests were performed with different acid concentrations and ratios that were prepared with deionized water (DW) and synthetic seawater (SW) to mimic onshore and offshore matrix acidizing operations.

Solubility tests were done to evaluate the acids' ability to dissolve carbonate formations and to investigate possible reaction products such as salt precipitation. Corrosion tests were performed with low carbon tubular steel coupons to assess how corrosive the acids are compared to HCl. Wettability evaluation was performed since acids can leak-off inside the formation and alter the wettability. Whole treatments were then simulated by coreflood, which returned results in terms of permeability improvement, required pore volume amounts to breakthrough, and optimum injection rate.

1.3 Research Objectives

This research is focused on lab-based experimental results. It includes the following five objectives.

- Determine a base case for lactic acid reaction with carbonate rock and lactic acid interaction with low carbon tubular steel coupons.
- Improve lactic acid reaction with calcite and prevent calcium lactate precipitation deposition by the addition of gluconic acid. The acid concentrations and molar ratios were manipulated to achieve an optimum acidizing fluid recipe that can achieve acceptable dissolving capacity. The improved system was also tested for corrosion rate where it was kept below the acceptable corrosion rate.
- Evaluate the two-acid system performances when the acids are mixed by seawater. This step produced more knowledge about the two-acid dissolving capacity when seawater ions are dissolved in solution. Existing ions in seawater can affect calcium ion diffusion rates in the acid-calcite reaction.
- Investigate the two-acid system effects on carbonate rock wettability by testing the spent solution effect on calcite particles by measuring the alteration of calcite rock surface charges.
- Simulate the two-acid system using a coreflood apparatus to accomplish a solid foundation of utilizing lactic acid with gluconic acid in stimulation operations. This simulation includes the pre-treatment, treatment, and post-treatment stages.

1.4 Tested Materials and Fluids

This research has been performed to promote lactic acid as a stimulation fluid for carbonate formations. Gluconic acid was chosen to be a complementary acid to increase reaction product salt

solubility in solution. Crushed pink desert limestone cores were used to conduct solubility tests for acids prepared with deionized water and seawater. Coreflood tests were conducted on low permeability Indiana limestone cores that have an average permeability of 2 to 4 md and an average porosity of 12 to 14%. Steel coupons, cut from N-80 pipe, were used for corrosion tests. All fluids and materials used in this research were publicly available except for the corrosion inhibitor provided from a local service company.

1.5 Thesis Overview

This dissertation is based on lab experimental work that is detailed in nine chapters. Chapter 1 introduces the motivation and objectives of the research. Chapter 2 presents the background and the literature review of reservoir stimulation and fluids used to stimulate carbonate formations. Chapter 3 shows the experimental setups, apparatus, procedures, and test principles.

Chapter 4 to Chapter 7 present the experimental results and discussion of the solubility, corrosion, wettability, and coreflood tests. Chapter 8 shows the application and benefits of implementing the lactic and gluconic acid mixture in oil and gas acidizing operations. Chapter 9 concludes this dissertation by combining the main highlights and by providing recommendations for future research.

CHAPTER 2

LITERATURE REVIEW

This chapter provides an intensive review of reservoir stimulation and its main methods. Further summaries about fluid systems used in acidizing operations are provided to establish a base background for introducing lactic and gluconic acids. Section 2.3 summarizes an overview of lactic and gluconic acids which includes chemical reactions with carbonate, chemical and physical properties, and processing and production methods. Later sections focus on the impact of utilizing seawater to prepare the acids and on the impact of acid invasion on carbonate formation wettability. This chapter also includes an overview about common additives that are essential in any acidizing operations.

2.1 Reservoir Stimulation

Reservoir stimulation was introduced in oil and gas operations to enhance well productivities and injectivities with a target to delay artificial lift usage, to redeem old wells, and to unlock new formations (Economides and Boney 2000). The two main methods of reservoir stimulation are hydraulic fracturing and matrix stimulation as these methods can improve reservoir and wellbore communication. This improvement can be easily noticed in the IPR curve for any well, where reservoir stimulation can reduce the well's skin factor and shift the inflow curve to the right. This shift would increase the well's productivity with a lower bottom hole pressure as can be seen in Figure 2.1.

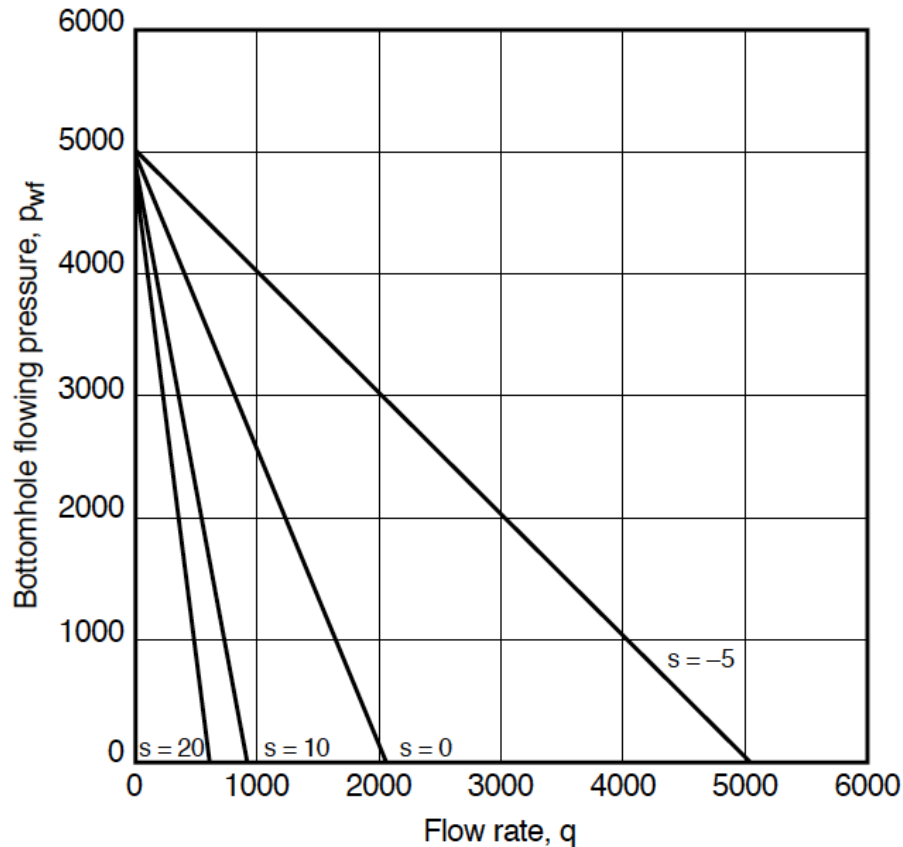


Figure 2.1 Skin factor effect on IPR curve. It shows the importance of restoring skin factor to lower values as doing so increases the flow rate at a specific bottomhole flowing pressure (From Economides and Boney 2000).

In addition to this improvement, the oil and gas industry is targeting new unconventional hydrocarbon reservoirs that cannot be unlocked without utilizing reservoir stimulation. Shale reservoir operations are examples of tight unconventional reservoirs whose production has risen significantly due to the extensive hydraulic fracturing and acidizing operations in the United States (Economides and Boney 2000).

Acid stimulation has been performed in the oil and gas industry for more than 120 years to maximize new wells' productivity or to restore old wells' productivity by removing formation damage and by creating new reservoir contact via wormholes (Economides and Boney 2000; Hill

and Schechter 2000; Nasr-El-Din et al. 2007; Mahmoud et al. 2011). This productivity improvement is mathematically manipulated by altering the skin effect, which was introduced by Van Everdingen and Hurst (1949).

2.1.1 Skin Effect

“Skin” is a dimensionless analog representing alterations in the near-wellbore zone. Any wellbore operations can cause these alterations from drilling to reservoir stimulation itself (Economides and Boney 2000). Lack of protective applications can severely reduce near wellbore permeability. In turn, this reduction would cause an alteration to the radial and lateral flow toward the wellbore due to an additional pressure difference in the near-wellbore zone, Figure 2.2.

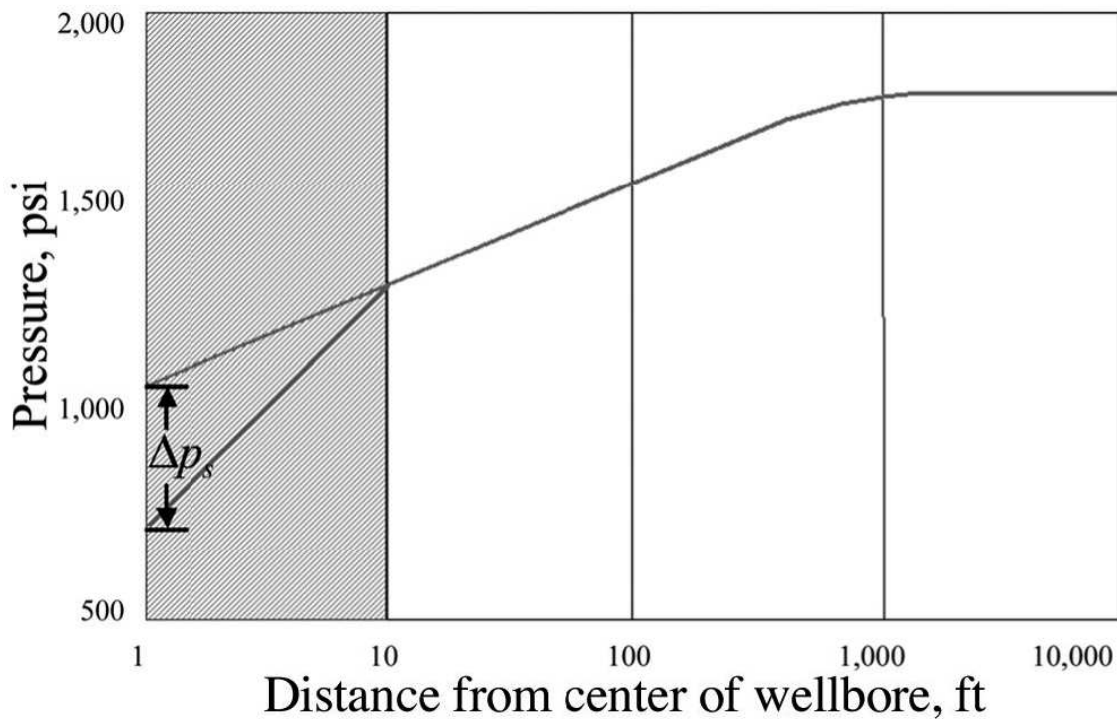


Figure 2.2 Additional pressure drop in the flow convergence region due to near wellbore alteration and damages (From Petrowiki 2015).

This additional drop in the altered zone is represented by Equation 2.1:

$$\Delta p_s = \frac{q\mu}{2\pi kh} s \quad (2.1)$$

The skin effect is the cause of this steady-state pressure drop, which is reflected in a two-zone region: damaged and undamaged zone. As a result, reservoir radius and permeability can be divided into two analogs, one representing the whole reservoir and the other representing the damaged zone as shown in Figure 2.3.

Hawkins formula, introduced by Hawkins (1956), is the most common skin effect representation in the industry as it is an easy tool to assess damage in a wellbore. This equation was derived through the steady-state flow equation. In an ideal situation, the flow is represented by Equation 2.2:

$$q = \frac{kh(p_s - p_{wf,id})}{141.2B\mu \ln\left(\frac{r_s}{r_w}\right)} \quad (2.2)$$

And in a damaged situation the flow is represented by Equation 2.3:

$$q = \frac{k_s h(p_s - p_{wf,d})}{141.2B\mu \ln\left(\frac{r_s}{r_w}\right)} \quad (2.3)$$

Where,

- Δp_s : altered zone additional pressure drop, psi
- q : flow rate at surface, STB/D
- μ : viscosity, cp
- B : formation volume factor, reservoir volume/ surface volume
- k : matrix permeability, md
- h : net formation thickness, ft
- s : skin factor, dimensionless

- p_s : damaged zone boundary pressure, psi
- $p_{wf,id}$: flowing bottom hole pressure in ideal case, psi
- $p_{wf,d}$: flowing bottom hole pressure in damaged case, psi
- r_e : drainage radius, ft
- r_w : wellbore radius, ft
- r_s : damaged zone radius, ft
- k_s : damaged zone permeability, md

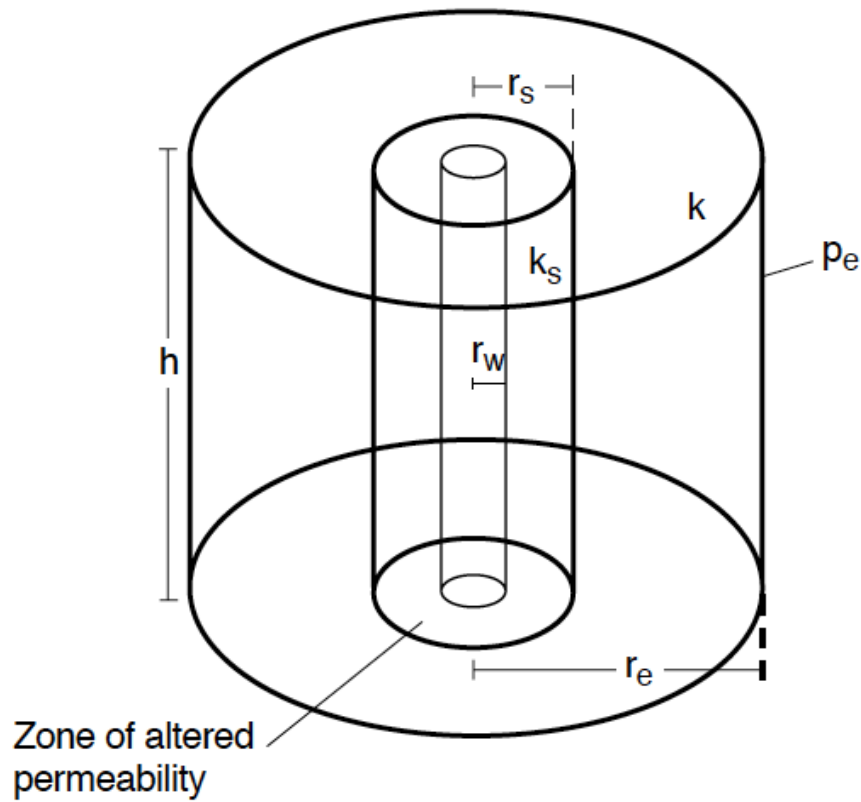


Figure 2.3 Two region zones caused by positive skin factor: damaged (r_s) and undamaged (r_e) (From Economides and Boney 2000).

The additional drop due to near-wellbore damage is represented by Equations 2.4 and 2.5:

$$\Delta p_s = p_{wf,id} - p_{wf,d} \quad (2.4)$$

$$\Delta p_s = \frac{141.2qB\mu}{h} \ln \left(\frac{r_s}{r_w} \right) \left(\frac{1}{k_s} - \frac{1}{k} \right) \quad (2.5)$$

By combining Equations 2.1 and 2.5, the Hawkins equation is:

$$s = \left(\frac{k}{k_s} - 1 \right) \ln \left(\frac{r_s}{r_w} \right) \quad (2.6)$$

If k_s is larger than k , then the well is stimulated, and the skin effect is negative. While in the case of k_s being smaller than k , then the well is damaged, and the skin effect is positive. If no damage or enhancement exists, k_s would equal to k , and the skin factor would be equal to zero.

2.1.2 Acid Stimulation and Dissolution Patterns

Acid stimulation includes three main treatment types: acid washing, matrix acidizing, and acid fracturing. The first two are performed below fracturing pressure while the last is performed above fracturing pressure.

Acid washing is applied to remove and to clean dissolvable precipitations deposited on the wellbore tubulars and the wellbore sandface. Matrix acidizing is applied to generate channels within a treated formation, which are called wormholes, by dissolving and bypassing near-wellbore formation damage. Eventually, hydrocarbon would flow through these channels due to an increase in near-wellbore permeability, which is reflected by a decrease in the skin effect. Acid fracturing is differed from matrix acidizing as it is applied above fracturing pressure. Mainly, it is applied to create fractures within a treated formation.

The most two commonly used acids are hydrochloric acid (HCl) and hydrofluoric acid (HF) where the last is used exclusively in sandstone acidizing to remove aluminosilicate particles. Organic acids and other chelating agents are used mainly in high temperature applications due to their slow reaction behavior with formations (Robert and Crowe 2000; Buijse et al. 2004; Mahmoud et al. 2011; Nasr-El-Din et al. 2007, 2009). Matrix acidizing in sandstone formations can only penetrate and remove formation damages within 1 ft of the wellbore (Hill and Schechter

2000). In carbonate matrix acidizing, acids can penetrate and can remove formation damage at much longer distances, through dominant wormholes, notably when the treated formation is naturally fractured or is highly vugular (Hill and Schechter 2000).

The injected acid's ability to create dominant wormholes is the key for a successful carbonate matrix acidizing treatment (Fredd and Fogler 1998; Akanni and Nasr-El-Din 2016). When the acid is injected, large pores consume most of the acid and start to get larger than the smaller pores do. As more acid is pumped, these large pores get more acid and grow in length until wormholes are formed. Dominant wormholes are one of several different possible wormholes pattern that can occur due to acid dissolution. These patterns, shown in Figure 2.4, include face dissolution, conical wormholes, dominant wormholes, ramified wormholes, and uniform dissolution (Economides and Boney 2000; Pandey et al. 2018). Formation of these patterns are highly dependent on the injection rate, reaction kinetics, flow geometry, formation heterogeneity, and fluid loss rate (Fredd and Fogler 1998; Economides and Boney 2000; Akanni and Nasr-El-Din 2016; Pandey et al. 2018).

The optimum injection rate can lead to dominant wormholes as the acid is consumed at the tip of the evolving flow channel and penetrates the channel (Al-Duailej et al. 2013). At low injection rates, a high volume of the acid would be spent in the rock surface, and a face dissolution or a conical wormhole patterns would occur. At a very high injection rate, a ramified wormhole can occur, which consists of many small branches, due to the acid being forced inside small pores (Fredd and Fogler 1998; Al-Duailej et al. 2013; Akanni and Nasr-El-Din 2016).

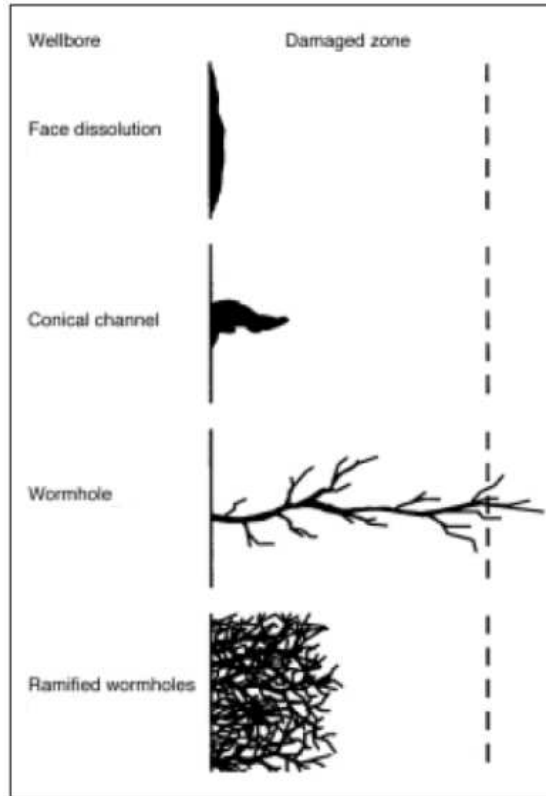


Figure 2.4 Schematic of common dissolution patterns. Maintaining the optimum injection rate can lead to dominant wormhole pattern (From Economides and Boney 2000).

In matrix acidizing the main goal is to lower the skin effect and to increase or to restore production. Manipulating acid dissolution patterns is a critical step toward developing dominant wormholes. These wormholes are essential to increase the permeability of the near-wellbore zone. In fact, in many cases, matrix acidizing cannot be very beneficial without this optimum connection between formation and wellbore (Akanni and Nasr-El-Din 2016; Pandey et al. 2018).

2.1.3 Manipulating Skin Effect and Damage Distance

The following scenarios illustrate the benefits and gains from acidizing conventional carbonate formations. It also shows how removing formation damage without dominant wormholes is only slightly beneficial in tight carbonate formations as the increase of productivity is not very remarkable.

Equation 2.7 is used to represent a steady-state flow case where all parameters were kept constant with the exception of flow rate (q) and skin effect (s).

$$q = \frac{kh(p_e - p_{wf})}{141.2B\mu \ln\left(\frac{r_e}{r_w} + s\right)} \quad (2.7)$$

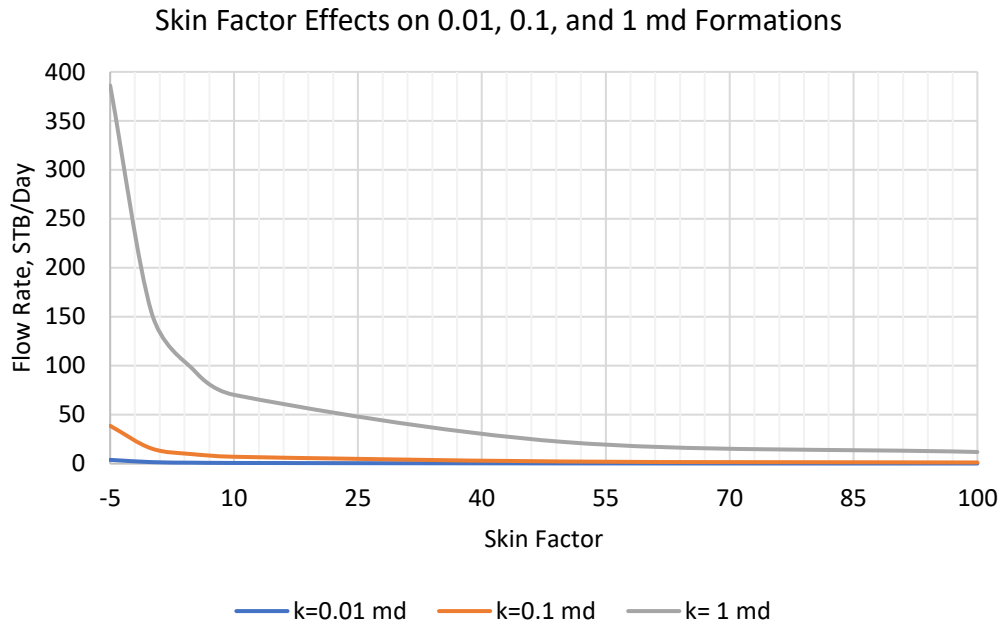


Figure 2.5 Skin factor effect on steady state flow rate. It shows that reducing the skin factor by damage removal can be very beneficial in conventional formations while it is less so in tight formations.

In this scenario shown in Figure 2.5, it can be noticed that restoring the skin factor, or removing formation damage, from 40 to -5 was very beneficial when the formation permeability was set to 1 md as the flow rate increased from 32 to 386 STB/Day or 12 folds of increase. While in moderate permeabilities formations, the flow rate increased from 2.5 to 38 STB/Day, which is still 12 folds of increase. However, in the tight formation case, the flow rate increased from 0.32 to 3.88 STB/Day, which is only 3.56 STB/D of gain. Although it is also 12 folds of production increase, this low increase is not very beneficial. The optimum result is obtained when the flow

permeability and skin effect are improved and manipulated through wormhole creation and removing formation damage.

As mentioned before, carbonate acidizing can bypass and penetrate a few feet inside the treated formation. However, formation damage removal is not practical after these few feet since formation damage can only restrict hydrocarbon flow in the stream convergence zone. This is illustrated in the following scenarios, shown in Figure 2.6, where the Hawkins equation was used again to manipulate the skin factor value when damage distance was changed as shown in Equation 2.8.

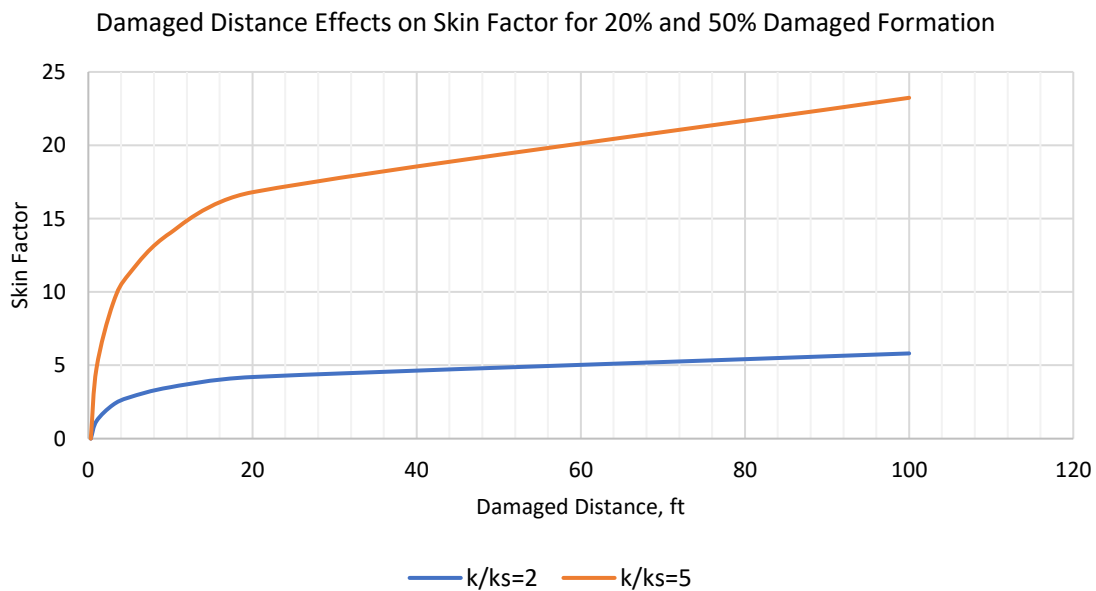


Figure 2.6 Damage distance effect on reducing the skin factor. The skin factor can be highly reduced when formation damage within 0 to 20 ft of the wellbore is removed.

From the previous two scenarios, it can be presumed that damage beyond the near-wellbore region would not be a vital factor in hydrocarbon flow restriction. A few feet of acid penetration can restore the skin factor significantly without the need to inject large volumes of acid into the formation.

2.2 Acid Used in Matrix Acidizing

The following sections talk about the primary acids used in carbonate formation acidizing with HCl being the most common, followed by organic acids.

2.2.1 HCl Applications and Limitations

HCl is the most commonly used acid in carbonate acidizing due to its relatively low price, availability, dissolving power, and soluble reaction product (Buijse et al. 2004; Nasr-El-Din et al. 2007). In 1932, the Pure Oil Company used inhibited HCl to stimulate a limestone formation, and since then HCl became the choice to replace the explosive stimulation of open-hole wells (Elbel and Britt 2000). HCl reacts with calcium carbonate (CaCO_3), and produces soluble calcium chloride, CO_2 gas and water:



However, the high reactivity and corrosivity of HCl obstruct its usage at high temperature applications due to the following reasons:

- Etching pattern.
- Wormhole pattern.
- Sludge, emulsion, wettability, and leak-off.
- Corrosion and pitting.

HCl has an extreme dissolution rate that leads to a high reaction rate. HCl's strong reactivity leads to poor etching patterns within the formation. Poor etching patterns can compromise stimulation treatments as etching is an important parameter that helps conductive wormholes to sustain formation closure stress (Blauch et al. 2003).

HCl dissolution patterns are another concern in acidizing treatments. Where dominant wormhole patterns are the most optimal results, HCl cannot, in most cases, create a dominant wormhole pattern in high downhole temperatures due to its high reactivity. In high temperature applications, the optimum HCl injection rate is avoided as it is generally higher than the maximum allowable surface injection pressure (Akanni and Nasr-El-Din, 2016). As mentioned before, a low injection rate can lead to face dissolution, which is not the most efficient pattern for matrix acidizing, as shown in Figure 2.7.



Figure 2.7 A carbonate core that was coreflooded using HCl at high temperature. The high reactivity and dissolving power caused a face dissolution to this core (From Akanni and Nasr-El-Din 2016).

HCl's effects can be delayed or retarded using emulsified acid, gelled acid, or surfactants, but these methods have their disadvantages such as corrosion, emulsion, sludging, and wettability alteration. Another challenge for HCl and other HCl combined fluids is the leak-off rate. One of the factors for a successful acidizing treatment is leak-off control, as insufficient control can result in short wormhole length, which leads to low productivity improvement (Blauch et al. 2003). The oil and gas industry has developed different methods to control leak-off rate in acidizing carbonate formations that are presented in Table 2.1 along with their main limitations:

Table 2.1 Limitations for Controlling Leak-off Rate Methods (Blauch et al. 2003)

Controlling leak-off rate methods	Limitations
Building filter cake by using polymers	Difficult to degrade all polymers that can reduce the pore throat flow path.
Mixture of soluble and insoluble solids	Insoluble particles can plug pore throats if they remain in wellbore.
Viscosity enhancement	Polymers are used to increase the viscosity which can lead to reducing the pore throat flow path. Also, it lowers the diffusion rate of the acid and acid/ rock reaction products.

HCl's strong dissolution associated with high downhole temperature makes HCl a very corrosive acid toward wellbore tubulars. HCl inhibition is required in these conditions by adding expensive corrosion inhibitors and intensifiers (de Wolf et al. 2017; Ng et al. 2018). Still, corrosion damage can occur, causing additional costs due to maintenance and replacements (de Wolf et al. 2017; Ng et al. 2018). Along with that, safety concerns have encouraged researchers to look for alternative acidizing fluids that are less corrosive and less hazardous. Table 2.2 shows that HCl possible protection time is limited and is much less than acetic acid, as an example.

Table 2.2 Achievable Protection Time for HCl at Different Temperatures Compared to The Achievable Corrosion Protection for Acetic Acid Time (Robert and Crowe 2000)

Acid	Temperature (°F)	Maximum Protection Time (hours)
15 wt% HCl	375	8
15 wt% HCl	400	4
28 wt% HCl	350	4
10 wt% Acetic	400	24
10 wt% Acetic	500	16

These limitations and challenges motivated the industry's research and development divisions to develop alternative acids and fluids that can deliver a successful treatment with the best production enhancement possible.

2.2.2 Organic Acids

Organic acids were introduced in acidizing operations to reduce the associated limitations of other methods. Organic acids are less corrosive than HCl and do not dissociate completely in water, which make them weaker acids. The two primary organic acids are acetic and formic acids, where formic is used less often as it is harder to be inhibited than acetic acid (Robert and Crowe 2000). In addition, formic acid reaction products are less soluble than acetic acid reaction products, which restricts formic acid to be prepared above 9 wt% (Robert and Crowe 2000).

Citric and lactic acids are less commonly chosen fluids for acidizing than acetic and formic acids. These acids are not new to the oil and gas industry as they represent most of the iron control agents in many treatment fluids, specifically citric acid. Hall and Dill (1988) mentioned the use of citric acid as an iron control agent to avoid precipitation of ferric hydroxide or iron sulfide. Also, lactic acid has been used to serve the same purpose along with removing drilling filter cake (Elkatatny and Nasr-El-Din 2012).

The conventional organic acids, formic and acetic, tackled some of the main challenges such as tubular corrosion, acid penetration, and reaction rate. Citric acid was introduced in capsule forms to generate in-situ acid (Al-Khaldi et al. 2003). However, there are two unique properties of these organic acids that can restrict their results. The first property is the low solubility of some of their reaction products such as calcium acetate and calcium citrate. Low solubility can impose a large risk on hydrocarbon flow paths due to reaction product salt deposition. Table 2.3 shows the solubility of formic, acetic, citric, and lactic acids reaction products. The second drawback is the

reaction behavior of those acids with carbonates as it is reversible, which prevents the acid from reaching a complete reaction stage (Nasr-El-Din et al. 2007).

Table 2.3 Solubility of Salts Produced From Common Organic Acid Reactions With Calcium Carbonate

Acid	Reaction Product	Solubility
Acetic	Ca acetate	300 g/L (Rabie et al. 2015)
Formic	Ca formate	166 g/L (Rabie et al. 2015)
Citric	Ca citrate	0.85 g/L (Nasr-El-Din et al. 2007)
Lactic	Ca lactate	79 g/L (Rabie et al. 2015)
Lactic and Gluconic	Ca lactate gluconate	400 g/L (Rabie et al. 2015)

Mixing gluconic acid with lactic acid can produce a salt that has much better solubility than calcium lactate. This salt is called calcium lactate gluconate and has a solubility of 400 g/L compared to 79 g/L of calcium lactate. This idea was first approached by Gerstner and Ladenburg (2002), who reported an increase of 33% of calcium lactate salt with the combination of sodium gluconate. Phadungath and Metzger (2011) applied this novel approach in the food industry to avoid calcium lactate precipitation that appears on the cheese surface after six months of aging, and they reported also promising results in this situation.

2.3 Lactic and Gluconic Acids

Lactic acid is an α -hydroxy carboxylic acid that has served the oil and gas industry as an iron control agent and as a component in drilling fluid mud filter cake (Elkatatny and Nasr-El-Din 2012). Lactic acid produces calcium lactate salt when it reacts with carbonate under specific temperature and pressure. This salt has a solubility of 4.5 gram/100 gram H₂O at 25°C or 79 g/L at 30°C (Nasr-El-Din et al. 2007). Table 2.4 shows the physical and chemical properties of lactic acid (Martinez et al. 2013).

Table 2.4 Physical and Chemical Properties of Lactic Acid (Martinez et al. 2013)

Property	Description
Relative molecular mass	90.08
Chemical formula	C ₃ H ₆ O ₃
Synonym	S-2-Hydroxypropanoic acid
pKa	3.86
Boiling point (50% solution)	200°C
Density	1.2060 g/cm ³
Appearance	Clear
Solubility	Soluble in water

Lactic acid can be used in solid form as a precursor that hydrolyzes with water under a specific temperature to release acid in-situ. This advantage can bring good treatment results as corrosion challenges can be alleviated due to the in-situ released acid where a well tubular would not be exposed to the acid. Along with that, lactic acid precursors can serve as a diverting agent in multi-zone acid stimulation treatments or in hydraulic fracturing treatments.

Diversion can be done by redirecting the main treatment from the untargeted zone by plugging the zone with precursors of lactic acid. After running the treatment, lactic acid precursors would start the hydrolysis process to give more stimulation to the diverted zone. In terms of leak-off rate, solid lactic acid reduces the risk of losing the treatment's fluid into the formation as the acid would be released when it is in the targeted place.

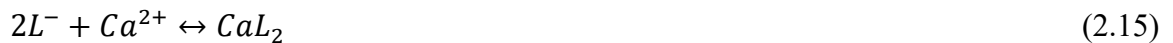
Lactic acid dissociates partially in water to give lactate and hydrogen ions as in the following reaction:



Where H^+ is a hydrogen ion, and L^- is a lactate ion $[CH_3CH(OH)CO_2^-]$. In this research, the concern is about the reaction between lactic acid and calcite. This reaction has been a subject of study for many researchers such as Lund et al. (1973a; 1973b), Plummer et al. (1978), and Sjoberg and Rickard (1984). This reaction can be classified into three reactions: hydrogen ion reaction, water reaction, and carbonic acid reaction with calcite as shown in Equations 2.10 to 2.12, respectively:



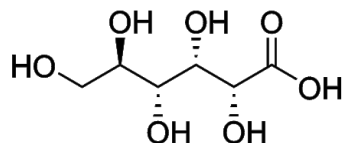
The hydrogen ion reaction is represented by Equation 2.10, and it is the dominant reaction at low pH values. Equation 2.11 represents the water dissolution reaction that is dominant at high pH values. The last reaction, Equation 2.12, represents the carbonic acid reaction with calcite. It is only considered when CO_2 partial pressure is higher than 0.1 atm and the solution pH is higher than 5. Since this study focuses on the reaction of lactic acid with calcite under acidic solutions with low pH values, the hydrogen ion reaction was only considered. The following sequence of reactions, Equations 2.13 to 2.15, represent lactic acid reaction with calcite for this research:



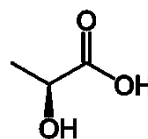
Rabie et al. (2015) introduced an idea to improve lactic acid performance in reservoir stimulation and to improve reaction product solubility in solution. The suggested mixing of

gluconic acid with lactic acid can produce a salt that has much better solubility than calcium lactate. This salt is called calcium lactate gluconate and has a solubility of 400 g/L compared to 79 g/L of calcium lactate. It is a result of calcium binding to the two acid legends as can be seen in Figure 2.8.

(a) Gluconic Acid



(b) Lactic Acid



(c) Calcium Lactate Gluconate

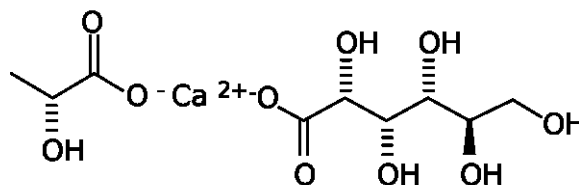


Figure 2.8 Chemical structures for (a) gluconic acid, (b) lactic acid and (c) calcium lactate gluconate.

Gluconic acid is an environmentally friendly compound that can be extracted from natural materials through the oxidation of glucose. It is a noncorrosive, mildly acidic, less irritating, and nontoxic organic acid. According to the US Food and Drug Administration, sodium gluconate is a safe additive to food and can be used without any limitation (Abdel-Rahman et al. 2011).

In oil and gas operations, gluconic acid has been utilized as a chelating agent for iron control, as an additive to study viscoelastic surfactant-based acid, as a corrosion inhibitor, and as

a scale inhibitor. Table 2.5 shows the physical and chemical properties of gluconic acid (Ramachandran et al. 2006).

Table 2.5 Physical and Chemical Properties of Gluconic Acid (Ramachandran et al. 2006)

Property	Description
Nature	Noncorrosive, mildly acidic, less irritating, non-odorous, nontoxic, easily biodegradable, nonvolatile
Relative molecular mass	196.16
Chemical formula	$C_6H_{12}O_7$
Synonym	2,3,4,5,6-pentahydroxhexanoic acid
pKa	3.7
Boiling point (50% solution)	102°C at 760 mmHg
Density	1.24 g/cm ³
Appearance	Clear to brown
Solubility	Soluble in water
Sourness	Mild, soft, refreshing taste
Degree of sourness (sourness of citric is 100)	29-35
Biodegradability	98% at 48 h

2.3.1 Lactic Acid Manufacturing and Production

Lactic acid was discovered in 1780 in sour milk and was fermented in 1839 with sugar, milk, starch, and dextrin (Holten et al. 1971). In recent years, lactic acid has gained much attention in various industries due to its ability to be a monomer in the processing of polylactic acid (PLA). As a result, production of lactic acid has increased significantly, and it is expected to be one of the main components for future products as The U.S. Department of Energy has listed it as a potential building block for the future (Abdel-Rahman and Sonomoto 2016). In 2013, lactic acid demand

was 714.2 kilotons, and it is expected to reach 1,960.1 kilotons by 2020 (Abdel-Rahman and Sonomoto 2016). The pie chart in Figure 2.9 shows the uses and demands of lactic acid.

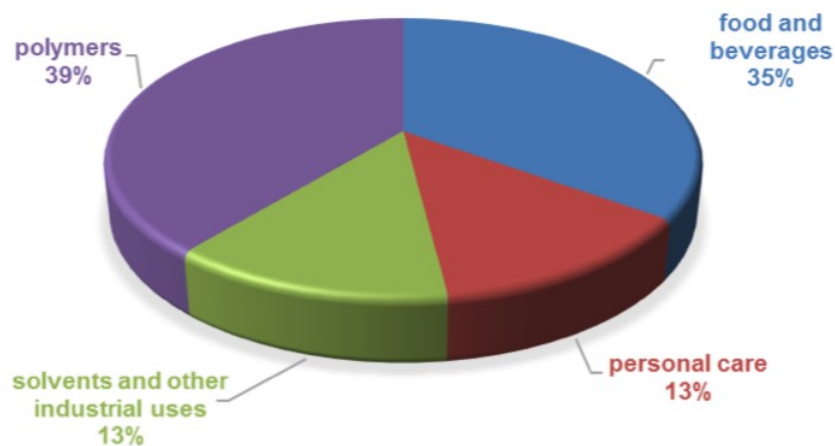


Figure 2.9 Uses and demands of lactic acid among different industries (From Komesu et al. 2017).

Lactic acid blocks can be found in many renewable resources and natural orgasms. It can be produced from coal, petroleum products, natural gas, plants, microorganisms, and animals. It is produced through two manufacturing methods. The first one is called chemical synthesis, while the second one is called microbial fermentation. The favorable production method is the microbial fermentation as it offers low production temperature and low energy consumption along with affordable production cost as compared to the chemical synthesis (Abdel-Rahman et al. 2011).

The microbial fermentation is started with raw materials of carbohydrates such as glucose, sucrose, or lactose along with water, lime, and chalk. These raw materials are fermented to produce crude calcium lactate with impurity from gypsum compound. Then, gypsum is removed to form crude lactic acid. Lastly, pure lactic acid is produced by purification and concentration processes (Abdel-Rahman et al. 2011; Abdel-Rahman and Sonomoto 2016; Komesu et al. 2017).

2.3.2 Gluconic Acid Manufacturing and Production

Gluconic acid was recognized in 1870 and found in *aspergillus niger* in 1870. Naturally, gluconic acid is produced through the glucose oxidase catalysis process, which includes the dehydrogenation reaction that forms gluconic acid (Ramachandran et al. 2006). Gluconic acid has a wide range of applications in the food industry as it is part of meats, dairy products, baked goods, and flavoring agents.

The most common production method is microbial fermentation, which consumes a wide range of organisms to produce gluconic acid. Among other production methods, the microbial fermentation is the easiest and cheapest method. Ramachandran et al. (2006) reported gluconic acid production can rely on fungal species, such as *aspergillus niger* or *penicillium*, and bacterial species, such as genera *Gluconobacter*, *Pseudomonas* or *Acetobacter*. Both sources can be used to produce gluconic acid by microbial fermentation through oxidation of glucose molecules.

2.4 Presence of Sulfate Ions in Acidic Solutions

The reactions of calcite with HCl or organic acids produce high amounts of calcium ions. In the presence of sulfate ions, calcium sulfate precipitation can occur due to the combination of calcium ions and sulfate ions, as shown in Equation 2.16. This scale has a very low solubility that favors decreasing more when the acid is spent, which can cause formation damage within formations pores and flow channels. Moreover, this precipitation can compromise the matrix acidizing procedure as calcium sulfate may act as a blockage or as a barrier between the carbonate formation and the acid.



The tendency of calcium sulfate precipitation increases when seawater is being used to prepare the acid as seawater usually contains high level of sulfate ions. Ahmed et al. (2017) mentioned the following considerations before using seawater with acids:

- Acid needs to be compatible with seawater without any precipitation.
- The acid recipe has to remove anticipated formation damage.
- The treatment results should increase the formation's permeability.
- The formation's integrity should be stable during the treatment.

Two methods can be used to avoid calcium sulfate deposition in seawater: extracting sulfate ions from the seawater, which costs a lot, or using scale inhibitors which is more economical (Fan et al. 2010). Three kinds of scale inhibitors have been used in the oil and gas industry to mitigate scale deposition. The first kind is chelating agents that can form a soluble complex to be in the solution under specific conditions. The second kind is retarders, which prevent the growth of calcium sulfate crystals, and the third kind is threshold inhibitors which prevent the initiation of the supercritical nuclei (Al-Khaldi et al. 2011).

In this research, a synthetic seawater was prepared with different amount of sulfate ions (3000 to 5000 ppm) to investigate the compatibility of lactic acid with seawater. Three scale inhibitors, that are commercially available, were chosen to mitigate calcium sulfate precipitation. Table 2.6 shows these scale inhibitors along with their based chemistry.

Table 2.6 Scale Inhibitors Used in This Research and Their Chemistry Base

Scale Inhibitor	Chemistry Base
SI-A	Diethylenetriaminepentakis(methylphosphonic acid)
SI-B	Poly(acrylic acid sodium salt)
SI-C	Nitrilotri(methylphosphonic acid)

2.5 Corrosion

Corrosion protection and maintenance costs the US industries around \$170 billion a year, and the oil industry takes a substantial portion from this amount (Brondel et al. 1994). Corrosion is linked to every phase of oil and gas field life from drilling to abandonment. It is difficult and nearly impossible to prevent corrosion, but it is more attainable and economical to manage it.

Corrosion occurs by following the basic battery concept with a metal acting as a cathode and another metal acting as an anode. The metal with a higher corrosion tendency becomes the negative pole and acts as an anode. Free positive ions can be lost from the anode and cause a loss of free electrons; this is called an oxidation process. These free electrons can be built upon the anodic site and impose an electrical potential, inviting a reduction process where these electrons would flow to the cathode site and would be combined and neutralized with other ions.

Figure 2.10 illustrates this experience. In the anodic site, iron is released to solution as iron ions Fe^{++} (oxidation) that can complex with oxygen, hydrogen sulfide, or carbon dioxide. A reduction process would occur at the same time at the cathodic site where hydroxyl ions or hydrogen gas is produced from oxygenated water.

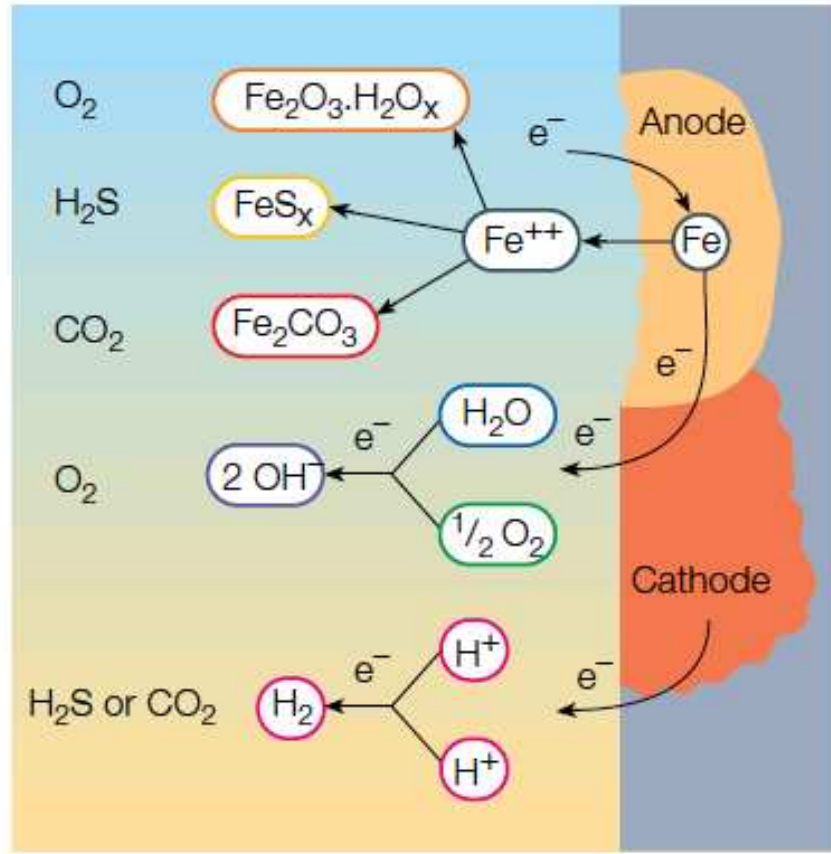


Figure 2.10 Anodic and cathodic sites corrosion on metal surface (From Brondel et al. 1994).

In acidizing operations, steel is attacked by dissociated hydrogen ions in the acid solution causing an oxidation and a reduction in the anodic and cathodic sites. Iron is released to iron ions in the anodic site by following this Equation 2.17:



While hydrogen ions form hydrogen gas in the cathodic site by following Equation 2.18:



And the overall reaction is:



2.5.1 Corrosion Inhibition in Acidizing Operations

The most common method for corrosion inhibition is the addition of chemicals that can interfere with the reaction between acids and cathodic or anodic sites. This interference occurs by building a protective film on the metal surface to prevent any interaction between acids and the metal surface. Adsorption phenomena is responsible for the adherence of the protective film on the metal surface (Nathan 1973). Sulfur, nitrogen and oxygen groups that are in corrosion inhibitors build Van der Waals forces against the metal surface, which gets strengthened by chemisorption attachment (Rozenfel'd 1981; Weder et al. 2016).

These chemicals consist of two groups: organic and inorganic corrosion inhibitors. Organic corrosion inhibitors are built from one or multiple polar groups, mostly sulfur, nitrogen, and oxygen. They work by building the mentioned protective film and by demobilizing of hydrogen ion at the cathodic site. On the other hand, inorganic corrosion inhibitors consist of different metals such as nickel, copper, arsenic, antimony, and salts of zinc with the arsenic group being the most common. It works by building an iron sulfide (protective film) that acts as a barrier between the acid and the metal surface. However, inorganic corrosion inhibitors are highly hazardous and cause iron sulfide insoluble precipitation.

2.5.2 Corrosion Inhibitors for HCl and Organic Acids

HCl acid is usually combined with inorganic corrosion inhibitors that are based on quaternary ammonium. The presence of chloride ions in the acid solution invites positively charged inhibitor molecules to attach to the metal surface. Organic acids do not contain chloride ions which make HCl based corrosion inhibitor inadequate for usage (de Wolf et al. 2017). Organic acid counter ions, such as acetate, formate, and lactate, cannot attach to the metal surface strongly. In that case, the sulfur-based corrosion inhibitor is essential. SH^- molecules in the sulfur-based

corrosion inhibitor are attached and can attract the positively charged molecules in the corrosion inhibitors (Frenier and Ziauddin 2008).

In this research, a sulfur-based corrosion inhibitor was selected to reduce the corrosion rate caused by lactic and gluconic acid. This corrosion inhibitor is classified as one of the thiourea groups that combine with different fatty acids. These fatty acids work as aids to improve corrosion control by adding more attachment to the metal surface through covalent bonds. Table 2.7 shows the used corrosion inhibitor composition and concentration.

Table 2.7 Sulfur-Based Corrosion Inhibitor Chemical Composition

Substance	Concentration
Ethylene glycol	10-30%
Thiourea	10-30%
Surfactant	1-5%
Fatty amine salt	1-5%

2.6 Wettability Alteration

During matrix acidizing, spent acid invades the near-wellbore area, which mainly contains calcium and water. An entirely successful matrix acidizing treatment can be achieved when the spent acid is recovered completely. The stimulation treatment can create small wormholes within a stimulated zone near the wellbore. However, the spent acid can go deeper to invade, as in Figure 2.11, which can alter the relative permeability. Spent acid invasion has a direct effect on production enhancement and recovery of spent acid. Spent acid recovery can be affected by the acid additives' surface-active properties and formation's rock wettability. Controlling these properties can lead to better recovery of the acid and better production enhancement (Saneifar et al. 2010).

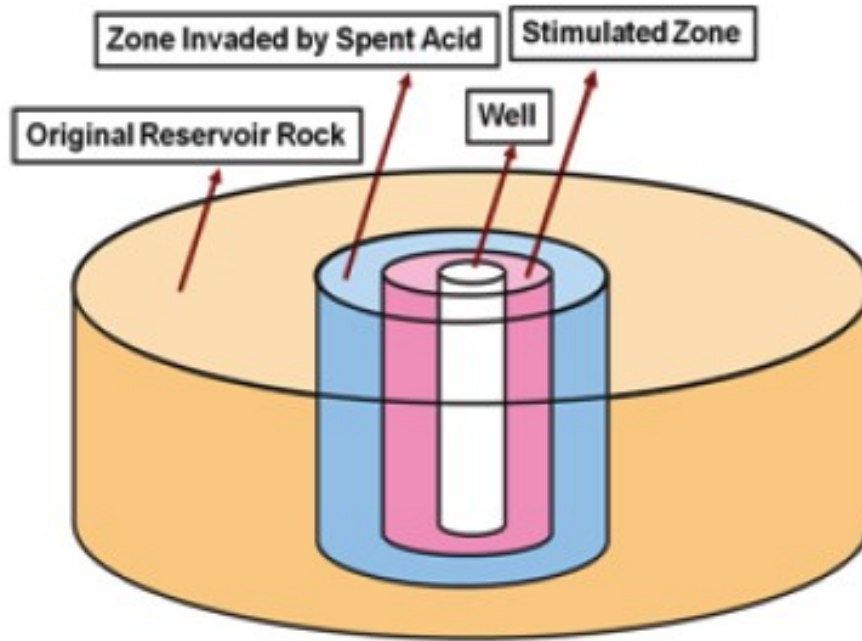


Figure 2.11 Zones affected by matrix acidizing due to spent acid invasion into the treated formation (From Saneifar et al. 2010).

A three-phase system can be found in matrix acidizing system including: rock surface, spent acid and hydrocarbon (gas or oil). The rock surface wettability is defined by the contact angle of the other phases. On a gas or oil wet rock surface, an angle that is larger than 90 degrees for a water droplet is created. While in a water wet rock surface, an angle that is less than 90 degrees for a water droplet is created, as seen in Figure 2.12.

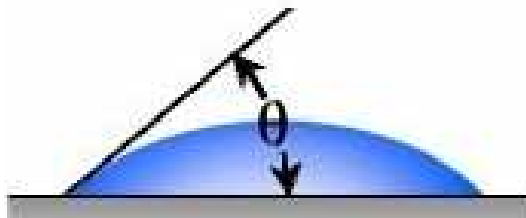


Figure 2.12 Wettability contact angle.

Due to capillary forces and wettability, the wetting phase tends to occupy smaller pores compared to the non-wetting phase. As a result, the wetting phase has lower relative permeability and mobility. Irreducible water saturation is a function of the previous parameters. Lowering the irreducible water saturation would give better mobility, and hence better spent acid recovery. An understanding and prediction of wettability status after the acid treatment is critical in order to avoid alteration that can lower hydrocarbon flow within pore channels.

CHAPTER 3

TESTING PROTOCOLS

This chapter explains the tests conducted to complete this dissertation. The main tests are detailed by test principle, apparatus, and methodology.

3.1 Solubility Test

This test was performed to assess lactic and gluconic acid reactions with calcium carbonate rock. Reaction products and dissolved ions determined the optimum ratio between lactic and gluconic acids.

3.1.1 Test Principle

The solubility test is run to evaluate an acidizing solution's dissolving capacity by measuring the tested material weight before and after the carbonate-acid reaction. A specific crushed core amount is mixed with an acid mixture inside a confined test vessel. Calcium ion concentrations are then monitored by analyzing several samples taken from the solution during the reaction process. Acid reaction with crushed calcium carbonate rocks diffuses calcium ions into solution. Calcium ions keep diffusing and increasing in solution throughout the acid reaction until reaching an equilibrium state. However, calcium ions can chelate with other ions within a solution, which reflects in a decrease of calcium ions in a concentration plot.

This test achieves the following purposes:

- Evaluating different acid ratios and concentrations;
- Determining acid dissolving solubility with different amounts of crushed calcium carbonate core plugs; and,

- Investigating potential calcium-based precipitation during acid- carbonate reaction.

3.1.2 Test Apparatus

Acid mixtures and crushed calcium carbonate core plugs were mixed in PARR 4760 Series general purpose vessels that can be pressurized up to 3,000 psi. The temperature was simulated through conduction using a Mtops heating mantle. A magnetic bar was used to keep the reaction under a dynamic state. Schematics and a photo of the test apparatus are shown in Figure 3.1.

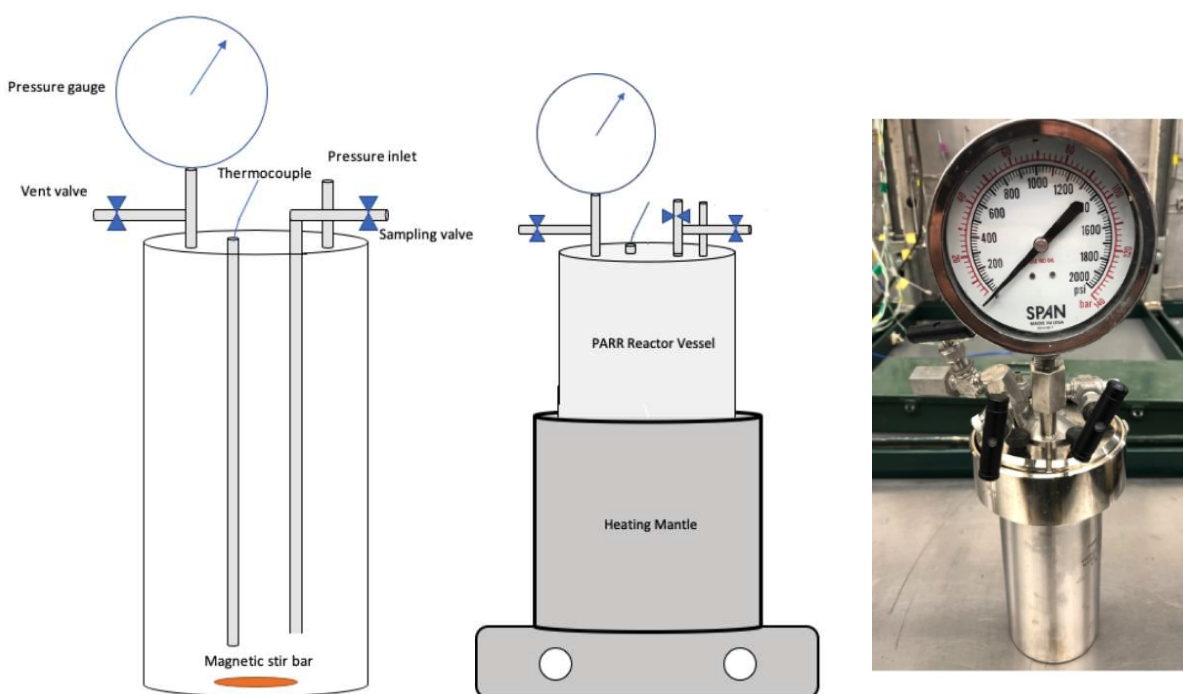


Figure 3.1 Schematics of solubility test apparatus. PARR 4760 test vessel schematic is shown on the left side, Mtops heating mantle schematic is shown in the middle, and a photo of the test vessel is shown on the right side.

3.1.3 Test Procedure

Pink desert limestone plugs of 1 inch diameter and 4 inch thickness were crushed and sieved. The fractions of the crushed plugs were collected over sieve trays with 20 to 100 mesh sizes. Fractions collected from the 100 mesh size sieve were used for the solubility test. The

crushed core amount for each test was calculated based on the number of moles of acid solution used to dissolve such amount. Pink desert limestone cores were tested by the supplier using Fourier Transform Infra-Red (FTIR), and the results showed 100% purity of calcium carbonate. For that, the impurity fraction was neglected in the crushed core amount calculation. Equation 3.1 shows how calcium carbonate crushed core amounts were calculated.

$$W_{CaCO_3} = M_{CaCO_3} \times n_{acid\ solution} \quad (3.1)$$

Where,

W_{CaCO_3} : Weight of crushed core used in the test, gram

M_{CaCO_3} : Crushed core molar mass, g/mole

$n_{acid\ solution}$: Number of moles within acid solution, moles

The acid solutions were prepared based on the molarity ratio between lactic and gluconic acids. The total number of moles was determined based on the acid mixtures solution volumes. Equation 3.2 shows how the acid volume was determined. Acid stock volumes were diluted using solution's additives (such as the paired acid or corrosion inhibitor), and the final solution volume was adjusted using deionized water.

$$V_{acid\ stock} = \frac{X_a V_f d_a}{X_s d_s} \quad (3.2)$$

Where,

$V_{acid\ stock}$: Volume amount taken from an acid stock, mL

X_a : Desired acid concentration, frac

V_f : Solution final volume, mL

d_a : Density of the acid at the desired concentration, g/mL

X_s : Acid stock initial concentration, frac

d_s : Acid stock density, g/mL

The test was started by preparing both the acid solution and the crushed core. Then, the acid solution would be placed in the test vessel and heated up to 100°F. The test vessel contained a magnetic stirrer that would make the test run under dynamic conditions. After that, the calculated amount of crushed core was put inside the test vessel, which was the start of the two hours test duration. The test vessel was locked carefully and was pressurized by N₂ up to 800 psi. CO₂ from the acid reaction and temperature would adjust the pressure to be around 1,000 to 1,200 psi. The magnetic stirrer was set to 500 rpm, and the test was run for two hours after placing the test vessel in the heating mantle. During the test, different solution samples were drawn using a sampling valve to analyze them using an ICP. Samples were filtered using a 0.45 micron syringe filter to separate any solids from the extracted sample solution.

Once the test was completed, the heating mantle was turned off, and the vessel was set to cool down. The spent acid solution was then filtered using a filtration kit with a 20 micron Whatman filter paper. Unreacted solids were weighed, and acid solubility was calculated as per Equation 3.3.

$$\text{Acid Solubility} = \frac{W_0 - W_1}{W_0} \times 100 \quad (3.3)$$

Where,

W_0 : Crushed core weight before test, gram

W_1 : Unreacted crushed core weight after test, gram

3.1.4 Calculation Example

The following calculations show an example of how an acid solution was prepared. The acid has a total strength of 14 wt%, which is the sum of 4.5 wt% of lactic acid and 9.5 wt% gluconic acid.

- Determining number of moles in solution is shown in Equation 3.4:

$$C_m = \frac{10 \times C_p \times d_a}{M_{acid}} = \frac{10 \times 4.5 \times 1.0086}{90.08} = 0.5 \text{ moles/mL} \quad (3.4)$$

Where,

C_m :	Molarity, mole/mL
C_p :	Acid concentration, frac
d_a :	Density of acid at the desired concentration, g/mL
M_{acid} :	Acid molar mass, g/mole

For 4.5 wt% lactic acid, molarity would equal 0.5 moles per milliliter, as shown in Equation 3.5:

$$C_{m_{lactic}} = \frac{10 \times 4.5 \times 1.009}{90.08} = 0.5 \text{ moles/mL} \quad (3.5)$$

For 9.5 wt% gluconic acid, molarity would equal 0.5 moles per milliliter, as shown in Equation 3.6:

$$C_{m_{gluconic}} = \frac{10 \times 9.5 \times 1.035}{196.16} = 0.5 \text{ moles/mL} \quad (3.6)$$

The number of moles was calculated based on solution volume. In this example, the final volume was set to 150 mL and the calculated number of moles was 0.15 moles, as per Equation 3.7:

$$n_{acid\ solution} = C_{m_{total}} \times \frac{V_f}{1000} = 1 \times \frac{150}{1000} = 0.150 \text{ moles} \quad (3.7)$$

- Determining crushed core amount.

Recalling Equation 3.1, 15.01 gram was needed to set a molarity ratio of 1:1 between the acid solution and crushed core, as calculated in Equation 3.8

$$W_{CaCO_3} = M_{CaCO_3} \times n_{acid\ solution} = 100.0869 \times 0.150 = 15.01 \text{ gram} \quad (3.8)$$

- Determining acid stock volumes to prepare 4.5 wt% lactic acid and 9.5 wt% gluconic acid.

From Equation 3.2, lactic and gluconic acids volumes taken from the stock solutions were calculated as shown in Equation 3.9 and 3.10. Volume of deionized water was calculated as shown in Equation 3.11:

$$V_{lactic\ acid\ stock} = \frac{4.5 \times 150 \times 1.009}{85 \times 1.209} = 6.62 \text{ mL} \quad (3.9)$$

$$V_{gluconic\ acid\ stock} = \frac{9.5 \times 150 \times 1.035}{50 \times 1.234} = 24.18 \text{ mL} \quad (3.10)$$

$$V_{deionized\ water} = 150 - 24.18 - 6.62 = 119.2 \text{ mL} \quad (3.11)$$

3.2 Solubility Test using Synthetic Seawater

This test was performed to evaluate the acid mixtures' performance when seawater was used instead of deionized water to prepare the acids. The principle, apparatus, and procedure were explained in the solubility test (Section 3.1). Seawater and scale inhibitor preparation are explained in this section.

3.2.1 Seawater Preparation

A synthetic seawater recipe was prepared based on the Arabian Gulf seawater composition, shown in Table 3.1. The sulfate ion concentration was changed between 4,000 ppm and 12,000

ppm to cover different seawater salinities. Salts used to prepare the seawater were provided by Sigma-Aldrich and used as received. Based on the Arabian Gulf seawater composition, different salts were mixed together to produce a synthetic seawater. The sodium sulfate salt loading was changed three times to manipulate the sulfate ion concentration. Three sulfate concentrations were tested, including 4,000, 6,000, and 12,000 ppm.

Table 3.1 Typical Composition for Arabian Gulf Seawater (Ahmed et al. 2017)

Ions	Concentration (ppm)
Sodium	18,300
Calcium	650
Magnesium	2,110
Sulfate	4,290
Chloride	32,200
Bicarbonate	120
TDS (total dissolved solids)	57,670

3.2.2 Scale Inhibitors Preparation

Three scale inhibitors were selected to keep the sulfate ion concentration as high as possible as a severe drop in this ion's concentration can lead to calcium sulfate precipitation. Scale inhibitors A and C are based on phosphonic acid, while scale inhibitor B is based on acrylic acid. 5 to 10 ppm was found to be the recommended loading range based on the industry usage of these inhibitors to prevent different scale deposition. These inhibitors were tested at the mentioned loading to eliminate calcium and sulfate complexing processes in acid solutions.

These scale inhibitors were purchased from Sigma-Aldrich and were handled based on their state. Scale inhibitors A and C were in the liquid state with a high concentration (more than 10,000 ppm). A specific amount was taken from the stock solution and was diluted using deionized

water to produce a new stock solution with 100 ppm. Then, 10 or 5 ppm concentrations of the scale inhibitor was delivered by adding a calculated amount from the new stock to the prepared acids' mixture solutions. Scale inhibitor B was in the solid state where a certain amount was dissolved in deionized water to follow the same procedure used for scale inhibitors A and C.

3.3 Corrosion Test

This test was performed to evaluate the corrosiveness of lactic and gluconic acids when mixed with an N-80 low carbon steel coupon. The test showed that an appropriate CI would eliminate corrosion risk from these organic acids.

3.3.1 Test Principle

Corrosion testing is an essential step to evaluate any new fluid for acidizing operations as it helps to identify the potential of corrosion toward well tubulars in terms of corrosion rate and pitting rating. Hydrogen ions from dissociated acids attack steel layers causing oxidation and reduction in the anodic and cathodic sites that result in losing steel material. Iron ions are also released and dissolved into solution, which can impose another type of formation damage risk through iron ions bonding with other ions. Such new complexes can have low solubility in water and become stable to precipitate immediately. This test is done in order to evaluate lactic and gluconic acid contributions toward steel corrosion and to investigate potential associated damage.

This test achieves the following purposes:

- Corrosion and pitting evaluation of different acid ratios and concentrations;
- Investigating the potential of iron-based precipitation in the case of high iron ions in solution; and,
- Determining the appropriate CI to eliminate acid corrosion.

3.3.2 Test Apparatus

N-80 low carbon steel coupons were used to mimic wellbore tubulars. The coupons are mainly iron by weight with some traces of manganese, sulfur, and phosphorus. It is important to identify the main elements in the tested steel coupons to track them from tested solution samples using the ICP test.

The PARR 4760 vessel was used as well for corrosion tests due to its ability to sustain acid corrosiveness and its ability to withstand test pressure. Schematics and a photo of the test apparatus are shown in Figure 3.1 with the magnetic stirrer replaced with a steel coupon. In the industry, corrosion tests usually run between 2 hours and up to 16 hours (Ng et al. 2018). For this research, a 4-hour test period was chosen in order to evaluate how corrosive the acids are. Then, the most corrosive acid solution was mixed with a CI and tested for 12 hours.

3.3.3 Test Procedure

The test was performed by placing the acid solution in the test vessel and heating it up to 100°F. Then, a tubular coupon, with known weight and surface area, was soaked in the center of the vessel to allow interaction between the acid and the coupon. It is important to apply an appropriate pressure to keep the solution in the liquid phase, so the vessel was pressurized up to 800 psi as the temperature would then adjust the pressure to be around 1,000 to 1,200 psi. The test vessel was then placed in the heating mantle, and the test was run for the necessary test period. During the test, different samples were drawn from the acid solution to track iron ions in solution, which would help to investigate acid corrosion levels and precipitation potential.

When the test was completed, the heating mantle was turned off, and the vessel was allowed to cool down. Then, the pressure was bled off, and the vessel was opened to extract the steel coupon. The steel coupon was washed with distilled water and left at room temperature for

drying. The weight was recorded, and the corrosion rate was calculated. Corrosion rate can be calculated using Equation 3.12 (Fann 2017):

$$\text{Corrosion rate in [lb/ft}^2\text{/test period]} = \frac{\text{weight loss in miligram}}{453,600} \times \frac{144}{\text{Area in in}^2} \quad (3.12)$$

The results were evaluated based on commonly used evaluation criteria in the industry. Smith et al. (1978) reported that there is no standard procedure or standard corrosion rates that can be followed to examine acid performance in terms of corrosion area. However, they reported that the most common acceptable ranges vary based on the reservoir temperature as acid becomes more aggressive when the temperature increases. Table 3.2 represents the acceptable ranges of corrosion rates followed in this research.

Table 3.2 Acceptable Ranges of Corrosion Rate Based on Temperature Ranges.

Temperature, °F	Corrosion Rate, lb/ft² /test period
To 200	0.02
201 to 250	0.05
251 to 275	0.075
276 and up	0.09

Another important evaluation in terms of corrosion is the pitting rating, which scales how the acid pits tubular coupons. Corrosion rates can be low enough to be acceptable but can be accompanied by a high level of pitting (Smith et al. 1978). The pitting rating has a scale from zero to nine and is rated by visual evaluation. The pitting scale definition is illustrated by Figure 3.2 that represents comparable tubular coupons that exhibited different pitting rates.

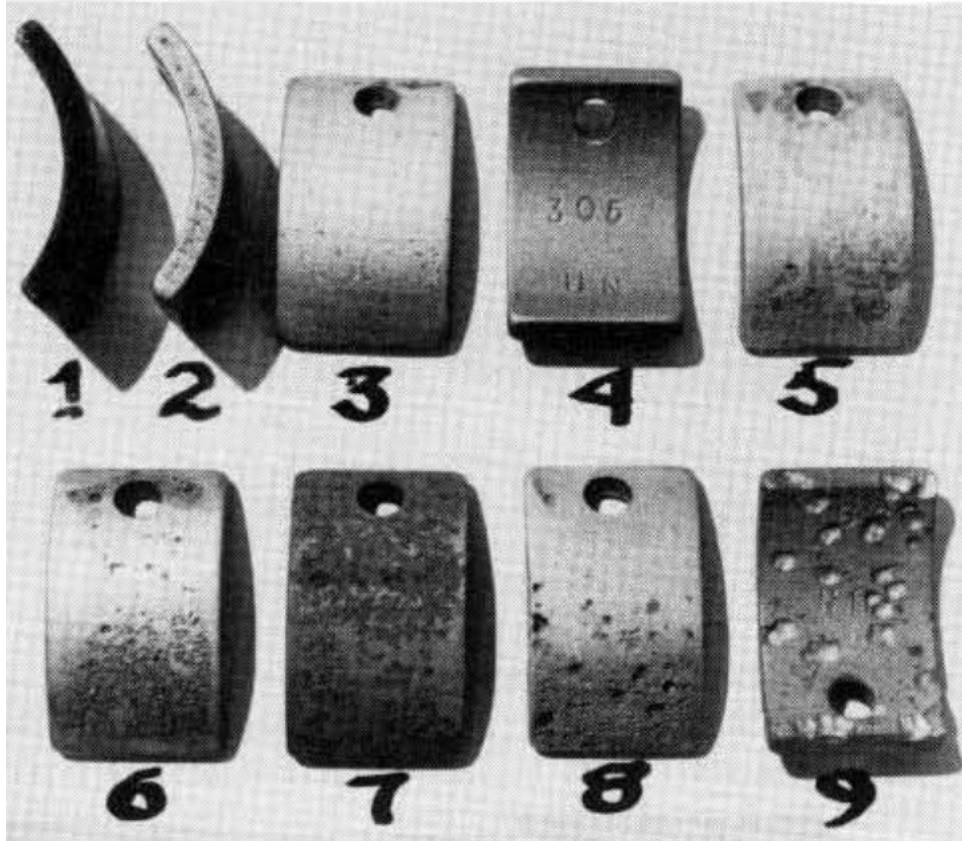


Figure 3.2 Comparable tubular coupons that exhibited different pitting rates caused by acid exposure (From Smith et al. 1978).

3.4 Wettability Test

Spent acid can go deep inside a treated formation to invade, which can alter the treated formation's relative permeability. This test was performed to investigate the spent acid alteration of carbonate rock wettability.

3.4.1 Test Principle

This test was performed by evaluating spent acid effects on carbonate core wettability through the use of zeta potential. Zeta potential is the electrical potential developed at the shear plane at a solid-liquid interface. It is a result of the relative movement of fine particles and water. Hunter (1981) mentioned that particles and surface behavior in a solution could be understood by

zeta potential measurements under liquid flow. The change in rock surface charge and rock wettability can be qualitatively measured using zeta potential.

A high zeta potential value is usually expected in high salinity formation water, which makes the rock more oil wetting. Mahani et al. (2015) investigated the zeta potential values of different carbonate rocks by changing different parameters. Their study showed that zeta potential value decreased when brine salinity was decreased to seawater level. Also, they found a high dependency between solution pH and zeta potential, which showed that low pH solutions tend to have fewer surface charges.

3.4.2 Test Apparatus

The test was run using a Zetasizer Nano series, as it measures electrophoretic mobility of carbonate particles dispersed in a brine of different spent acid solutions. The instrument uses the Smoluchowski approximation of Henry's equation to measure the electrophoretic mobility that is utilized to calculate the zeta potential (Hunter 1981). A photo of the test apparatus is shown in Figure 3.3.

3.4.3 Test Procedure

Four base solutions were prepared without any acid where three of them contained seawater with different sulfate concentrations, and one contained deionized water. Then, a 14 wt% and a 27 wt% of lactic and gluconic acid mixtures at 1:1 molar ratio served as the control solutions. The other solutions varied based on corrosion inhibitor and scale inhibitor loadings. A total of 12 tests were performed by taking three measurements for each test. The average zeta potential of the three measurements was taken and evaluated.

Solutions with acids were neutralized using calcium carbonate until there were no more reactions, and the solution's pH became neutral. Then, tested solutions were prepared for the test by suspending 0.1 grams of crushed carbonate core in a 10-gram solution. Later, each solution was shaken three minutes. After 6 hours and ten days of aging and shaking, the zeta potential measurements were done and reported.



Figure 3.3 A photo of the Zetasizer Nano series used to measure the Zeta potential.

3.5 Coreflooding Test

Coreflood tests were used to mimic in-situ conditions that can be faced with any acidizing operation. Different results were obtained from this test that was a main feature of this research's outcomes.

3.5.1 Test Principle

Coreflood testing was the simulator of the acidizing treatments in this research. It delivered a representable evaluation of lactic and gluconic acid mixtures used to stimulate Indiana limestone

cores. One of the main disadvantages of HCl in high temperature applications is the poor dissolution pattern, which can be overcome by exceeding the fracturing pressure. The injection rate is the main factor in this issue, which can be easily manipulated through coreflood testing.

The differential pressure across the tested core was measured through two pressure transducers that were placed on the inlet and outlet lines. Permeability measurements were performed based on Darcy's equation that is suitable for laminar, linear, and steady-state flow of Newtonian fluids. Equation 3.13 shows Darcy's equation.

$$k = \frac{245 \times L \times q_i \times \mu}{\Delta P \times A} \quad (3.13)$$

Where,

k :	Calculated permeability, md
L :	Core length, cm
q_i :	Injection rate, cm ³ /min
μ :	Injected fluid viscosity, cp
ΔP :	Differential pressure across the tested core, psi
A :	Core area, cm ²

This test achieves the following purposes:

- Evaluating different acid strengths when stimulating carbonate cores;
- Investigating the potential of calcium-based precipitation on the tested cores inlet and outlet faces;
- Identifying the effect of temperature, acids concentrations, and injection rates on the pore volumes required to breakthrough the tested core; and,

- Evaluating the dissolution pattern and the generated wormholes due to the injection of acid solutions.

3.5.2 Test Apparatus

A Chandler 6100 formation response tester (FRT) was used to conduct coreflood tests due to its ability to measure the permeability changes across the core when exposed to different fluids. Nitrogen gas was injected by a pressure regulator to apply a back pressure of 500 psi on the core holder chamber. Pumped oil was used to apply an overburden pressure of 1,500 psi on the core sleeve. The pressure drops were recorded through computer connected transducers that can accurately measure the pressure as a function of time across the tested cores. The temperature was simulated by a built-in electric jacket that covers the core holder and acid accumulator. Figure 3.4 shows a schematic of the coreflood.

3.5.3 Test Procedure

The first step to conduct a coreflood test was preparing the acid solution and the tested core. The acid solution was prepared based on mixing specific volumes of lactic and gluconic acids to reach the required total acid concentration. The tested core was vacuumed in a container filled with a 5 wt% KCl brine that has a known density. The weight difference before and after brine saturation was recorded, which was then used to calculate the core pore volume and porosity. Equations 3.14 and 3.15 show how the pore volume and porosity were calculated.

$$PV = \frac{\text{Mass difference (g)}}{d_{5 \text{ wt\% KCL}}} \quad (3.14)$$

$$\phi = \frac{PV}{V} \quad (3.15)$$

Where,

PV :	Core pore volume, cm^3
$d_{5 \text{ wt\% KCL}}$:	Density of 5 wt% KCl brine, g/ cm^3
ϕ :	Core porosity, frac
V :	Core volume, cm^3

The second step was loading the core to be tested in the core holder and the subject solution in the accumulator. Then, a confining pressure of 1,500 psi was applied on the core sleeve, and the nitrogen gas regulator was turned on to increase the backpressure to 500 psi. Once these pressures were applied, the heating jackets were turned on to increase the temperature up to the required level.

The third step was scheduling and pumping the fluids, which included 5 wt% KCl brine and the acid mixture solution. Pumping was started by closing all fluid lines except the pumped fluid source, inlet, and outlet lines. This was done to keep the pumped fluid going through only the tested core. 5 wt% KCl was first pumped until a stabilized pressure difference was reached between the inlet and the outlet pressures. This injection served as the preflush step that provided the initial core permeability.

The acid solution was then pumped by closing the KCl brine source valve and opening the accumulator valve. Acid introduction to the core increased the inlet pressure due to the high viscosity of the mixture and due to the reaction with the core. The acid solution was pumped until reaching a breakthrough or until pumping a large amount of the mixture. A breakthrough can be easily recognized by a sharp drop in the differential pressure due to wormhole generation inside the tested core.

A 5 wt% KCl brine was injected again after the acid solution to compare the initial core permeability with the stimulated core permeability. Three to four pore volumes of brines were injected before the test was stopped.

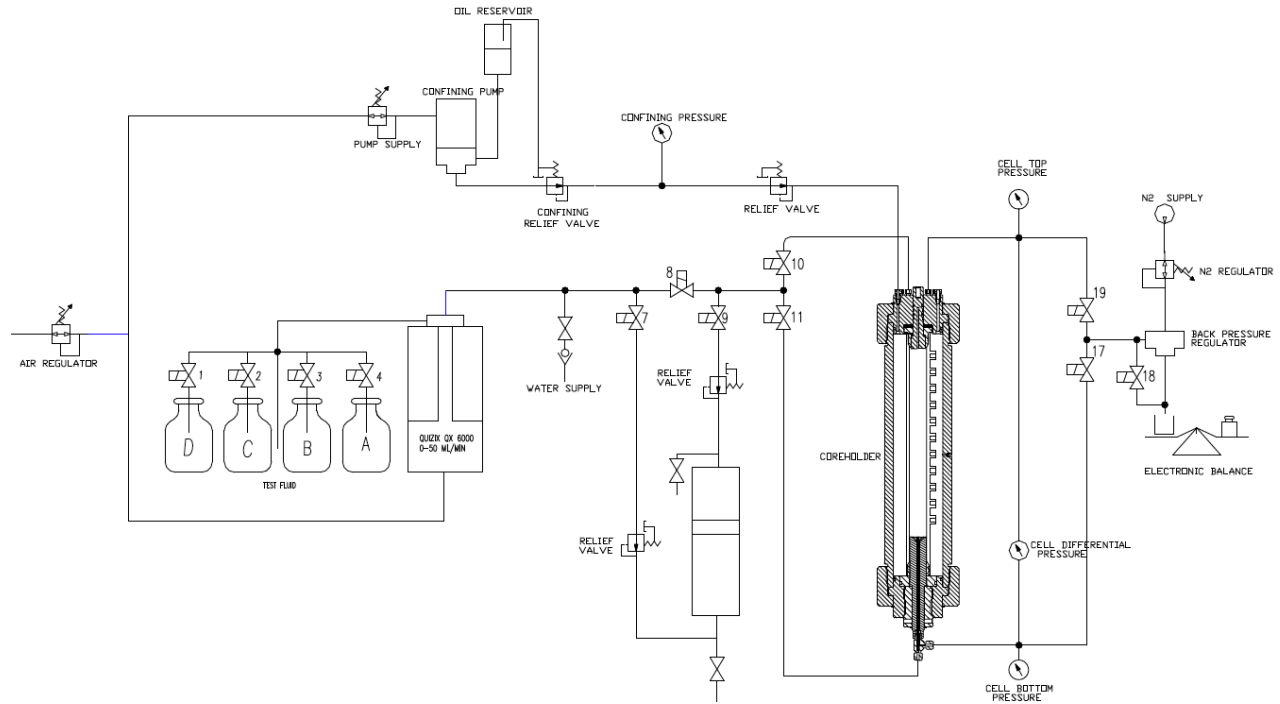


Figure 3.4 A schematic of the Chandler 6100 FRT.

3.6 Experimental Repeatability and Reproducibility

The previous experiments were set up and prepared using equipment and analytical testing that are available in most research labs. Results' reproducibility is highly anticipated if the two-acid mixture is evaluated again in other research. However, slight variations in solubility and corrosion testing results are expected.

In this research, results' repeatability was confirmed in solubility and wettability tests to ensure a high level of accuracy of the generated data. The solubility test contained different runs that were associated with specific acid concentrations and test temperatures. Each run was repeated

between two and three times, and showed a low variation in solubility percentage. The quality of the ICP and IC results were also considered to ensure proper calcium and sulfate ion measurements. Calcium and sulfate ion measurements are strong indications of any calcium-based and sulfate-based precipitations. Based on this, the used ICP and IC machines were calibrated with calibration fluids between every five to ten samples to avoid contamination that can reduce accuracy.

The wettability test was performed by zeta potential measurement that is a highly sensitive procedure. Repeatability of the test was done by taking three runs for each sample and reporting the average value. However, the reproducibility of the test can have moderate variations. The process of shaking each sample for some time every day before taking the measurement can induce the mentioned variation. Nevertheless, the change in zeta potential values between each sample was easily reproducible.

Corrosion testing runs were performed one time for each case as the main objective was to show the corrosivity of the acids and the effectiveness of utilizing a corrosion inhibitor. Coreflood tests were also run one time for each case. The results were compared with previously published results for other organic acids and showed similar pressure profile behavior.

CHAPTER 4

SOLUBILITY TEST: RESULTS AND DISCUSSION

This chapter discusses and evaluates the performance of different LA:GA acid mixtures based on the dissolving capacity of crushed Pink Desert limestone cores and associated reaction product precipitations. Preparing the LA:GA acid mixtures with synthetic seawater was also investigated and is discussed in this chapter. Calcium and sulfate binding was found to be a significant problem in utilizing seawater with rich sulfate ions levels.

4.1 Solubility Test of Acids Prepared Using Deionized Water

Lactic and gluconic acids were prepared and diluted using deionized water. Deionized water was used instead of tap water due to the need for mixing the acid mixtures with calcium carbonate without any ion contamination. The acid mixture solubilities were investigated based on changing lactic and gluconic acid molar ratio, total acid mixture concentration, test temperature, and crushed core amount. Along with calculating the solubility ratio, calcium ions concentration in solution was analyzed using the ICP to track any crystal deposition from calcium and lactate complexing.

4.1.1 Lactic Acid Reaction With Calcium Carbonate

Lactic acid was first tested with a crushed core of Pink Desert limestone rock to illustrate the deposition of calcium lactate precipitation. Deposited solids from the acid reaction were collected and analyzed using the XRD to confirm their composition and identity. Along with this, different samples were drawn from the reaction solution to track calcium ion concentrations in solution.

A 12 wt% (1.4 M) lactic acid solution was prepared and tested with crushed core for two hours at 70°F and 1,000 psi. The amount of the crushed core was set to be in an equimolar ratio with the total acid strength. Different samples were taken during the reaction and were placed in sampling tubes. These samples were left at room condition for 24 hours to give enough time for the existed ions to reach chemical equilibrium. Figure 4.1 shows the sampling tubes after 24 hours of conducting the test. As can be seen, white precipitations appeared in all sampling tubes, which were filtered and collected for further analysis.

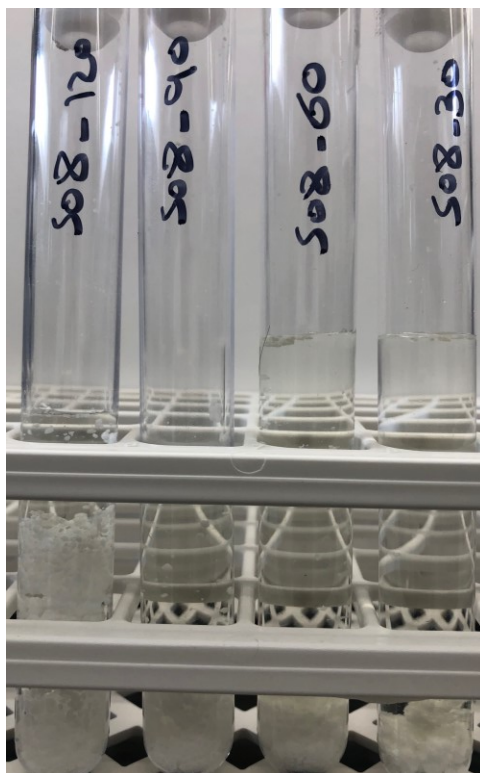


Figure 4.1 Sampling tubes from 12 wt% lactic acid reaction with crushed core at 70°F and 1,000 psi. White precipitation started to appear before 24 hours of conducting the test.

Calcium ion concentrations were analyzed using the ICP test, and the results were plotted versus time as shown in Figure 4.2. Due to the nature of the reaction and the high temperature condition, the acid was able to diffuse a high amount of calcium ions in the first few minutes of

conducting the test. However, as hydrogen ions were dissociated with more time from the lactic acid solution, lactate ions were dissociated as well. After a few minutes of starting the test, a large amount of lactate and calcium ions were above the saturation and solubility limit, which caused calcium lactate precipitation. The deposition of calcium lactate precipitation can be identified with a drop of calcium ion concentrations during the test duration that is shown in Figure 4.2.

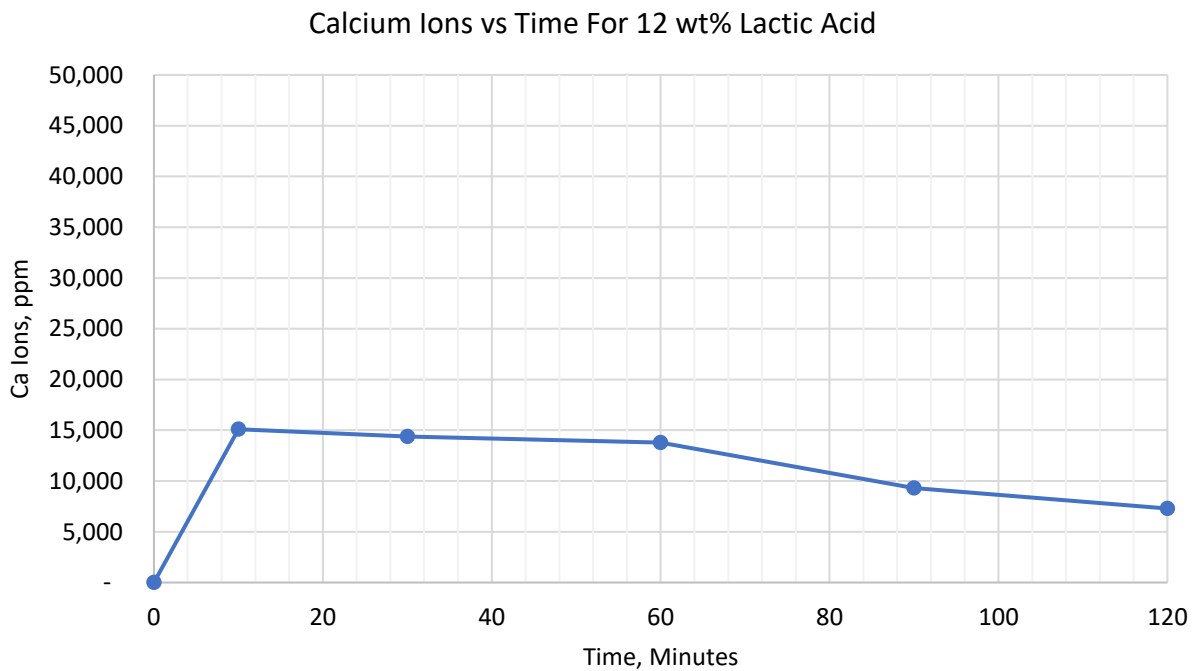


Figure 4.2 Calcium ion concentrations versus time for the reaction of 12 wt% lactic acid with crushed core at 70°F and 1,000 psi.

Nasr-El-Din et al. (2007) evaluated solids that release 10 wt% of lactic and concluded that the acid would deliver excellent results in terms of etching and dissolving of calcite and carbonate rocks. Based on this, lactic acid concentration was reduced and tested at 9 wt% (1 M) instead of 12 wt% (1.4 M) to investigate calcium lactate precipitation tendency at this strength. The two-hour test at 70°F and 1,000 psi showed that calcium lactate precipitation would precipitate even at this

strength when it was reacted with an equimolar ratio of the crushed core, as can be seen in Figure 4.3.

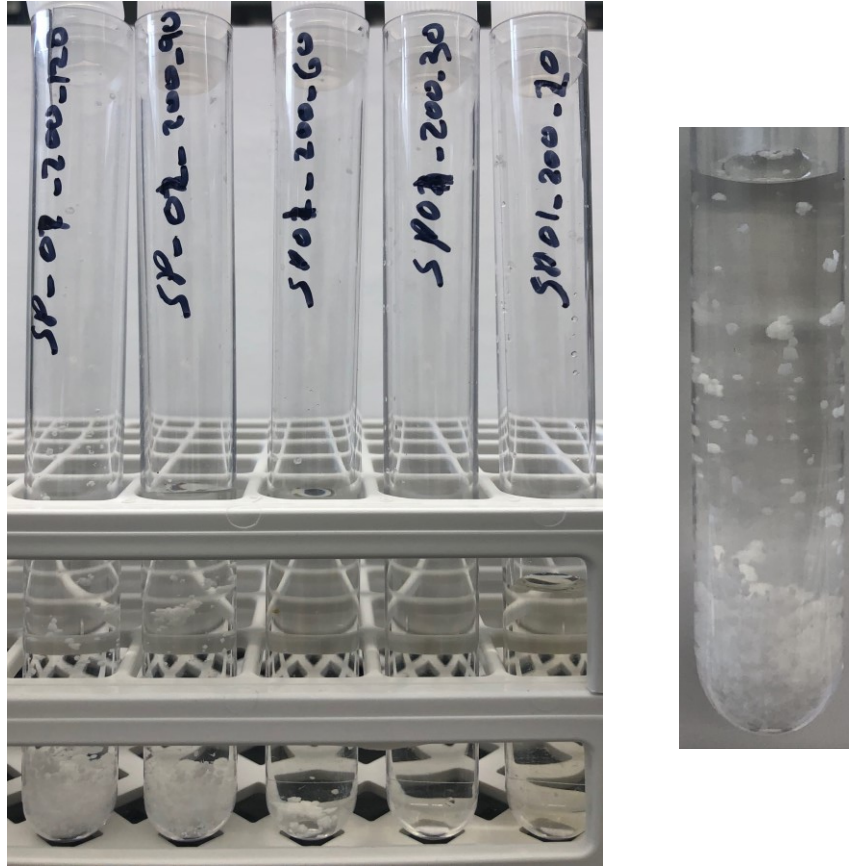


Figure 4.3 Sampling tubes from 9 wt% lactic acid reaction with crushed core at 70°F and 1,000 psi. White precipitation started to appear before 24 hours of conducting the test.

The ICP analysis also showed that calcium ion concentrations dropped after 30 minutes of running the test, as is shown in Figure 4.4. However, the ICP results showed that calcium ion levels in the 9 wt% lactic acid case was more than the 12 wt% case during the whole two-hour test period. The increase in calcium ion level was attributed to the difference in the dissociated lactate ions amount between the 9 wt% and 12 wt% solutions. At the 9 wt% solution, fewer lactate ions were available for calcium ions to complex with, which was reflected in an increase in the free calcium ion concentrations.

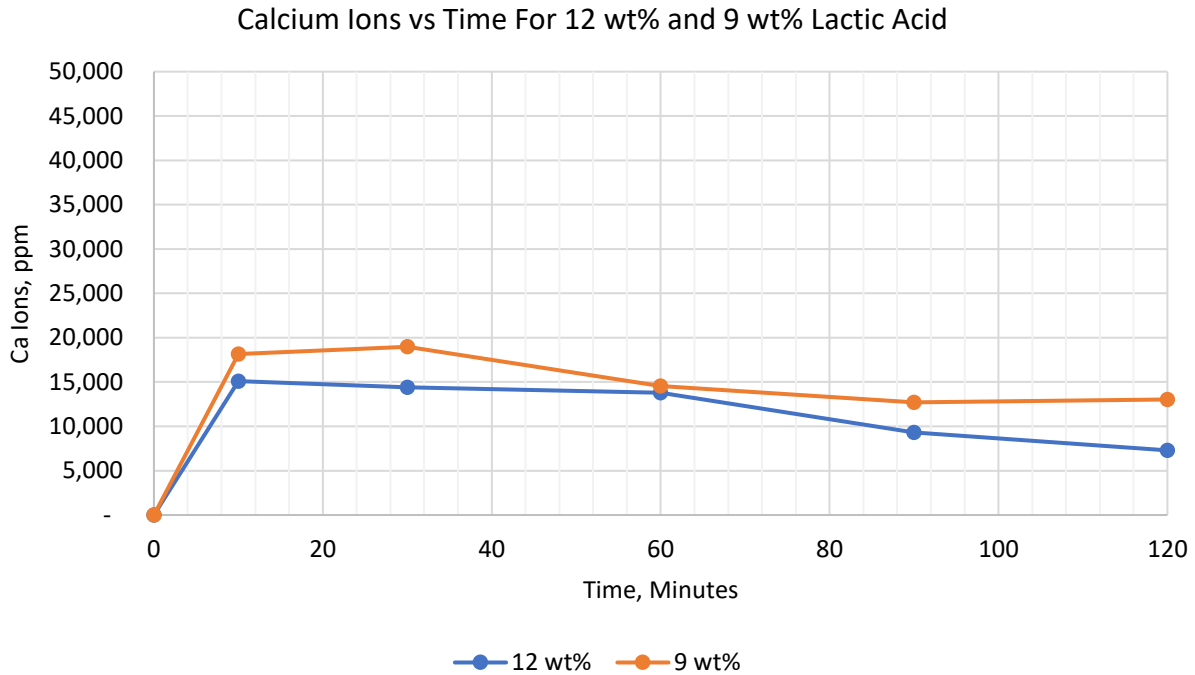


Figure 4.4 Calcium ion concentrations versus time for the reaction of 9 wt% and 12 wt% lactic acid with crushed core at 70°F and 1,000 psi.

Precipitated solids were collected and analyzed using the XRD test to validate calcium lactate precipitation. Figure 4.5 shows the XRD spectrum of the collected solids that confirmed calcium lactate precipitation. Calcium lactate ($\text{Ca}(\text{CH}_3\text{CHOHCOO})_2 \cdot 2.5\text{H}_2\text{O}$) is distinguishable with three peaks at diffraction angles (2θ) of 7.5, 9.5, and 14.5. The resulting spectrum nearly matched the spectrums reported by Tansam et al. (2014) and Rabie et al. (2015).

Kubantseva and Hartel (2002) reported the solubility of calcium lactate to be around 3.38 gram/100 grams in water at 4°C, which gives 0.62 grams of calcium and 2.76 g of lactate. Exceeding these values lets calcium and lactate ions move to nucleation sites to form calcium lactate precipitation due to a thermodynamic driving force. Nevertheless, calcium lactate interaction needs several days to reach equilibrium (Kubantseva and Hartel 2002).

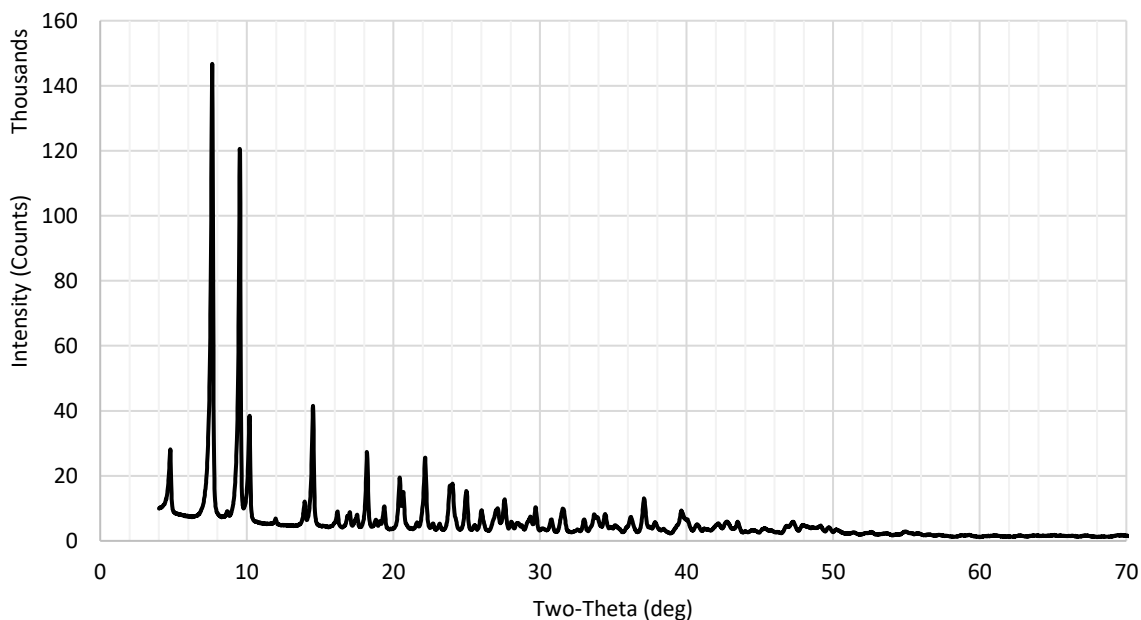


Figure 4.5 XRD spectrum of the collected solids that confirmed calcium lactate precipitation.

Based on these results, lactic acid should not be used as an acidizing fluid at high initial concentration by itself. Calcium lactate is the main drawback of dissolving calcium carbonate using lactic acid as lactate ions are high enough to complex with calcium ions. Therefore, an enhancement is needed to prompt lactic acid use in acidizing operations by manipulating calcium lactate precipitation tendencies.

4.1.2 Lactic and Gluconic Acids Reaction With Calcium Carbonate

Gluconate ions were added to the mixture solution by mixing gluconic acid with lactic acid using deionized water. Gluconic acid dissociates in water and produces hydrogen ions and gluconate ions, which can also add extra dissolution strength due to hydrogen ion attacks on calcium carbonate. Gluconic acid was mixed with lactic acid in a 1:1 molar ratio, where 4.5 wt% (0.5 M) of lactic acid was mixed with 9.5 wt% (0.5 M) of gluconic acid. The change of the strength in the weight percentage between the two acids was due to the difference in the molecular weights

between them. The amount of the crushed core was set to be in an equimolar ratio with the total acid strength.

The new mixture was tested for two hours at 70°F and 1,000 psi, where a solubility of 50% was achieved. The two-acid LA:GA mixture did not show any precipitation in the sampling tubes and did not show any drop in calcium ions concentration, as can be seen in Figures 4.6 and 4.7, respectively. Rabie et al. (2014; 2015) reported that the lactic acid calcite dissolution rate was slightly higher than the gluconic acid dissolution rate. This observation was also noticeable in this research, as can be seen in Figure 4.7 where both acids had the same molarity, but 9 wt% of lactic acid dissolved more calcium ions than 14 wt% mixture in the first 30 minutes before the precipitation of calcium lactate.

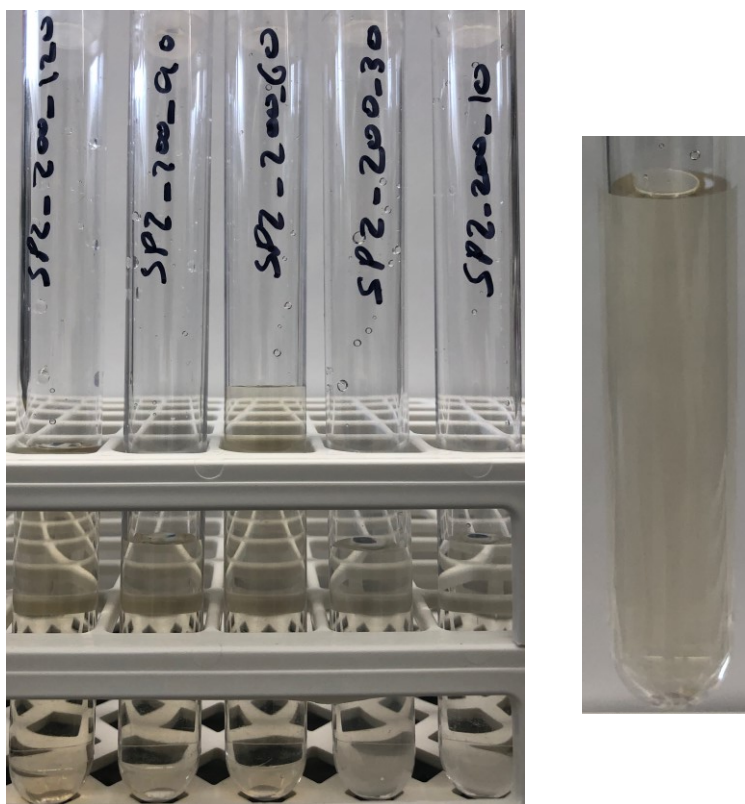


Figure 4.6 Sampling tubes from 14 wt% of (1:1) lactic and gluconic acid reactions with crushed core at 70°F and 1,000 psi.

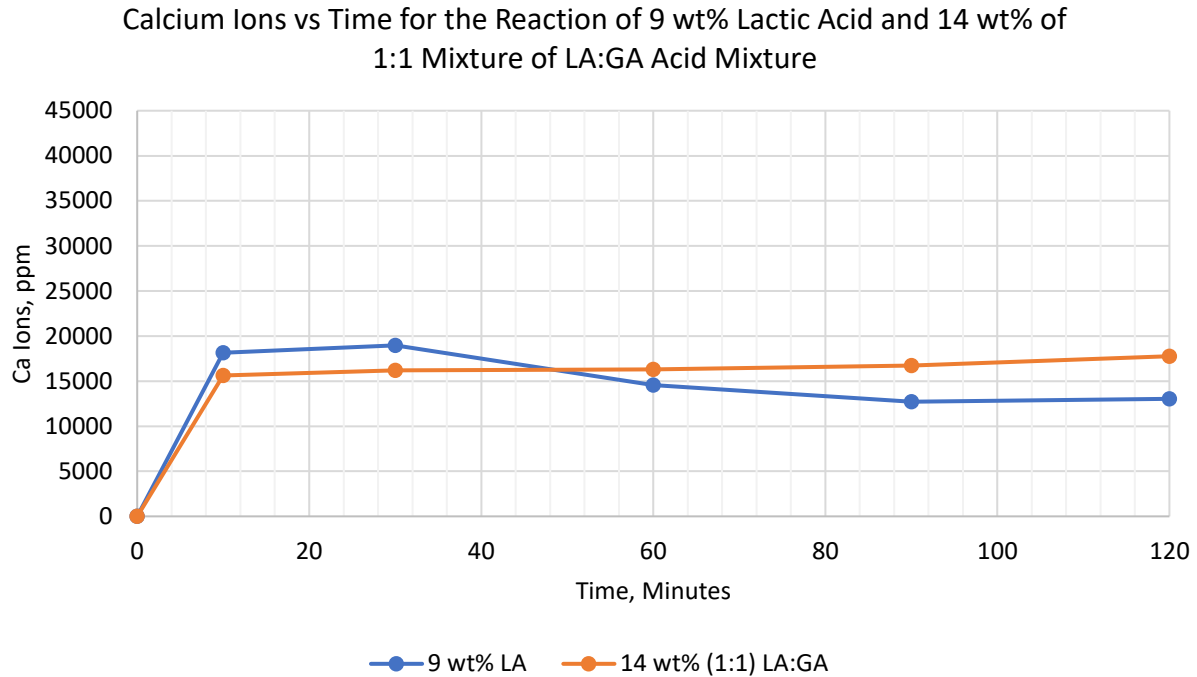


Figure 4.7 Calcium ion concentrations versus time for the reaction of 9 wt% lactic acid and 14 wt% (1:1) of lactic and gluconic acids with crushed core at 70°F and 1,000 psi.

Gluconate ions tend to bond with calcium ions through the hydroxy carboxylate group that is in the gluconic acid chemical structure. According to Phadungath and Metzger (2011), calcium ions and carboxylate groups interact through alpha mode interaction behavior. This happens by bonding a calcium ion with an oxygen atom from water molecules and oxygen atoms from the carboxyl and the hydroxyl groups. This process of interaction and bonding can produce calcium lactate gluconate complex instead of calcium lactate complex, with the first being more soluble in water.

Since lactic acid has a higher dissolution rate than gluconic acid, the molarity ratio between the two acids was investigated at 2:1 and 3:1 of lactic and gluconic acids ratio with a total acid strength of 1 M at 200°F and 1,000 psi. These ratios would add more moles of lactic acid in solution to increase the acid dissolution rate. When tested with crushed calcite, calcium lactate precipitation

was noticeable after a few days, as can be seen in Figure 4.8. A 1:1 molar ratio was the optimum ratio between lactic and gluconic acids due to its capability of providing calcium lactate solids free of spent acid solution and due to its capability of providing a higher solubility ratio than the other two molar ratios. The solubilities of the three ratios are given in Figure 4.9.

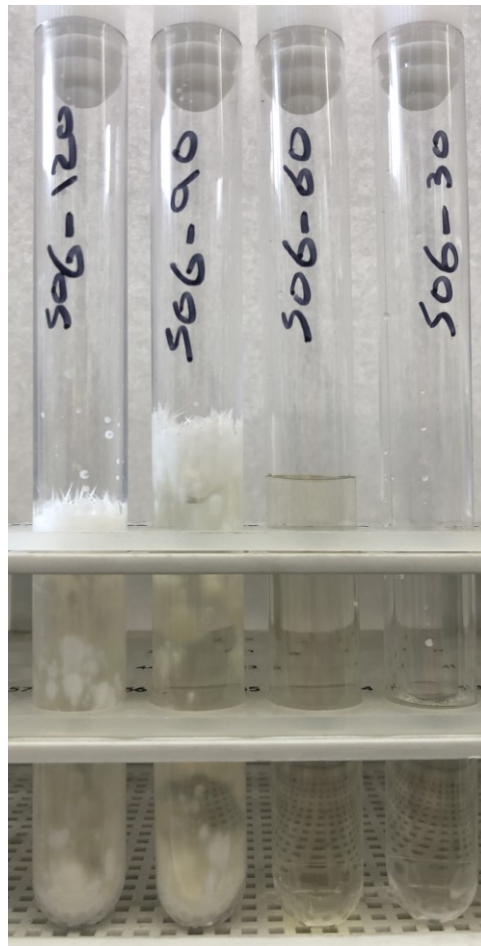


Figure 4.8 Sampling tubes from 1 M (2:1) of lactic and gluconic acid reactions with crushed core at 200°F and 1,000 psi. Calcium lactate precipitation can be seen deposited after a few days of conducting the test.

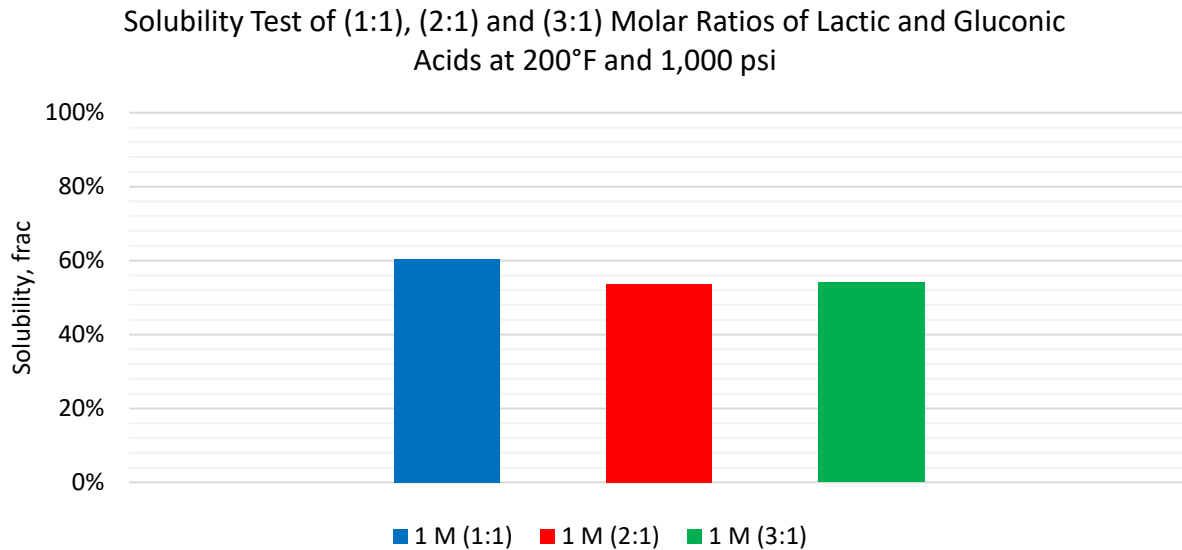


Figure 4.9 Solubility tests of (1:1), (2:1) and (3:1) molar ratios of lactic and gluconic acids with a total acid strength of 1 M at 200°F and 1,000 psi.

4.1.3 Total Acid Concentration and Temperature Effects on the LA:GA Acid Mixture Dissolving Capacity

The total LA:GA acid mixture concentration was also manipulated to investigate its effect on dissolving calcium carbonate. This step was needed to make sure no precipitation would occur when the acid solution was saturated with lactate and gluconate ions along with calcium ions. The results showed that the acid dissolving capacity would increase as the mixture concentration was increased. Along with that, no precipitation was observed even when the concentration was increased to 27 wt%. Figure 4.10 shows the solubility results of 10 (0.7 M), 14 (1 M), 20 (1.5 M), and 27 (2 M) wt% of (1:1) LA:GA acid mixtures at room conditions with constant amounts of crushed core.

The effect of temperature was also studied as it was expected to increase calcite solubility since the mixture dissolution rate would increase with temperature. Increasing the temperature would enhance ion mobility in solution that would be reflected in increases in calcium ion diffusion

rates and acid diffusivities. For example, the lactic acid diffusion coefficient at 80°F is 8.29×10^{-6} cm^2/s while it is 4.11×10^{-5} cm^2/s at 250°F, which indicates a faster flux of the acid passes through each unit of cross-section per unit of time from one region to another one.

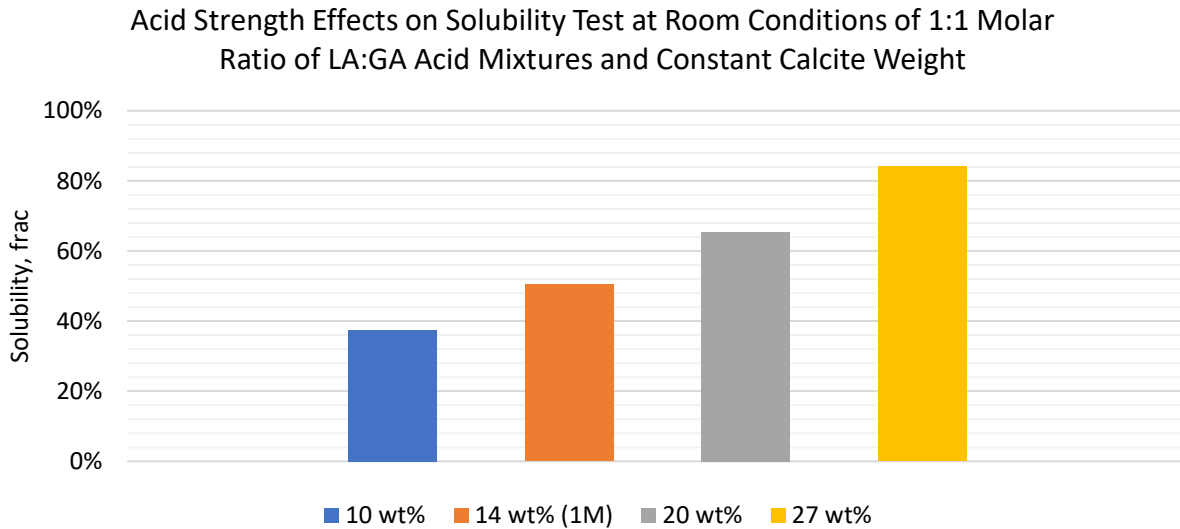


Figure 4.10 Solubility tests of different total acid strength of (1:1) lactic and gluconic acids at room conditions.

As was expected, increasing the temperature from 70 to 200 and 300°F increased the calcite solubility significantly when 27 wt% of 1:1 acid ratio was used. The calcium ion concentration plots are shown in Figure 4.11. Calcite solubilities, shown in Figure 4.12, were increased from 84% at 70°F to 94% and 99% at 200 and 300°F, respectively. The results from increasing the test temperature confirm the mixture applicability for acidizing high temperature formations.

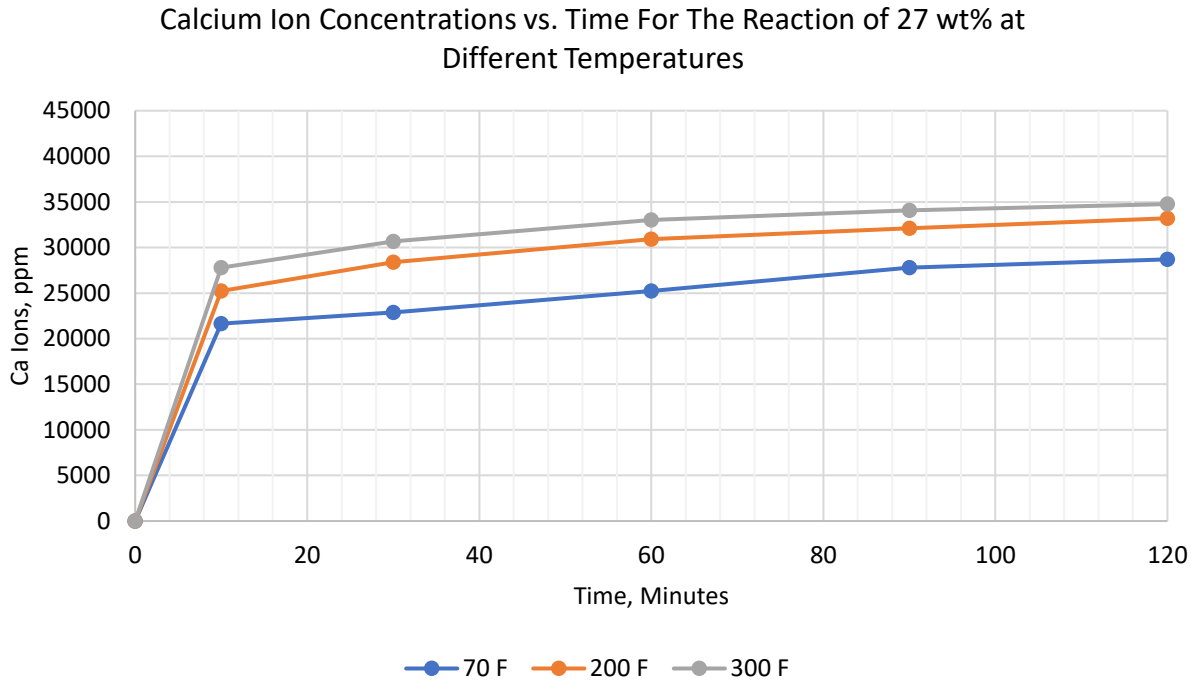


Figure 4.11 Calcium ion concentrations versus time for the reaction of 27 wt% of (1:1) lactic and gluconic acids with crushed core at 70, 200, and 300°F and 1,000 psi.

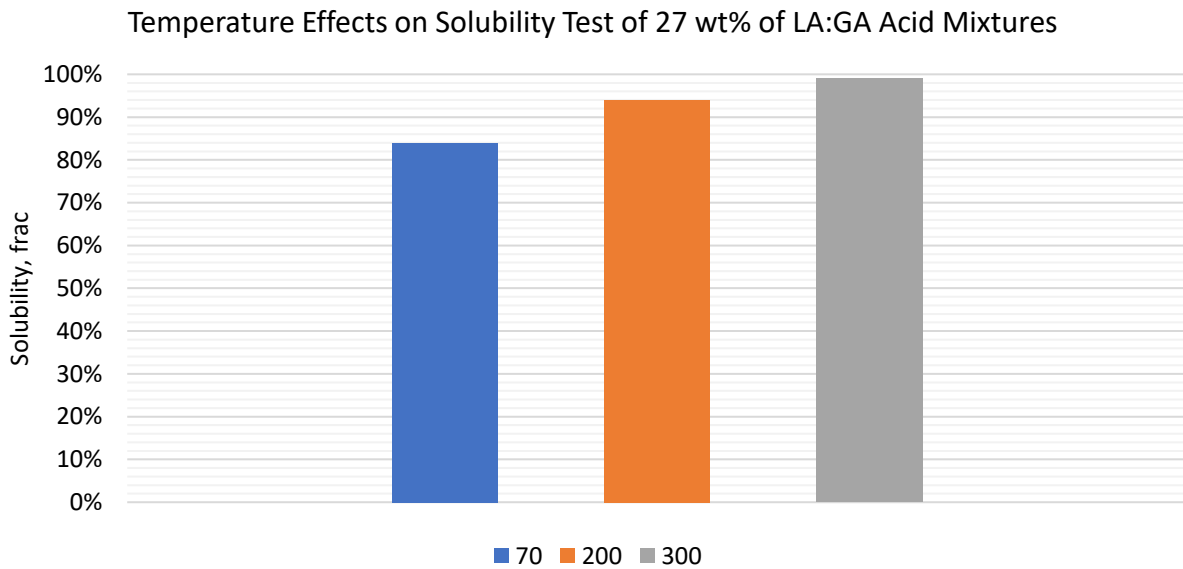


Figure 4.12 Solubility test of 27 wt% (1:1) lactic and gluconic acids at different temperatures using 1,000 psi of nitrogen pressure.

4.1.4 Crushed Core Amount Effects on the Acid Mixture Dissolving Capacity

In the previous tests, the molar ratio between calcium carbonate (crushed core) and total acid molarity was 1 to 1, except for the total acid strength test where the crushed core amount was fixed. In this section, the molar ratio was changed to 2:1 where the molarity of calcium carbonate was doubled to investigate the two-acid LA:GA mixture's ability to dissolve and etch a large amount of carbonate formation with minimum acid volume. Also, this test was performed to investigate calcium lactate tendency of precipitation when an excess amount of calcium ions are in solution.

Two LA:GA acid mixture solutions were tested - 27 wt% (2 M) and 33 wt% (2.5 M) of (1:1) lactic and gluconic acids. Low total acid concentrations were not tested due to the need for a high amount of dissociated hydrogen ions to dissolve the crushed core. Figure 4.13 shows the solubility results of the two-acid LA:GA mixtures were tested at 200°F and 1,000 psi. Calcium ions in solution are shown in Figure 4.14. The results illustrated that the two-acid LA:GA mixtures could dissolve at least 60% of the crushed core without any risk from calcium lactate precipitation.

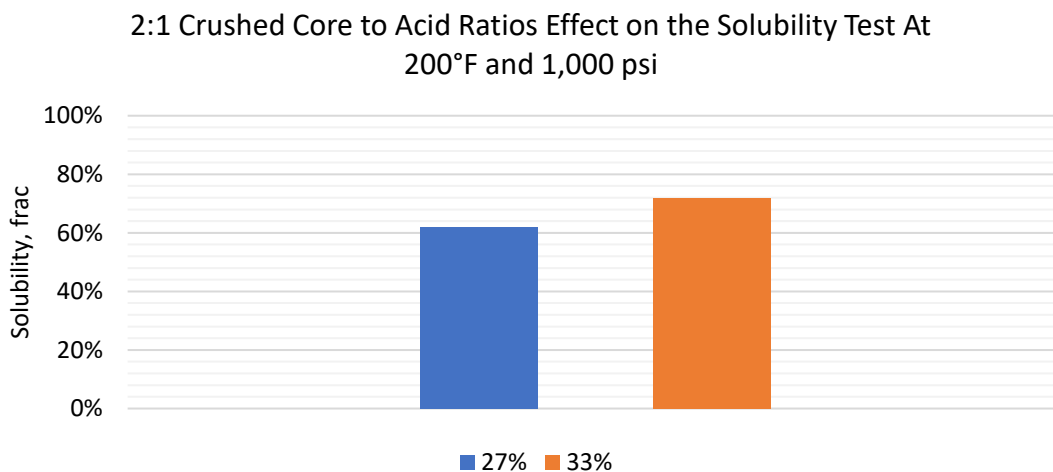


Figure 4.13 Solubility test of 27 wt% and 33 wt% using 2:1 crushed core-to-acid molarity ratio at 200°F and 1,000 psi.

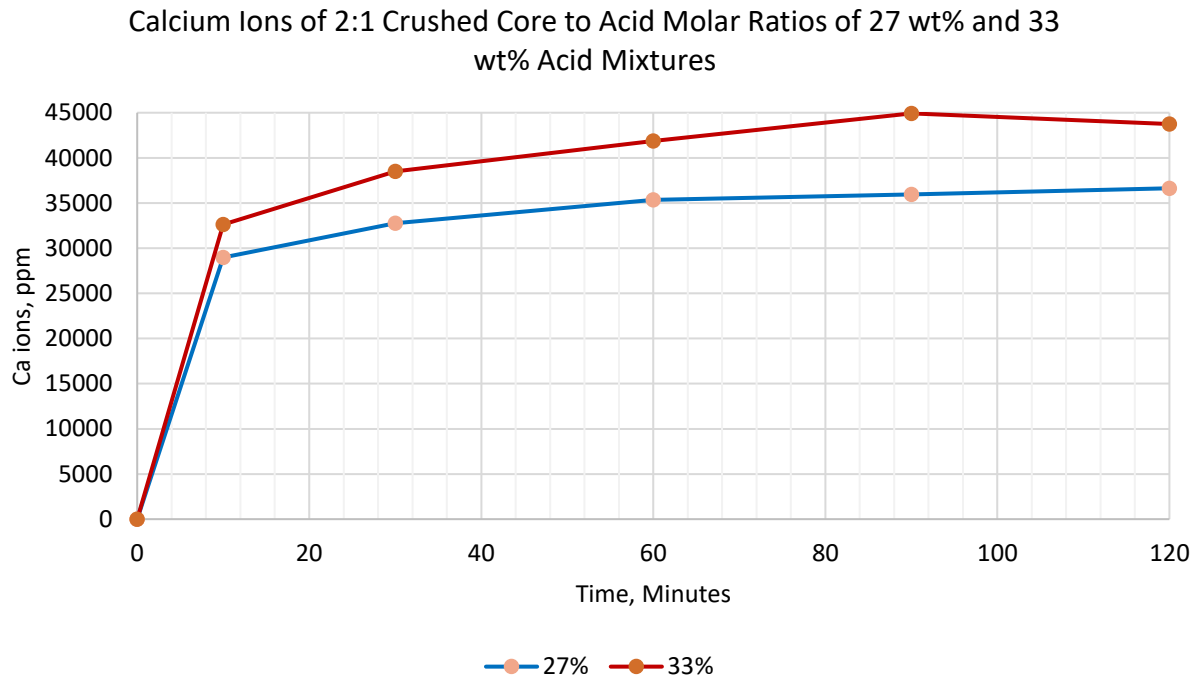


Figure 4.14 Calcium ion concentrations versus time for the reaction of 27 wt% and 33 wt% 2:1 crushed core-to-acid molarity ratio at 200°F and 1,000 psi.

4.2 Solubility Test of Acids Prepared Using Synthetic Seawater

Lactic and gluconic acids were prepared and diluted using synthetic seawater. Synthetic seawater was prepared and used to prepare 14, 20, and 27 wt% mixtures of lactic and gluconic acids. In the presence of sulfate ions, calcium sulfate precipitation can occur due to the combination of calcium ions and sulfate ions. This scale has a very low solubility in water that tends to decrease even more when the acid is spent, which can cause formation damage within formation pores and flow channels. Moreover, this precipitation can compromise the matrix acidizing treatment as calcium sulfate may act as a blockage between a carbonate formation and the treating acid.

4.2.1 Dissolving Capacity of Acid Mixtures Prepared by Seawater

Solubility tests were conducted using acids prepared with synthetic seawater that contained 4,000 ppm of sulfate at room conditions using a 1:1 molar ratio between the crushed core and the two-acid LA:GA mixture. The results showed less dissolving percentage than acids prepared with deionized water, as can be seen in Table 4.1. The lower solubility occurred due to the adverse effects of the different salts included in the synthetic seawater such as sodium chloride, calcium chloride, magnesium chloride, and sodium sulfate. Al-Khalidi et al. (2003) mentioned that organic acids reaction with calcite is thermodynamically limited by the presence of different ions in solution that can be deposited at the solution and calcite interface. This limitation can reduce the calcium ion concentration gradient, which would lower the acid dissolution rate.

Table 4.1 Solubility Comparison Between Acid Solutions Prepared With Deionized Water (DW) and Seawater (SW) at Room Conditions.

Acids	DW	SW (4,000 ppm of sulfate)
14 wt%	50%	46%
20 wt%	65%	60%
27 wt%	84%	79%

Further observation proved that calcium sulfate precipitated in solution as XRD analysis confirmed the identity of the collected solid that appeared in the sampling tubes. XRD results and calcium sulfate precipitation are shown in Figures 4.15 and 4.16, respectively.

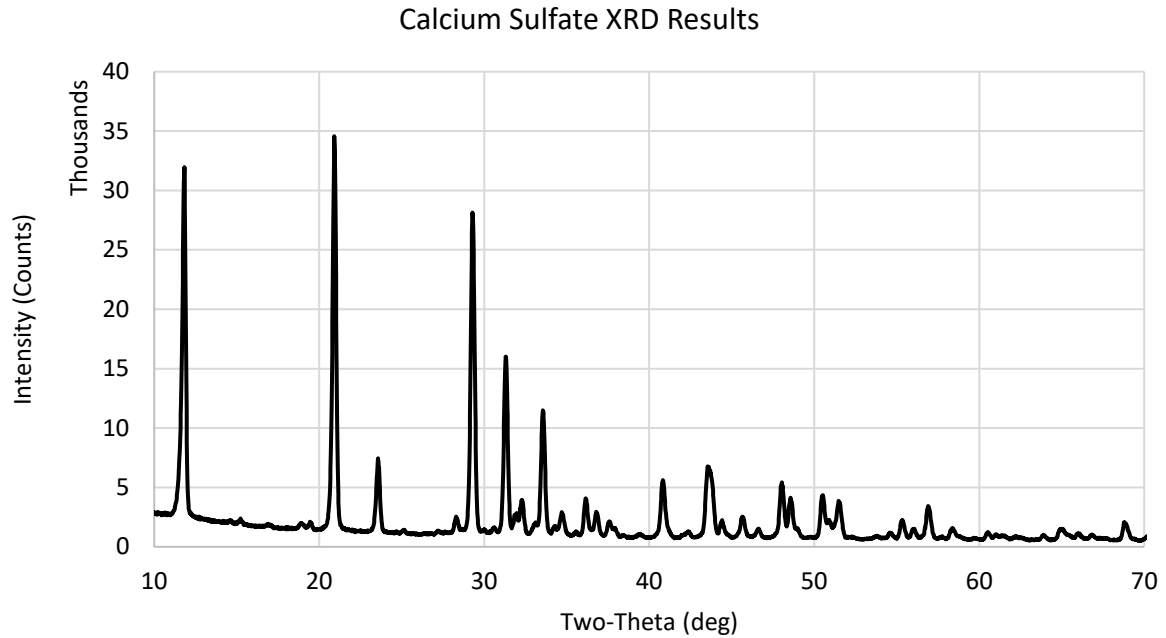


Figure 4.15 XRD spectrum of the collected solids from solubility tests of acids prepared with synthetic seawater that confirmed calcium sulfate precipitation.



Figure 4.16 Sampling tubes from acids prepared with synthetic seawater that were reacted with crushed core at room conditions. Calcium sulfate precipitation started to appear after a few days of conducting the test.

15 wt% HCl solution prepared with synthetic seawater was tested to demonstrate the difference between the two-acid mixture and HCl solution in terms of reaching an equilibrium state in the presence of sulfate ions. Figure 4.17 illustrates the difference between HCl and the 27 wt% mixture of lactic and gluconic prepared by seawater in terms of calcium sulfate risk. In the HCl case, calcium sulfate was deposited clearly after one hour of conducting the test. While in the other case, where a 27 wt% of the LA:GA mixture was tested, at least ten days were needed to observe calcium sulfate solids in the sampling tubes.

This delay in precipitation was due to the time needed to reach an equilibrium state between existing ions within a solution. It should also be noted that lactate and gluconate ions need several days to reach equilibrium with calcium ions in solution (Kubantseva and Hartel 2002). This fact gives sulfate ions enough time to complex with calcium ions and produce calcium sulfate precipitation.

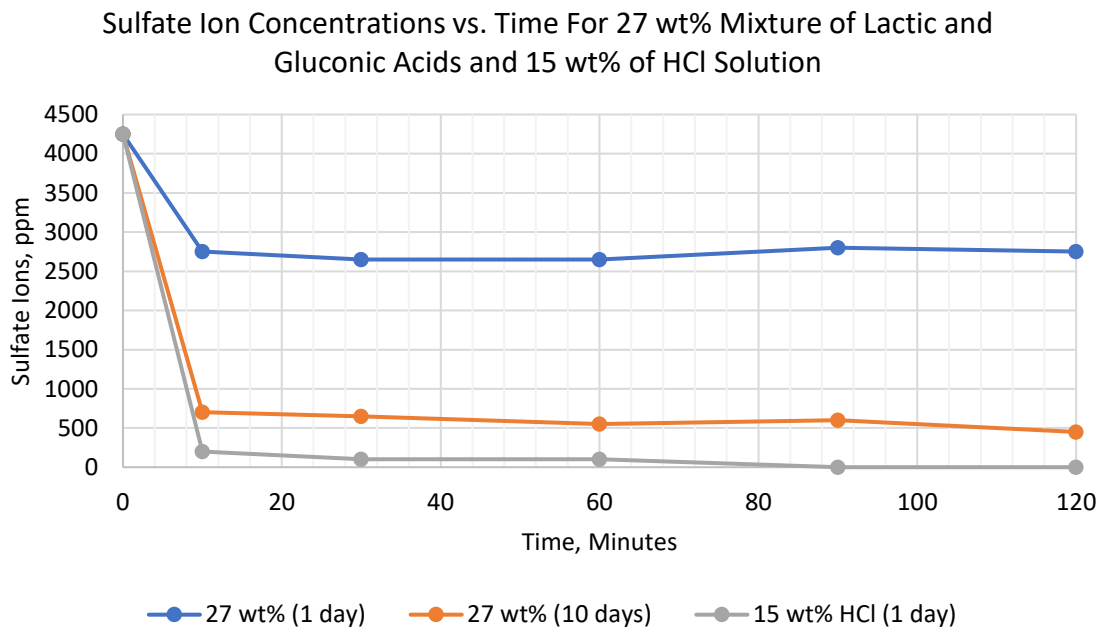


Figure 4.17 Sulfate ion concentrations of 15 wt% HCl and 27 wt% of (1:1) LA:GA acid mixture prepared by seawater that were tested at room conditions.

Total acid concentration and temperature effects were also studied for the solubility test of acids prepared with synthetic seawater. The results showed that the same behavior would be obtained when the temperature was increased as the ionic strength of the acids increased, causing higher solubility of the crushed core. When the total acid strength was increased, more hydrogen ions were dissociated, which was reflected in a higher reactivity of the tested solutions. However, more calcium ions were free in solution with the increase in crushed core solubility, which raised the risk of calcium sulfate precipitation. Figures 4.18 and 4.19 show the solubility results of acids prepared with synthetic seawater when the total acid concentration and temperature were manipulated.

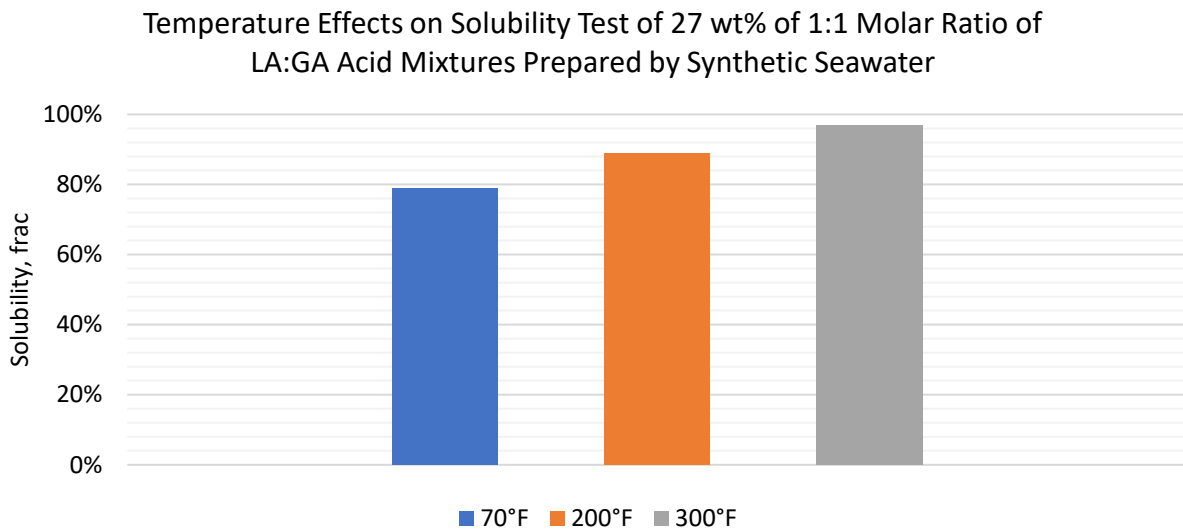


Figure 4.18 Solubility test of 27 wt% (1:1) lactic and gluconic acids prepared by synthetic seawater at different temperatures.

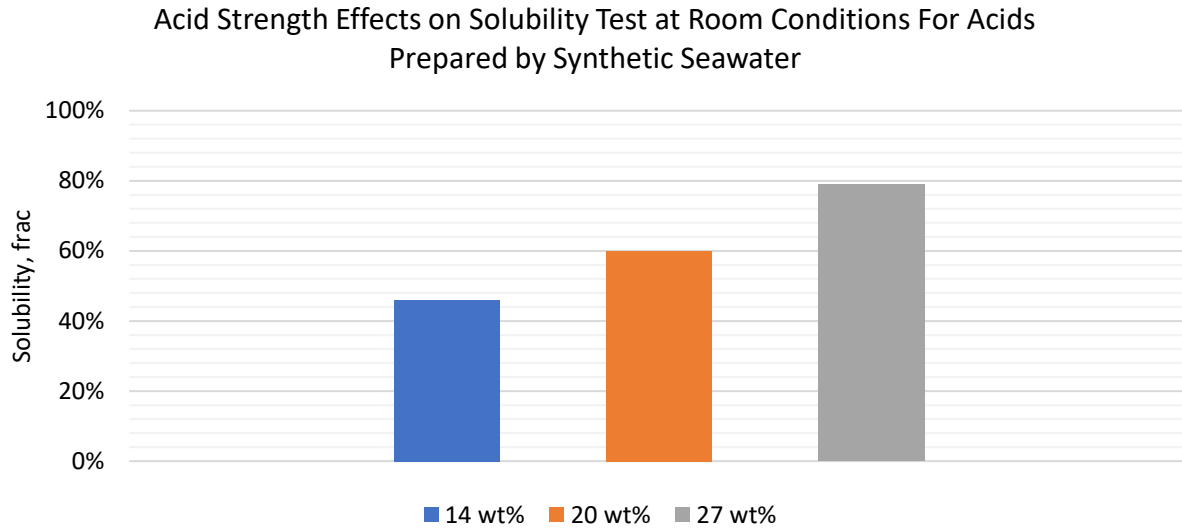


Figure 4.19 Solubility test results of different total acid strengths of (1:1) lactic and gluconic acids prepared by synthetic seawater at room conditions.

4.2.2 Scale Inhibitor Effects on Mitigating Sulfate Ions Bonding With Calcium Ions

Three scale inhibitors were selected to mitigate and reduce calcium sulfate precipitation. Scale inhibitors A and C are based on phosphonic acid, while scale inhibitor B is based on acrylic acid. These inhibitors have been used in the literature to prevent different scale deposition; 5 to 10 ppm was the recommended loading range. Therefore, these inhibitors were tested at these loadings to eliminate calcium and sulfate complexing processes in spent acid solutions. Three sulfate concentrations were tested, including 4,000, 6,000, and 12,000 ppm. Since calcium and sulfate ions need a few days to reach equilibrium, sulfate ion concentrations in solution were analyzed using Ion Chromatography (IC) after ten days of conducting the tests.

All inhibitors performed the same with lower sulfate levels in the higher acid concentration cases due to more calcium ions being diffused from the high calcite solubility. In the 4,000 and 6,000 ppm sulfate level case, 5 ppm of any scale inhibitors was enough to keep at least 80% of sulfate ions dissolved in the 14 wt% LA:GA mixture solution, while 50% were kept in the 27 wt%

LA:GA mixture solution. At the high sulfate level of 12,000 ppm, all scale inhibitors failed to keep more than 50% of the ions dissolved in both LA:GA acid mixture concentrations of the 14 wt% and 27 wt%. Figures 4.20 to 4.22 show the results of the scale inhibitors' performances in the acid solubility tests.

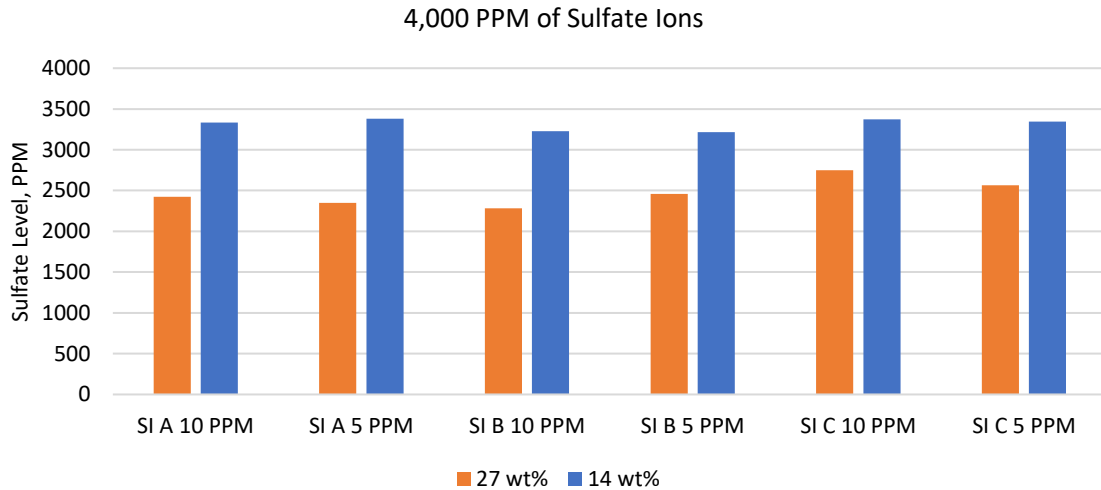


Figure 4.20 Sulfate ions levels within 14 & 27 wt% LA:GA acid solutions when 5 & 10 ppm of scale inhibitors were used with the solutions that contained 4,000 ppm of sulfate ions.

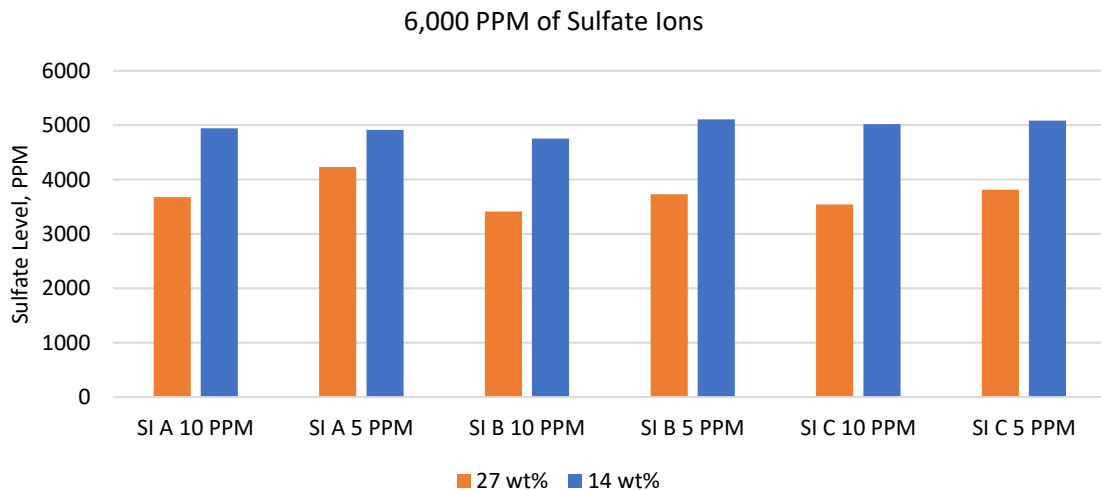


Figure 4.21 Sulfate ions levels within 14 & 27 wt% LA:GA acid solutions when 5 & 10 ppm of scale inhibitors were used with the solutions that contained 6,000 ppm of sulfate ions.

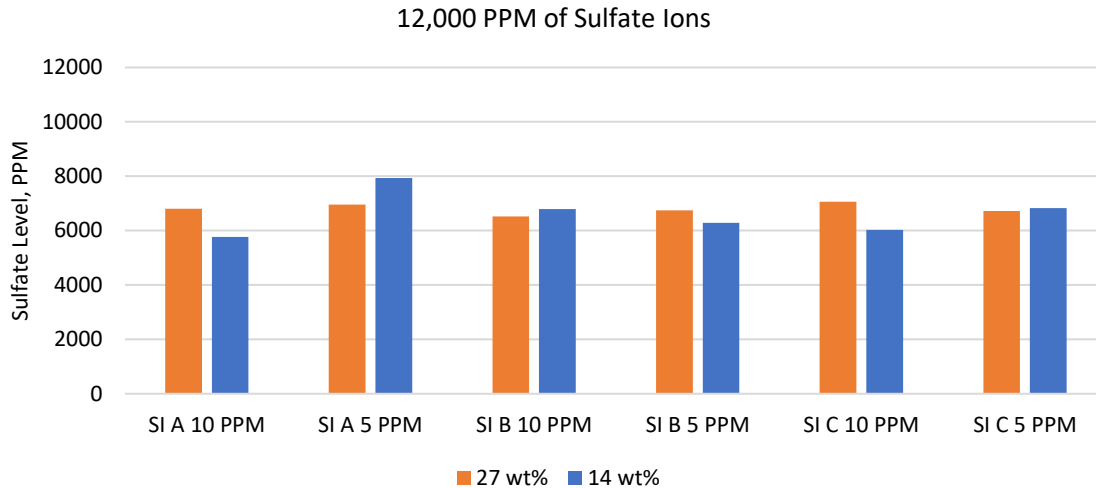


Figure 4.22 Sulfate ions levels within 14 & 27 wt% LA:GA acid solutions when 5 & 10 ppm of scale inhibitors were used with the solutions that contained 12,000 ppm of sulfate ions.

The results showed that even with an excellent mitigating of sulfate ions consumption in the 4,000 and 6,000 ppm cases, a more optimized scale inhibitor was needed to keep sulfate ions in the initial level. Acrylic acid-based inhibitors work by mitigating crystal growth of calcium sulfate precipitation after the initial nucleation of the crystal. However, these inhibitors cannot continue to retard the crystal growth due to the time degradation of the chemical structure of the inhibitor (Bin Merdhah 2010). Phosphonic acid-based inhibitors work better than acrylic acid-based inhibitors in terms of preventing crystal growth entirely (Chen et al. 2004).

According to a study conducted by Bin Merdhah (2010), phosphonic acid-based inhibitors outperform acrylic acid-based inhibitors. However, inhibition time and temperature have a significant impact on the overall inhibition efficiency. Arensman and Nasr-El-Din (2013) conducted a study on the effectiveness of different scale inhibitors to prevent calcium sulfate precipitation in spent HCl solutions prepared by synthetic seawater. Their results showed that phosphonic acid-based inhibitors mitigated calcium sulfate deposition more than acrylic acid-

based inhibitors. However, temperature and compatibility issues were drawbacks of these inhibitors to ultimately be effective in preventing calcium sulfate precipitation.

In this study, inhibition time was the main factor in reducing the efficiency of the mentioned scale inhibitors. The scale inhibitors were mixed with the spent acid and left in solution for approximately ten days, which was sufficient time to degrade and decrease these chemicals' effectiveness. Still, the two-acid mixture environment and the long time needed to reach equilibrium can allow a safe acidizing operation using seawater when the sulfate ion concentration is in the range of zero to 6,000 ppm. In the future, a phosphorus-based scale inhibitor can be utilized, which was tested in acidic and high temperature conditions and proved to be effective in keeping sulfate ions as high as possible (Bin Merdhah 2010).

CHAPTER 5

CORROSION TEST: RESULTS AND DISCUSSION

This chapter discusses and evaluates the corrosiveness of different acid mixtures based on corrosion and pitting ratings. The corrosion rating was calculated based on the weight loss method, and a pitting rating was assigned based on visual inspection of the acid effects on the tested steel coupons. Different tests were performed with and without a corrosion inhibitor (CI). The results showed that 5 gpt of an organic corrosion inhibitor could keep the corrosion and pitting ratings below the acceptable rating levels. Table 5.1 shows a summary of the corrosion rates of the conducted tests.

Table 5.1 Corrosion Rates of the Tested Solutions at 200 and 300°F.

4 hours of testing Corrosion rates in lb/ft ²		Acid Mixtures				
		9 wt% LA	9 wt% GA	14 wt% Mixture	27 wt% Mixture	15 wt% HCl
200°F	No CI	0.12	0.10	0.17	-	-
	5 gpt CI	-	-	0.003	0.004	-
300°F	No CI	0.45	0.15	0.29	0.54	0.56
	5 gpt CI	-	-	0.008	0.012	-

5.1 Corrosion Testing Without a Corrosion Inhibitor

This section shows the corrosion tests run for clean solutions without any corrosion inhibitor. 9 wt% lactic acid was tested first at 200 and 300°F to illustrate the corrosiveness of lactic acid. Then, 9 wt% gluconic acid was tested at the mentioned temperatures for the same reason. Further tests were then conducted at different temperatures using different total acid strengths to

show the effect of mixing the two acids on corrosion and pitting ratings. Lastly, HCl corrosiveness was shown via testing 15 wt% HCl at 300°F, which showed a high corrosion rating as expected.

The adsorption of organic acid conjugate base ion, such as lactate and formate ions for lactic and formic acids, respectively, on the metal surface was the main reason for the steel coupons corrosion. The adsorption occurs completely on the oxide layer and removes iron atoms from the steel structure. According to Rueda et al. (1985) and Panias et al. (1996), this process is highly affected by an increase in test temperature as it is associated with a high activation energy. The dissolution of the oxide layer is characterized by a formation of ferrous ions that can be anchored and removed by organic acid conjugate base ions.

5.1.1 Corrosion Testing Using 9 wt% Lactic Acid and 9 wt% of Gluconic Acid

A 9 wt% lactic acid solution was tested at 200 and 300°F at 1,000 psi for 4 hours. The steel coupon's initial weight was 37.05 grams, and it lost 1.5 grams after conducting the test at 200°F due to the lactic acid attack on the steel coupon surface. This weight's loss gave a 0.12 lb/ft² corrosion rating and 3 levels of pitting rating. At 300°F, the acid was more reactive, which resulted in a higher corrosion rating of 0.45 lb/ft² and a uniform pitting of a 3 rating. Figures 5.1 and 5.2 show the steel coupon of the tested solutions before and after performing the tests.

The increase in corrosion rating at 300°F was reflected in an increase in iron ion concentration in the samples taken from the tested solution during the 4-hour test. Figure 5.3 shows iron ion concentrations in the tested solution for the 9 wt% lactic acid solution tested at 200 and 300°F. Dissolved iron ions from the acid attack tended to complex with dissociated lactate ions from lactic acid dissociation. This affinity and the increase in iron ions in solution caused an iron lactate compound to precipitate in the sampling tubes of the solution tested at 300°F, as can be seen in Figure 5.4. Iron lactate precipitation can also be identified by a drop in iron ion

concentrations from Figure 5.3. The solution color was also affected by the increase in iron ion concentrations in solution as it changed from light greenish to dark greenish when the test temperature was raised to 300°F.

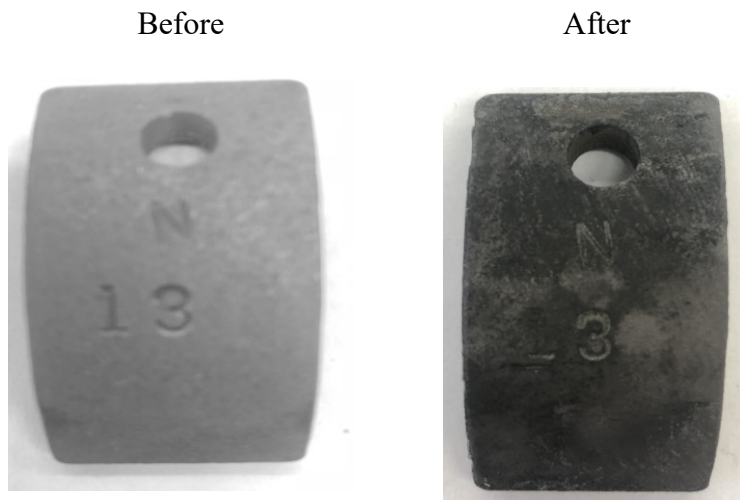


Figure 5.1 Tested steel coupon before and after soaking it at 200°F and 1,000 psi using 9 wt% lactic acid solution for 4 hours.

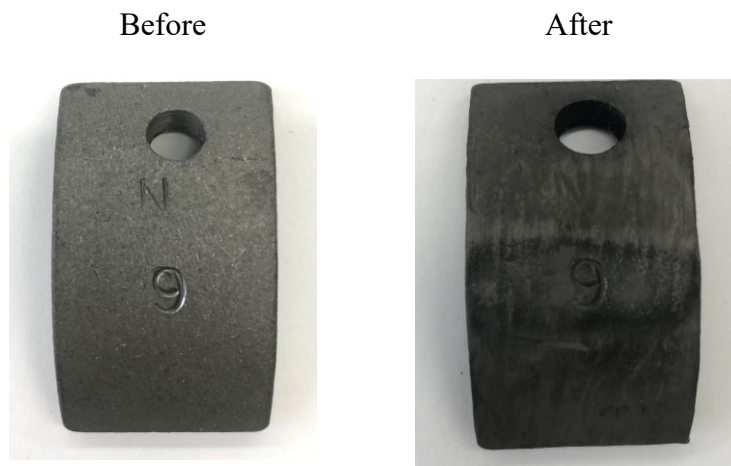


Figure 5.2 Tested steel coupon before and after soaking it at 300°F and 1,000 psi using 9 wt% lactic acid solution for 4 hours.

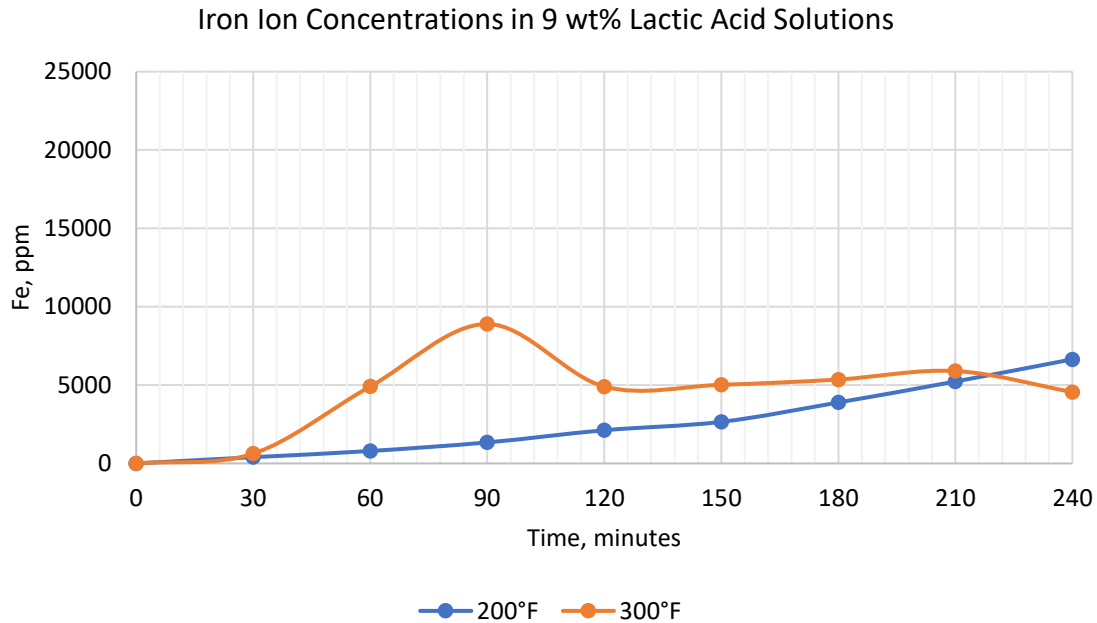


Figure 5.3 Iron ion concentrations in solution for 9 wt% lactic acid solution that was tested at 200 and 300°F at 1,000 psi for 4 hours.

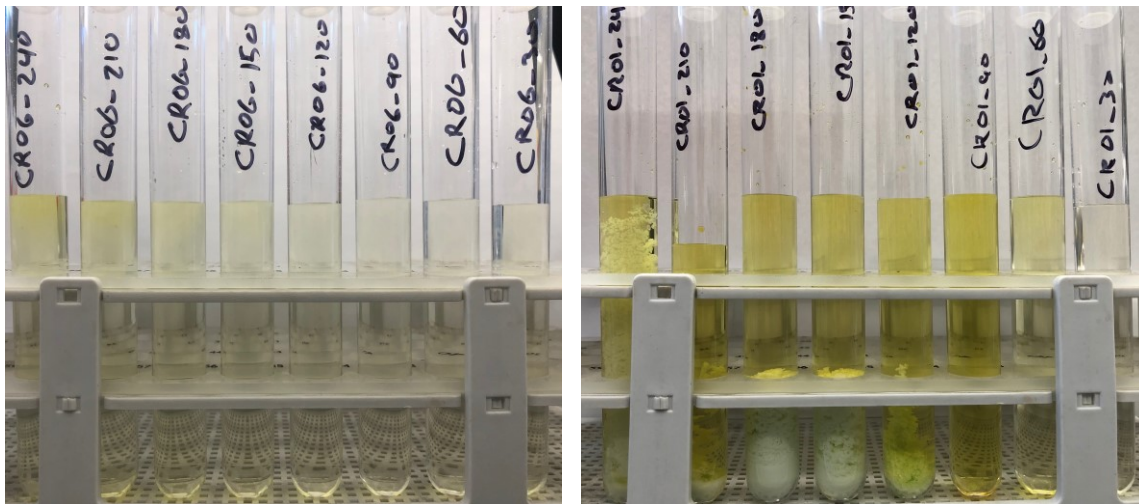


Figure 5.4 Sampling tubes of 9 wt% lactic acid solution that was tested at 200°F (on the left) and 300°F (on the right) at 1,000 psi for 4 hours. Iron lactate precipitation started to deposit after two hours of conducting the test at 300°F.

Iron lactate identity was also confirmed by conducting the XRD test on the collected solid samples. Figure 5.5 shows the XRD spectrum of the collected solids that shows a stable existence

of the molecules that build up the iron lactate compound. The compound consists of one atom of iron and two lactate anions with a chemical formula of $\text{Fe}(\text{C}_3\text{H}_5\text{O}_3)_2$. It should be noted that the XRD analysis identification process depends on the existence of standard patterns to do a qualitative examination on the tested solid. Otherwise, a relative estimation of the resulted peaks intensities is made to identify the tested solid.

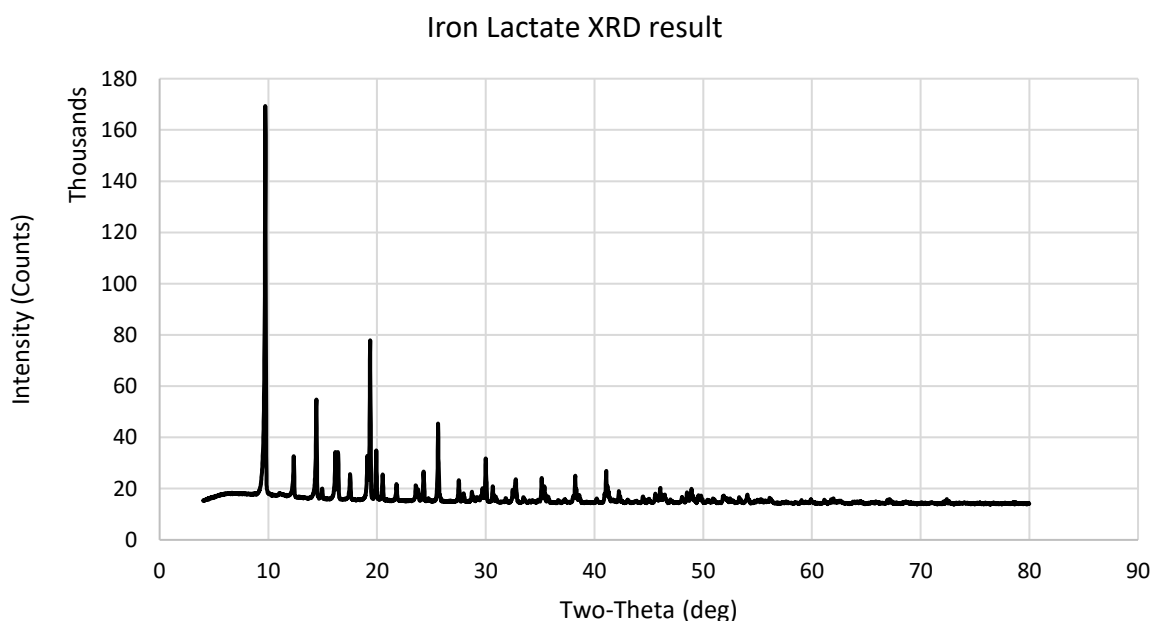


Figure 5.5 Spectrum of the collected solids that confirmed iron lactate precipitation.

Different programs were used to run a computer-based search on the resulted peaks, shown in Figure 5.5, to compare them with a standard database of peaks and intensities. However, no matches were discovered, and the adopted databases were found to be missing iron lactate compound. Therefore, a new search was done to estimate the existing elements within the tested solids. The new search was initiated by limiting the peaks identification process to those containing iron, carbon, hydrogen, and oxygen. These elements are the main elements of iron lactate compound. The results showed a high existence of these elements within the peaks and the

spectrum of the collected solids with minor traces of sulfur element. Sulfur can be found in the N-80 steel coupon composition, which can be the reason for its existence in the XRD analysis.

In both cases of testing the 9 wt% lactic acid solution at 200 and 300°F, the lactate ion amounts in solution were the same. However, the iron ion amounts in solution at 300°F were much more than the other case which caused the precipitation of the greenish crystal solid of iron lactate. Nevertheless, iron lactate has moderate solubility in water of 20.1 g/L at 10°C and 80.5 g/L at 100°C. It can be concluded from the previous tests that iron lactate precipitation would occur when the corrosion rating is high enough to raise the iron ion content in solution.

Gluconic acid was found to be less corrosive than lactic acid when tested using 9 wt% at 200 and 300°F for 4 hours at 1,000 psi. At 200°F, the corrosion rating was calculated to be 0.10 lb/ft², and the pitting rating was 0. A slight increase was noticed in the corrosion rating when the 9 wt% gluconic acid was tested at 300°F as a corrosion rate of 0.15 lb/ft² was calculated. The pitting rating did not change as the acid showed a low dependency between its corrosiveness and temperature. Figures 5.6 and 5.7 show the steel coupons of the tested solutions before and after performing the tests.

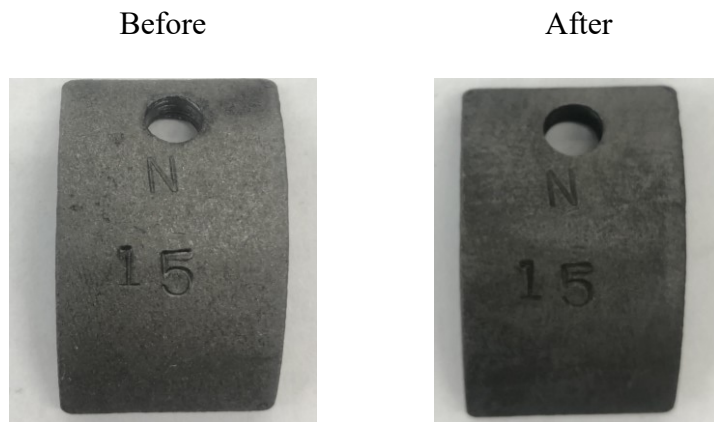


Figure 5.6 Tested steel coupon before and after soaking it at 200°F and 1,000 psi using 9 wt% gluconic acid solution for 4 hours.

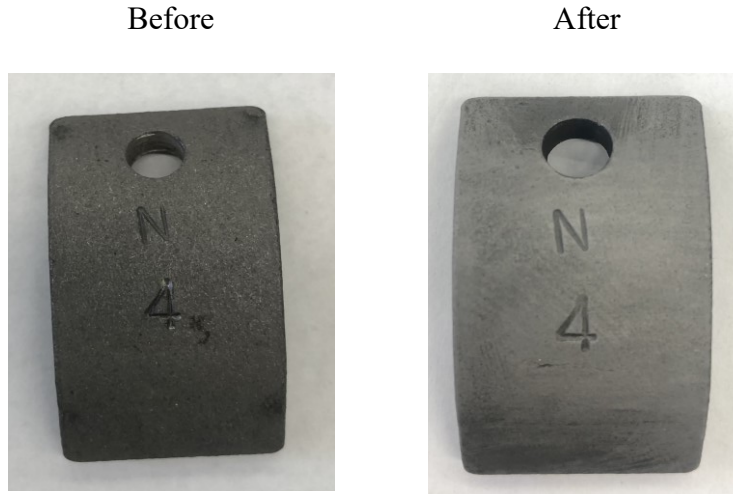


Figure 5.7 Tested steel coupon before and after soaking it at 200°F and 1,000 psi using 9 wt% gluconic acid solution for 4 hours.

Iron-based precipitation was not a concern in the gluconic acid corrosion tests due to low iron ion concentrations in solution and to the absence of lactate ions in solution. Gluconate ions were in solution instead of lactate ions and can complex with dissolved irons to produce an iron gluconate compound. However, the iron gluconate compound has a high solubility in water, which was reflected in clear sampling tubes of the tested solutions and in increases in the iron ion concentrations in solution, as can be seen in Figures 5.8 and 5.9.

The solutions' samples turned to yellowish to brownish colors as the test temperature was increased from 200 to 300°F. This change in color was attributed to gluconic acid behavior as its color changes to brown in high temperature conditions. This change in color was also confirmed by heating up a 9 wt% gluconic acid to 300°F where the solution's color changed from light yellow to dark brown.

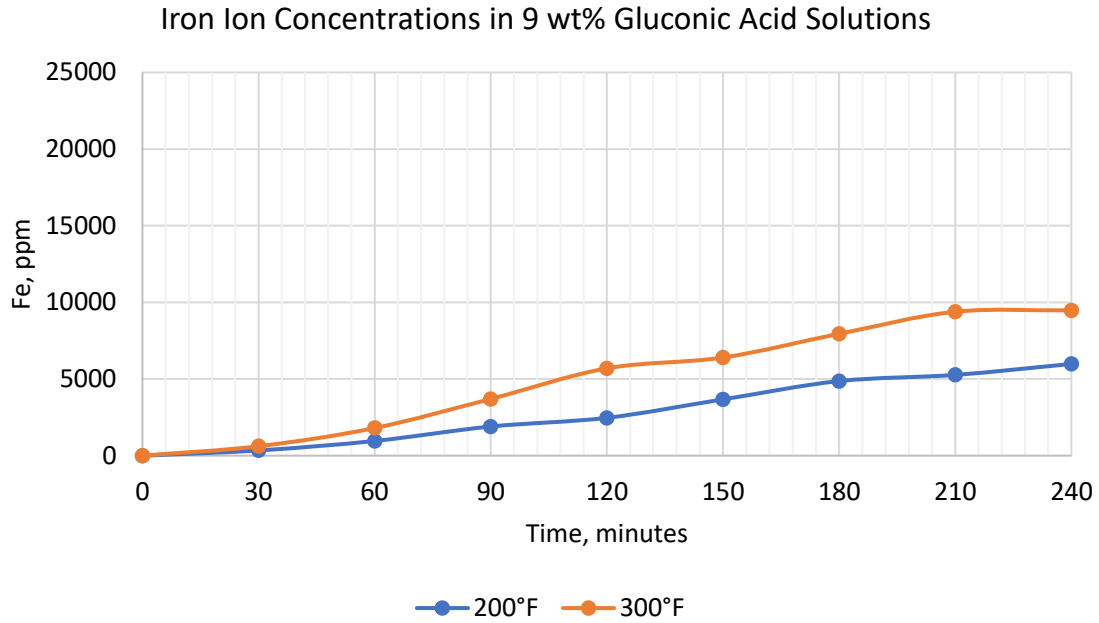


Figure 5.8 Iron ion concentrations in solution for 9 wt% gluconic acid solution that was tested at 200 and 300°F at 1,000 psi for 4 hours.

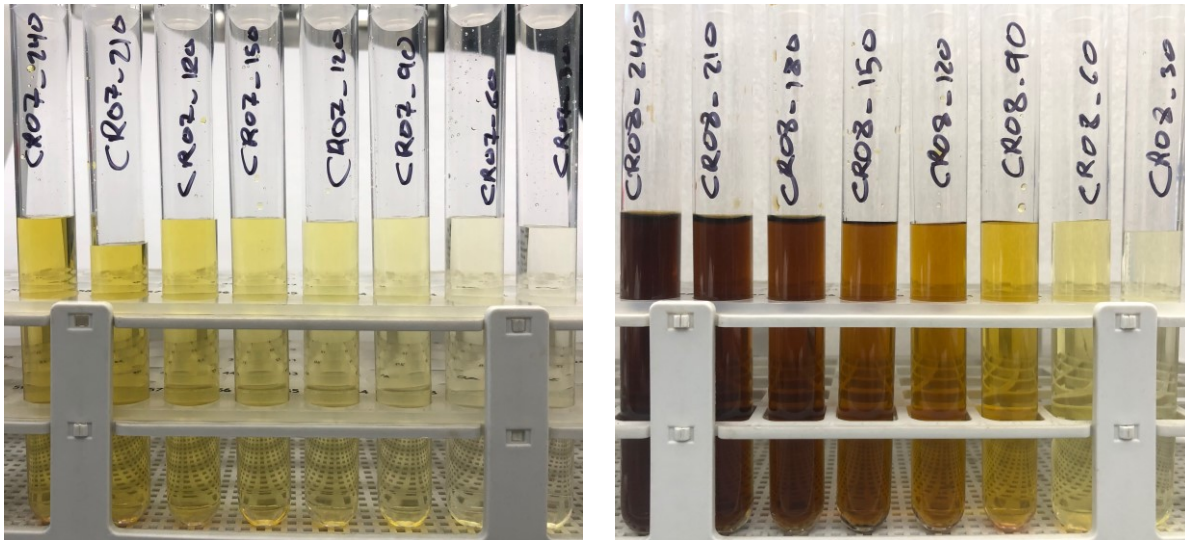


Figure 5.9 Sampling tubes of 9 wt% gluconic acid solution that was tested at 200°F (on the left) and 300°F (on the right) at 1,000 psi for 4 hours. The increase in temperature caused a change in the solution color.

5.1.2 Corrosion Testing Using 14 wt% and 27 wt% LA:GA Acid Mixtures at 1:1 Molar Ratio

Mixtures of the two acids were tested at total acid concentrations of 14 wt% and 27 wt% to illustrate the corrosiveness of the mixture solutions. The total acid concentration was manipulated to show the effect of increasing it on corrosion and pitting ratings. The 14 wt% LA:GA solution consisted of 4.5 wt% of lactic acid and 9.5 wt% of gluconic acid while the 27 wt% LA:GA solution consisted of 9.0 wt% of lactic acid and 18.0 wt% of gluconic acid. Iron lactate precipitation can occur due to lactate ions' existence at a high level in solution accompanied by a high level of iron ions. For that, iron lactate deposition was expected in the 27 wt% case since it had relatively similar lactate ion concentrations in solution like the 9 wt% lactic acid case.

As was expected, the 14 wt% acid mixture did not show any precipitation in the sampling tubes when it was tested at 200 and 300°F, as can be seen in Figure 5.10. The ICP analysis of the sampling tubes also did not show any sign of a drop of iron ion concentrations with time, which also ruled out any deposition of iron lactate precipitation in solution. The ICP analysis results are shown in Figure 5.11. The corrosion ratings were 0.17 lb/ft² at 200°F and 0.29 lb/ft² at 300°F. The pitting ratings were 2 for both cases, as can be seen from the steel coupons that are shown in Figures 5.12. and 5.13. Although the corrosion rates were lower than the 9 wt% lactic acid case at 300°F, it was still above the acceptable limit of 0.05 lb/ft².

It should also be noted that the 14 wt% LA:GA acid mixture had a higher total acid concentration, which caused an increase in the corrosion rate at 200°F when it was compared with the cases of 9 wt% of the lactic acid or gluconic acid. However, it caused a lower corrosion rate at 300°F than the 9 wt% of lactic acid case due to the low dependency of gluconic acid with temperature.

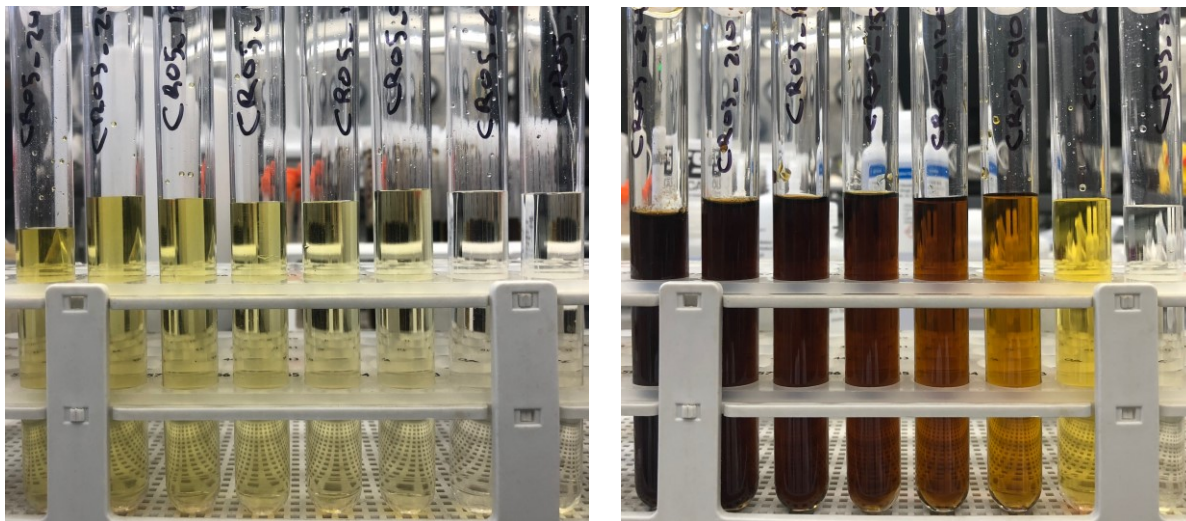


Figure 5.10 Sampling tubes of 14 wt% LA:GA acid mixture solution that was tested at 200°F (on the left) and 300°F (on the right) at 1,000 psi for 4 hours.

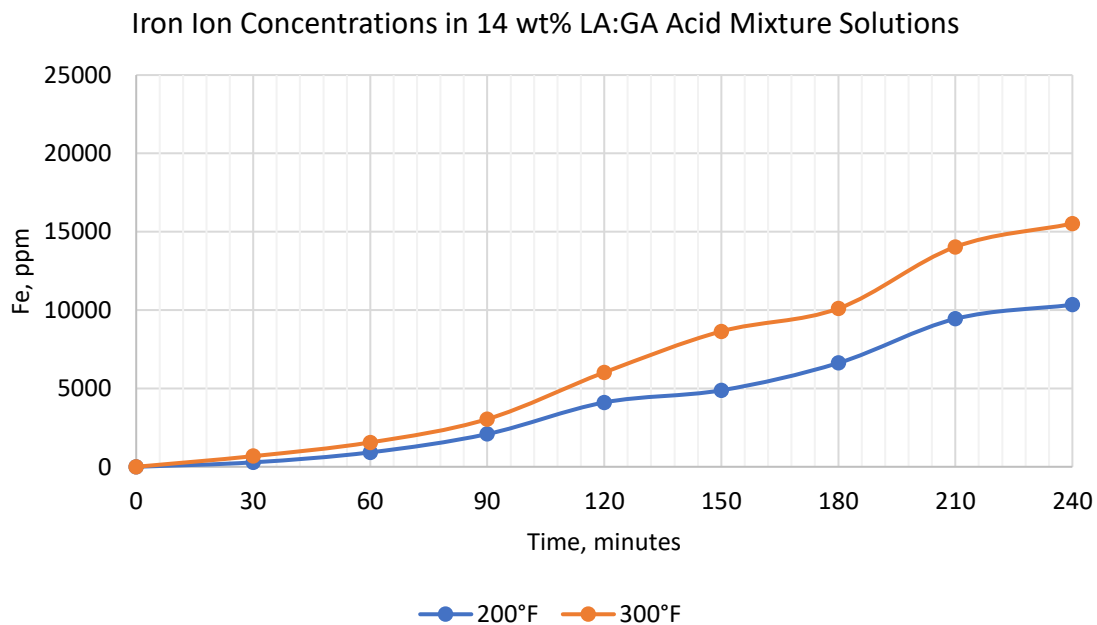


Figure 5.11 Iron ion concentrations in solution for 14 wt% LA:GA acid mixture solution that was tested at 200 and 300°F at 1,000 psi for 4 hours.



Figure 5.12 Tested steel coupon before and after soaking it at 200°F and 1,000 psi using 14 wt% LA:GA acid mixture solution for 4 hours.



Figure 5.13 Tested steel coupon before and after soaking it at 300°F and 1,000 psi using 14 wt% LA:GA acid mixture solution for 4 hours.

The 27 wt% LA:GA acid mixture was tested at 300°F to show its corrosiveness at high temperatures. The 4-hour test showed a corrosion rating of 0.54 lb/ft², which was more significant than the acceptable limit. The pitting rating was 4, as can be seen from the steel coupons in Figure 5.14. The increase in corrosion rating was mainly attributed to the increase of lactic acid

concentration when the 27 wt% LA:GA acid mixture case was compared to the 14 wt% LA:GA acid mixture at 300°F. This was also confirmed by the higher corrosiveness of lactic acid compared to gluconic acid that was discussed in Section 5.1.1.



Figure 5.14 Tested steel coupon before and after soaking it at 300°F and 1,000 psi using 27 wt% LA:GA acid mixture solution for 4 hours.

The high corrosion rating of the 27 wt% LA:GA acid mixture was reflected in an increase of iron ion levels in solution, which caused iron lactate precipitation as lactate ion existed in high concentration as well. Iron lactate precipitation can be seen in the sampling tubes that are shown in Figure 5.15. Additionally, the drop of iron ion concentrations versus time confirmed the formation of iron lactate compound, as can be seen in Figure 5.16.

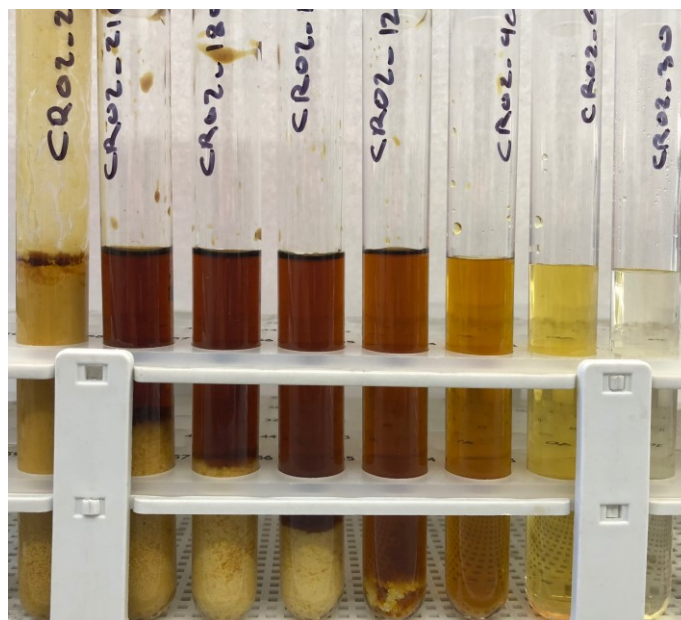


Figure 5.15 Sampling tubes of 27 wt% LA:GA acid mixture solution that was tested at 300°F and 1,000 psi for 4 hours.

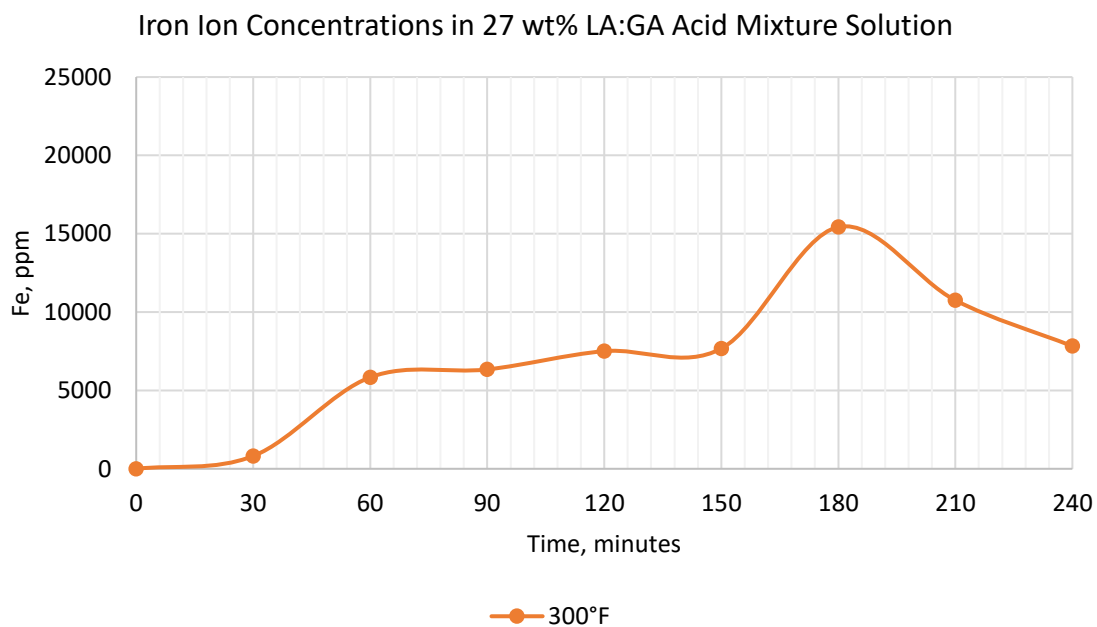


Figure 5.16 Iron ion concentrations in solution for 27 wt% LA:GA acid mixture solution that was tested at 300°F and 1,000 psi for 4 hours.

The previous tests and results indicated that a corrosion inhibitor is needed to keep corrosion and pitting ratings below the acceptable limits. Reducing the corrosion rating would decrease iron ions in solution, which would result in a clean solution without any risk of iron lactate precipitation. Therefore, a sulfur-based corrosion inhibitor was selected to reduce the corrosion rate caused by lactic and gluconic acid.

5.1.3 Corrosion Testing Using 15 wt% Hydrochloric Acid

HCl's strong corrosiveness toward steel tubulars undermines its applicability in high temperature treatments. HCl is usually used in 15 wt%, 20 wt%, and 28 wt% depending on the application conditions. The weakest concentration of 15 wt% HCl was prepared and tested for three hours at 300°F and 1,000 psi to illustrate the corrosion rating of this solution. It should be noted that the HCl solution was tested for three hours instead of 4 hours due to the test vessel limitation. The result was then compared with the strongest acid mixture of lactic and gluconic acids, which was the 27 wt% acid mixture.

The three hours test showed that 15 wt% of HCl was more corrosive than the 27 wt% LA:GA acid mixture as it caused 0.56 lb/ft² compared to 0.54 lb/ft². However, sampling tubes from the HCl solution did not show any precipitation, which resulted in a clean solution that was only rich with iron ions dissolved in solution. Figure 5.17 shows the steel coupon before and after conducting the test. Some pinholes can be seen in the steel coupon after performing the test due to localized attack by the HCl solution on the steel coupon. Pinholes in wellbore tubulars can create serious communication and fluid commingling problems (De Wolf et al. 2017). The HCl solution caused a pitting rating of 6 due to these localized holes.

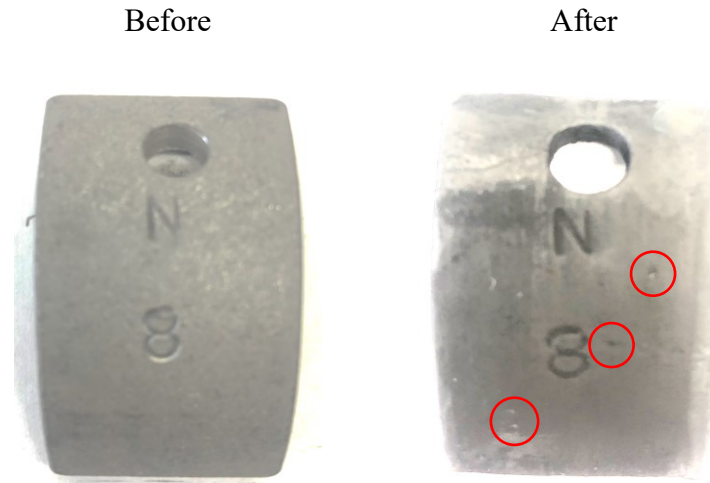


Figure 5.17 Tested steel coupon before and after soaking it at 300°F and 1,000 psi using 15 wt% HCl acid solution for three hours.

5.2 Corrosion Testing With a Corrosion Inhibitor

HCl acid is usually combined with inorganic corrosion inhibitors that are based on quaternary ammonium. The presence of chloride ions in the acid solution invites positively charged inhibitor molecules to attach to the metal surface. Organic acids do not contain chloride ions which make HCl-based corrosion inhibitors inadequate for usage (De Wolf et al. 2017). Organic acids counter ions, such as acetate, formate, and lactate, cannot attach to the metal surface strongly. In such cases, a sulfur-based corrosion inhibitor is essential. SH^- molecules in sulfur-based corrosion inhibitors takes the purpose of chloride ions in HCl solutions and can attract the positively charged molecules in sulfur-based corrosion inhibitors (Frenier and Ziauddin 2008).

A sulfur-based corrosion inhibitor was selected to reduce the corrosion rate caused by lactic and gluconic acid. This corrosion inhibitor is classified as one of the thiourea groups that combine with different fatty acids. These fatty acids work as aids to improve corrosion control by adding more attachment to the metal surface through covalent bonds. Based on literature review and the

manufacturer's recommendation, it was decided to add 5 gpt of the corrosion inhibitor in the different acid mixtures.

First, the 14 wt% LA:GA acid mixture was tested with 5 gpt of the corrosion inhibitor at 200 and 300°F at 1,000 psi for 4 hours. The results were above expectations as both steel coupons did not lose more than 0.11 gram, which gave corrosion rating of 0.0034 lb/ft² at 200°F and 0.0084 lb/ft² at 300°F. The pitting ratings were zero for both cases, as can be seen in Figures 5.18 and 5.19. These low corrosion ratings reduced significantly the iron ions dissolved in solution, which resulted in clean sampling tubes from the two cases.

The 27 wt% LA:GA acid mixture solution was also tested at 200 and 300°F with 5 gpt of corrosion inhibitor. Iron lactate precipitation, along with a high corrosion rating were the two main problems for this solution. However, reducing the corrosion rating would eliminate iron lactate precipitation by lowering the iron ion amounts in solution. In the absence of a high levels of iron ions, lactate ions cannot bond with iron ions to produce iron lactate precipitation.

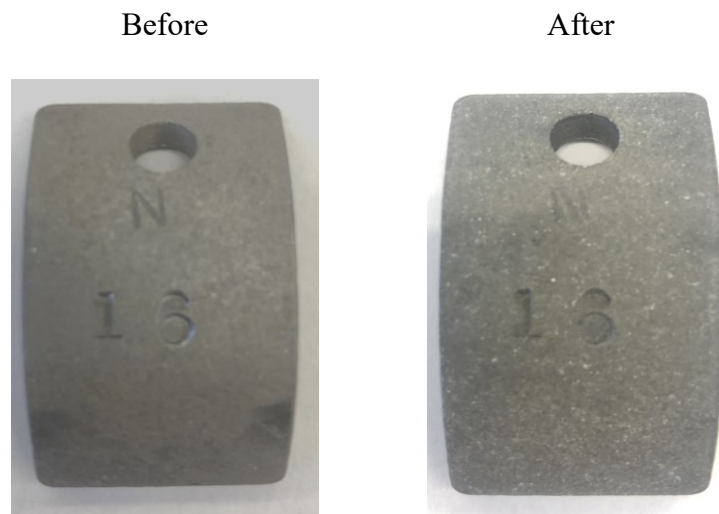


Figure 5.18 Tested steel coupon before and after soaking it at 200°F and 1,000 psi using 14 wt% LA:GA acid mixture solution for 4 hours with 5 gpt of corrosion inhibitor.



Figure 5.19 Tested steel coupon before and after soaking it at 300°F and 1,000 psi using 14 wt% LA:GA acid mixture solution for 4 hours with 5 gpt of corrosion inhibitor.

As it was expected, the corrosion inhibitor reduced the corrosion ratings significantly for both temperatures. At 200°F, the corrosion rating was 0.0043 lb/ft², and at 300°F, the corrosion rating was 0.0118 lb/ft². The pitting ratings were zero for both cases, as can be seen in Figures 5.20 and 5.21. The stability of the corrosion inhibitor was also tested by conducting another test using 27 wt% LA:GA acid mixture at 300°F and 1,000 psi for 12 hours. The resulting corrosion rating was slightly higher, by 0.0006 lb/ft², than the 4-hour test, but still below the acceptable limit. The pitting rating was zero, as can be seen in Figure 5.22.

These tests proved that lactic and gluconic acid corrosiveness could be efficiently inhibited and reduced by utilizing the appropriate corrosion inhibitor. Even with increasing the test temperature and test duration, there was not any need to increase the corrosion inhibitor loading of 5 gpt (0.5 vol%). Various studies reported that wellbore tubulars can be protected by 1 %vol and, more often 2 vol%, of corrosion inhibitors along with including different kinds of expensive corrosion inhibitor intensifiers based on the treatment design and wellbore conditions (Nasr-El-Din et al. 2002, 2003; Al-Mutairi et al. 2005). Overall treatment cost, spent acid effect on treated

formation wettability, and environmental impact of the treatment can be all significantly minimized by any reduction in the corrosion inhibitor and intensifier loadings for the treatment (De Wolf et al. 2017).



Figure 5.20 Tested steel coupon before and after soaking it at 200°F and 1,000 psi using 27 wt% LA:GA acid mixture solution for 4 hours with 5 gpt of corrosion inhibitor.



Figure 5.21 Tested steel coupon before and after soaking it at 300°F and 1,000 psi using 27 wt% LA:GA acid mixture solution for 4 hours with 5 gpt of corrosion inhibitor.



Figure 5.22 Tested steel coupon before and after soaking it at 300°F and 1,000 psi using 27 wt% LA:GA acid mixture solution for 12 hours with 5 gpt of corrosion inhibitor.

In the HCl case, a single corrosion inhibitor would not be enough to eliminate its corrosiveness in a high temperature environment. A corrosion inhibitor intensifier would be needed to enhance the corrosion protection method (Ng et al. 2018). Figure 5.23 shows the corrosion ratings of the 15 wt% HCl tested for 3 hours, the 27 wt% acid mixture without corrosion inhibitor tested for 4 hours, and the 27 wt% LA:GA acid mixture with 5 gpt of corrosion inhibitor tested for 12 hours.

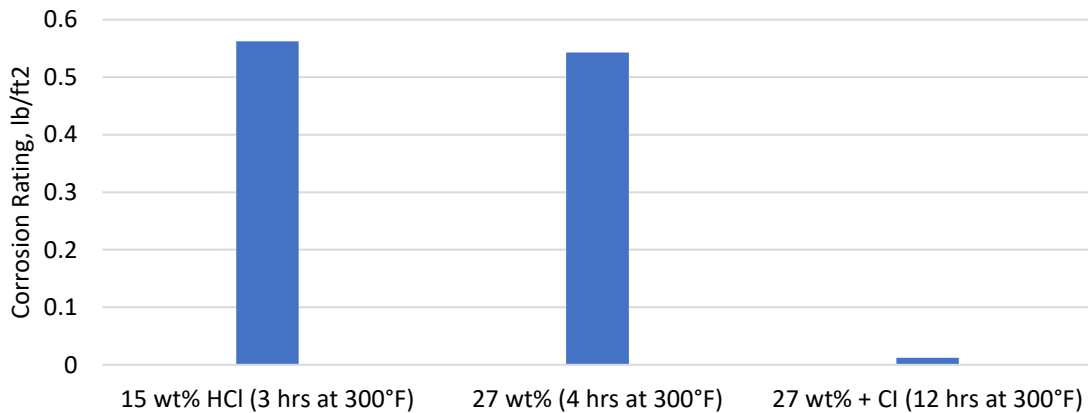


Figure 5.23 Corrosion ratings of the 15 wt% HCl tested for 3 hours, the 27 wt% LA:GA acid mixture without corrosion inhibitor tested for 4 hours, and the 27 wt% LA:GA acid mixture with 5 gpt of corrosion inhibitor tested for 12 hours.

CHAPTER 6

WETTABILITY TEST: RESULTS AND DISCUSSION

This chapter discusses and evaluates the effects of lactic and gluconic spent acid mixtures on carbonate rock wettability by utilizing zeta potential measurements. The spent acid invasion has a direct effect on the production enhancement and on the recovery of the spent acid. The spent acid recovery can be affected by the acid additives' properties and formation's rock wettability. Understanding these effects can lead to better recovery of the acid and better production enhancement (Saneifar et al. 2010).

Different cases were tested at room temperature, based on solution acidity, additives added to the solution, and seawater sulfate ion concentrations. The zeta potential measurements for these cases were taken after six hours and after ten days of suspending the calcite particles in solutions. These changes in conditioning time were done to illustrate the effect of soaking the acid mixtures (that contain different additives and ions) for a period of time after conducting the acidizing treatment.

6.1 Zeta Potential and Tested Rock Wettability

The primary purpose of this section is to show the relationship between zeta potential and the tested rock wettability. Zeta potential is a measurement of the electrical potential between a solid and a liquid interface in the plane of shear within the electrical double layer (EDL). The EDL is the plane that separates the static suspended medium from the more diffuse and moving part. It is more appropriate to measure the electrical potential at the stern layer, but it is much harder to obtain it due to the non-conductive nature of most mineral rocks (Taqvi and Bassioni 2019).

According to Shehata and Nasr-El-Din (2015), zeta potential can be defined by the charge that develops in the boundary of hydrodynamic shear. This charge exists on solid surfaces as a product of the electrostatic repulsion and the attractive forces related to the Van der Waals' forces. Therefore, zeta potential is affected by the surface charge of the medium and the characteristics of the surrounding suspension medium. Due to this behavior, zeta potential is a representation of the surface charges that exist in medium or rock surfaces (Mahani et al. 2015). Qualitatively, the change in zeta potential measures the change in rock surface charge and wettability. Figure 6.1 illustrates the potential difference as a function of distance from the charged surface of a particle suspended in a dispersion medium.

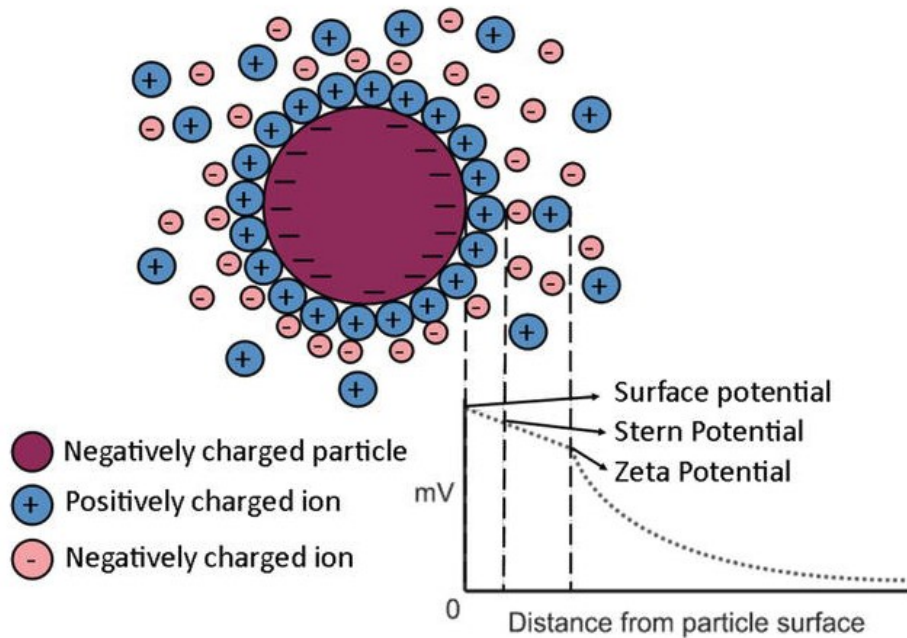


Figure 6.1 Illustration of potential difference as a function of distance from the charged surface of a particle suspended in a dispersion medium (From Taqvi and Bassioni 2019).

Zeta potential tests were carried out using a Zetasizer Nano Series system. The machine measures electrophoretic mobility of carbonate particles dispersed in brines of different spent acid solutions. The instrument uses the Smoluchowski approximation of Henry's equation to measure

the electrophoretic mobility that is utilized to calculate the zeta potential (Hunter 1981). Equation 6.1 shows the Smoluchowski approximation that was used in the Zetasizer Nano Series equipment:

$$\xi = 113000EM \frac{v_t}{D_t}$$

Where,

ξ : zeta potential, mV

EM : electrophoretic mobility at temperature t

v_t : viscosity of the suspending solution at temperature t

D_t : dielectric constant of the suspending solution at temperature t

6.2 Zeta Potential Measurements After Six Hours

Calcium carbonate particles were ground and suspended in 12 different solutions at a loading of 0.1 wt%. These solutions were varied based on water type, acidity, sulfate ion concentrations, and additives added to the solutions. Sulfate ion concentrations were changed between 4,000 and 12,000 ppm. The additives that were tested in the wettability tests included the corrosion inhibitor used in the corrosion test (Chapter 5) and the three scale inhibitors used in the seawater solubility test (Chapter 4). Table 6.1 shows the twelve different solutions that were tested using the zeta potential.

Table 6.1 The Twelve Different Solutions Tested Using Zeta Potential at Room Temperature.

Case	Solution and Additives	Solution Content
1	DW	Deionized water
2	SW4	Seawater with 4,000 ppm of sulfate
3	SW 6	Seawater with 6,000 ppm of sulfate
4	SW 12	Seawater with 12,000 ppm of sulfate
5	14 wt%	Control acid mixture
6	14 wt% + CI	14 wt% acids mixture with 5 gpt of corrosion inhibitor
7	SW 14 wt% + SI A	14 wt% acids mixture with 10 ppm of scale inhibitor A
8	SW 14 wt% + SI B	14 wt% acids mixture with 10 ppm of scale inhibitor B
9	SW 14 wt% + SI C	14 wt% acids mixture with 10 ppm of scale inhibitor C
10	SW 14 wt% + SI A + CI	14 wt% acids mixture with 10 ppm of scale inhibitor A and 5 gpt CI
11	SW 14 wt% + SI B + CI	14 wt% acids mixture with 10 ppm of scale inhibitor B and 5 gpt CI
12	SW 14 wt% + SI C + CI	14 wt% acids mixture with 10 ppm of scale inhibitor C and 5 gpt CI

Since the tested calcium carbonate particles were ground from clean calcite rocks with no residual oil in the pores, the zeta potential value was expected to be negative. As anticipated, calcite rock particles with free oil residual gave a negative zeta potential value of -12 mV when measured after six hours of suspension in deionized water. The deionized water was free from any ions dissolved in solution, which was intended to establish a control base for the other cases. It should also be noticed that the solution pH was around 7. Different studies showed that the zeta potential value increases positively when the tested solution pH is decreased and becomes more acidic (Buckley et al. 1998; Yukselen and Kaya 2003; Shehata and Nasr-El-Din 2015).

Seawater solutions with different sulfate ion concentrations were also used to measure the zeta potential at room temperature and after six hours of suspending the calcite particles. The results showed that increasing the solution salinity increases the zeta potential toward the oil wetting phase. This behavior was in agreement with other studies that were conducted to investigate salinity effects on zeta potential measurement (Shehata and Nasr-El-Din 2015; Mahani et al. 2015; Alarifi et al. 2018; Khaleel et al. 2019). The salinity effect on the zeta potential reading was attributed to the high concentrations of the cations adsorbed within seawater solutions such as Na^+ , Ca^{+2} , and Mg^{+2} . When the amounts of adsorbed cations decrease on the rock surface, the rock surface becomes more repulsive and negative (Legens et al. 1999; Alarifi et al. 2018). Figure 6.2 shows the zeta potential values for calcite particle suspension in deionized water and seawater solutions.

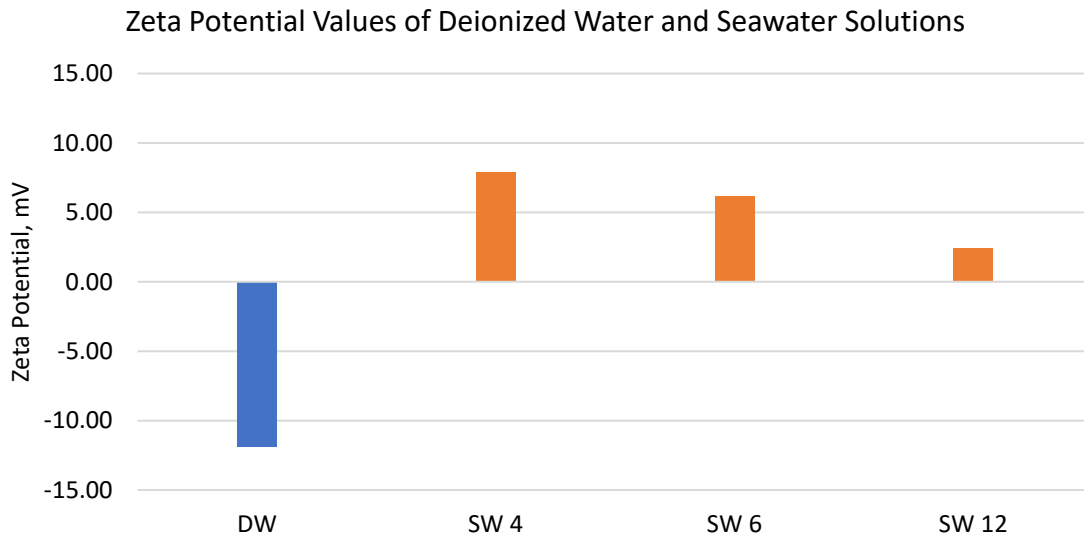


Figure 6.2 Zeta potential values of deionized water and seawater solutions after six hours of particle suspension at room temperature.

Sulfate ions are strong determining ions toward calcium carbonate particles (Pierre et al. 1990; Strand et al. 2008). The adsorption of sulfate ions on the surface of the particles causes more

repulsion force with oil molecules, which in turn changes the rock wettability toward the water wetting phase. This behavior was noticed in the tested cases of seawater with 4,000, 6,000, and 12,000 ppm of sulfate ions. Although cation ions within seawater solutions increased the zeta potential significantly compared to the deionized water case, the strong adsorption of sulfate ions reduced the zeta potential as sulfate ion concentrations were increased. These zeta potential values can be seen in Figure 6.2.

Lactic and gluconic acids are considered organic compounds that belong to the family of carboxylic acids, where carboxylate molecules are part of their chemical structures. Carboxylate molecules, within carboxylic acids, tend to adsorb on the calcite surface, which alter the wettability of the particles from hydrophilic (water wetting) to more hydrophobic (non-water wetting) (Legens et al. 1999). In addition to the lactic and gluconic acids, fatty acid is also part of the family of the carboxylic acids with a high number of carbon atoms in its chemical structure. The fatty acid is one of the substances that is within the used corrosion inhibitor composition. Along with the fatty acid, a surfactant was also used to produce the corrosion inhibitor.

In the zeta potential measurements, organic acids and the fatty acid-based corrosion inhibitor increased the surface charge of the suspended particles due to direct adsorption of the carboxylate molecule. This phenomenon was noticed when 14 wt% LA:GA acid mixture prepared by deionized water was used to suspend the calcite particles. The zeta potential value was increased to 1 mV compared to -15 mV in the deionized water case. The increase of zeta potential value was more significant when the corrosion inhibitor was added to the solution as the measurement was 4 mV, as can be seen in Figure 6.3. This also indicated that the used surfactant is a cationic surfactant that alters the wettability of calcite particles to be more oil wet. Additionally, the solution's pH was around 4 to 5, which played a significant part in increasing the calcite particles' zeta potential.

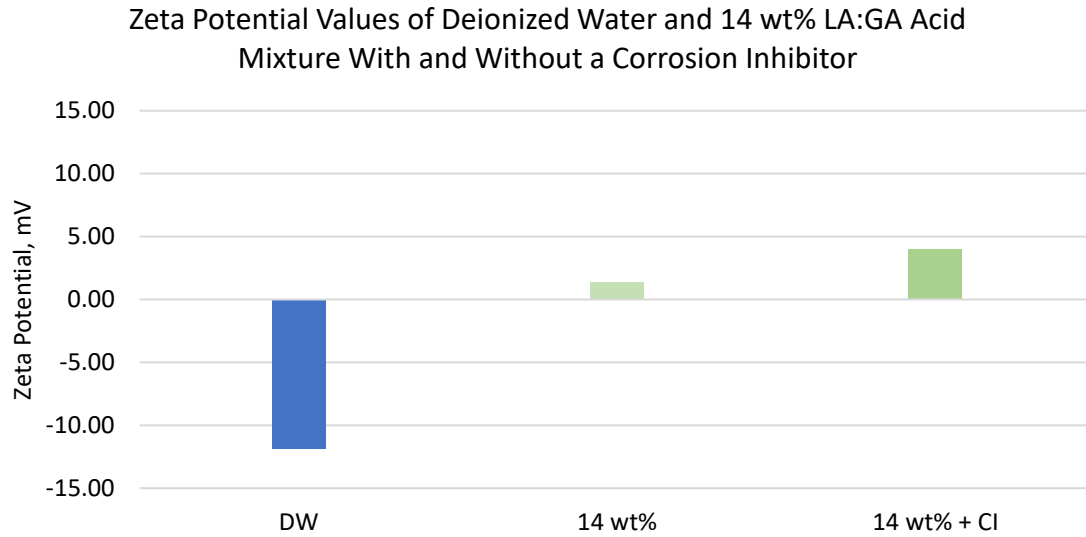


Figure 6.3 Zeta potential values of deionized water and 14 wt% LA:GA acid mixture with and without a corrosion inhibitor after six hours of particle suspension at room temperature.

The addition of the three scale inhibitors showed different results when the zeta potentials were taken after six hours of calcite particle suspension at room temperature using seawater with 4,000 ppm of sulfate. Scale inhibitor A, which is identified as diethylenetriaminepentakis (methyl phosphonic acid) or DTPMP, showed a significant reduction in the zeta potential reading comparing to the case of seawater with 4,000 ppm of sulfate as it was -1 mV. Scale inhibitor B and scale inhibitor C are identified as poly(acrylic acid) sodium salt, and nitrilotris (methylene) (phosphonic acid), respectively. These two inhibitors showed slight decreases in zeta potential values. Figure 6.4 shows the zeta potential values of these solutions compared to the case of seawater with 4,000 ppm of sulfate ions. It should be noted that calcium sulfate needed almost 10 days to precipitate in the acid mixture, and the scale inhibitors were able to inhibit at least 80% of sulfate ions. Based on that, calcium sulfate precipitation had no effect on the 6-hour zeta potential measurements.

Zeta Potential Values of Seawater with 4,000 ppm of Sulfate and 14 wt% LA:GA Acid Mixtures Prepared with the Same Seawater With Scale Inhibitors

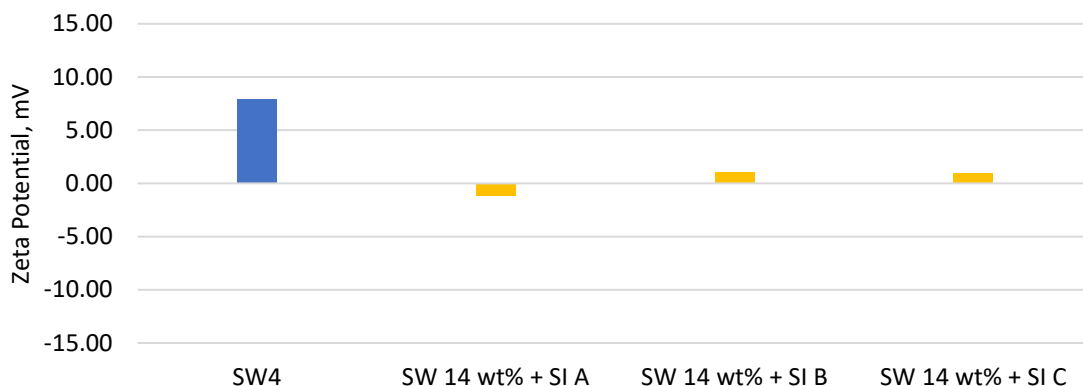


Figure 6.4 Zeta potential values of seawater with 4,000 ppm of sulfate and 14 wt% acid mixtures prepared with the same seawater with scale inhibitors.

The adsorption of hydroxide ions or OH^- would reduce the magnitude of the zeta potential increase. Hydroxide ions can be found in the chemical structure of the inorganic acids of scale inhibitor A and C, as can be seen in Figures 6.5 and 6.6. Scale inhibitor A caused more reduction as it contains more hydroxide ions than scale inhibitor C. Scale inhibitor B is based on acrylic acid, which is part of the carboxylic acids' family. It can be inferred from the results that acrylic acid's molecules had better adsorption than the different cations within seawater composition. This advantage created a competitive adsorption effect, which put scale inhibitor B in advantage to affect the surface charge on the calcite particle surfaces. The chemical structure of scale inhibitor B is shown in Figure 6.7.

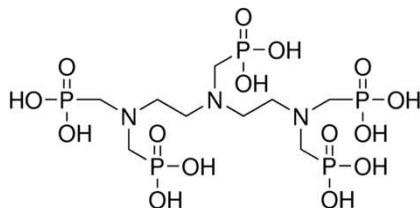


Figure 6.5 The chemical structure of scale inhibitor A.

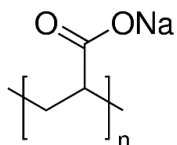


Figure 6.6 The chemical structure of scale inhibitor B.

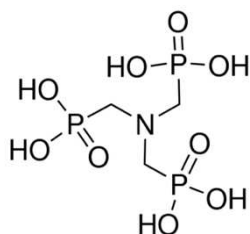


Figure 6.7 The chemical structure of scale inhibitor C.

The last measurements were done on the same previous solutions with the addition of the corrosion inhibitor. In these tests, all additives and seawater ions were mixed and kept with calcite particles for 6 hours. The zeta potential values did not change considerably, compared to the previous cases without the used corrosion inhibitor, except for the case of the mixture with scale inhibitor A. In that case, the zeta potential increased from -1 mV to 2 mV, as can be seen in Figure 6.8. The resulted zeta potential values for the three cases were compared with the zeta potential of the acid mixture with only the corrosion inhibitor. This behavior showed that the corrosion inhibitor molecules, at least at a short conditioning time with calcite particles, had stronger adsorption energy, which overcame the scale inhibitors' affinities to calcite particles.

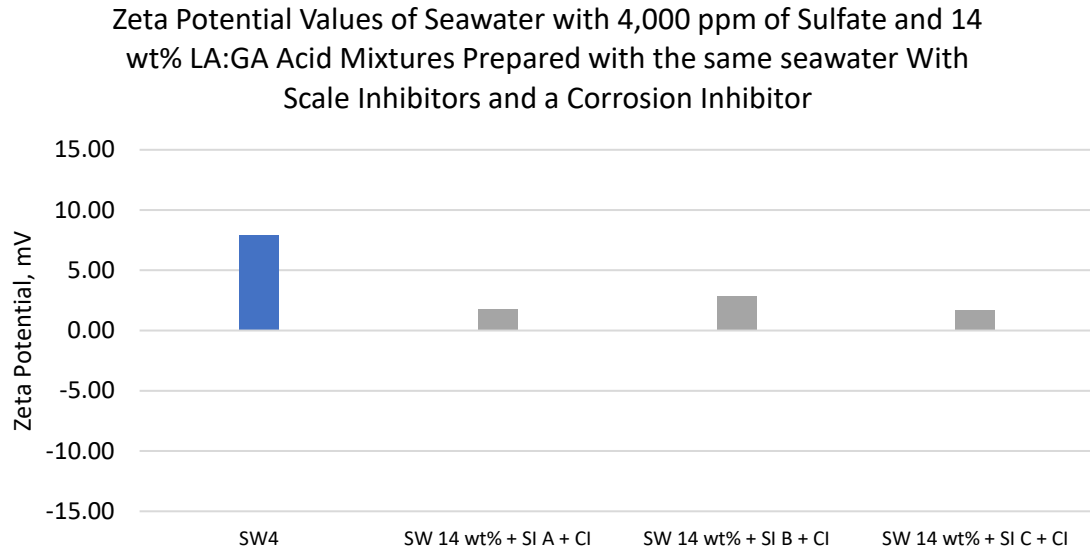


Figure 6.8 Zeta potential values of seawater with 4,000 ppm of sulfate and 14 wt% LA:GA acid mixtures prepared with the same seawater with scale inhibitors and a corrosion inhibitor.

Based on these results, it can be concluded that the LA:GA acid mixture would increase the oil wetting characteristics of a carbonate formation when the acid is spent and intrudes inside the treated formation due to carboxylate molecules. Additionally, seawater usage would have the same negative effect due to the high salinity created from the different ions dissolved in solution. The addition of scale and corrosion inhibitors would alter the rock wettability toward the oil-wetting phase. A recommended procedure is provided in Chapter 8 to reduce the negative effect of these acids, ions, and chemicals.

6.3 Zeta Potential Measurements After Ten Days

Conditioning time was also set to ten days to cover the late stages of flowing back a treated well. As mentioned before, spent acid invasion has a direct effect on production enhancement and recovery of spent acid. Spent acid recovery can be affected by the acid additives' surface-active properties and the formation's rock wettability. Leaving the spent acid mixture with its additives for a more extended period of time could have different outcomes than a few hours.

Different ions and additives' molecules within the solution can cause the equilibrium state to take several days to be reached. The final adsorption on calcite particles and effects on wettability can be concluded when all ions and molecules within the solution are in equilibrium. For example, calcium sulfate precipitation needed a few days to precipitate in the acid mixtures prepared with seawater. Before precipitation, sulfate and calcium ions were free in solution and free to proceed with bonding together.

Figure 6.9 shows a comparison between zeta potential measured after six hours with zeta potential measured after ten days for the case of deionized water and seawater with different sulfate ion concentrations. As can be seen, the negative effect of increasing the zeta potential values was noticeable for the seawater cases due to the salinity of the solution. However, the magnitude of zeta potential values was different due to different cations and anions being adsorbed differently after reaching ion stability.

Extending the conditioning time changed the trend between increasing the sulfate ion concentrations and the measured zeta potential values. Sulfate ions in the seawater composition were obtained through dissolving sodium sulfate salt (Na_2SO_4). Increasing sulfate ion concentrations were associated with increasing the positively charged cations of sodium. Thus, increasing the conditioning time gave sodium ions enough time to be adsorbed on the suspended calcite particle surfaces.

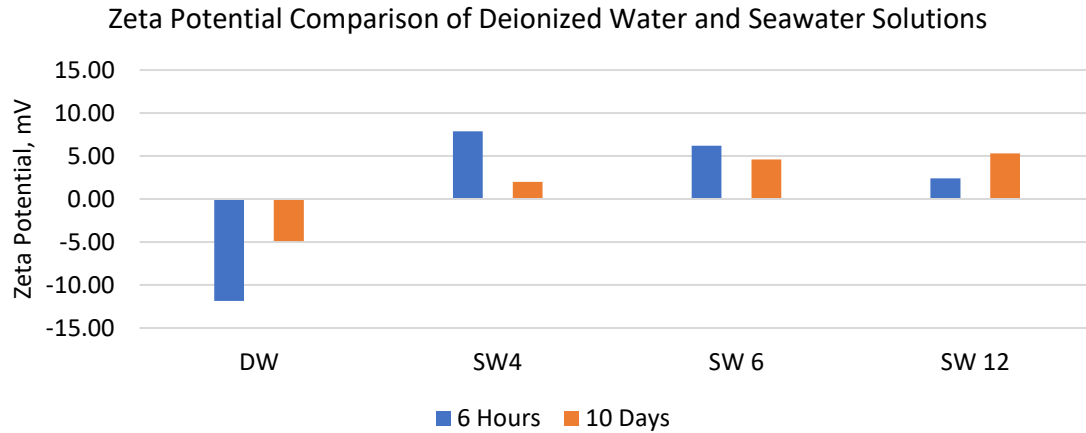


Figure 6.9 Zeta potential values of deionized water and seawater solutions after six hours and ten days of particle suspension at room temperature.

Ion stability and equilibrium effects on the suspended calcite particles were also noticeable in the other cases. When 14 wt% LA:GA acid mixture solutions were tested after ten days of suspending the calcite particles, the zeta potential decreased to almost -1 mV. This value was obtained for both solutions with and without the corrosion inhibitor. Although this decrease of zeta potential was favorable, it was still higher than the zeta potential value measured for the case of suspending calcite particles in deionized water. Figure 6.10 shows the zeta potential of the mentioned cases.

The last six cases were prepared with seawater with 4,000 ppm of sulfate ion concentrations, three solutions containing only a scale inhibitor of A, B, or C and another three duplicate solutions with the corrosion inhibitor. The zeta potential values for all cases were different from the values obtained from the six-hour zeta potential measurements. Accordingly, there are two possible explanations for this alteration in zeta potential values. The first one is the precipitation of micro-sized calcium sulfate precipitation, and the second one is the ion stability and equilibrium effect. In these cases, 20% of sulfate ions were free to complex with free calcium

ions in solution to producing a calcium sulfate compound. Figure 6.11 shows the zeta potential values of these cases.

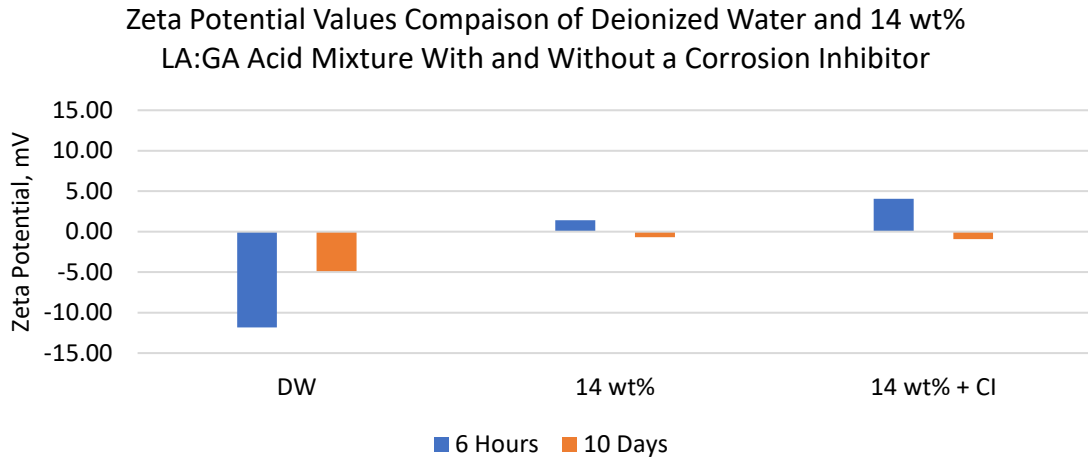


Figure 6.10 Zeta potential values of deionized water and 14 wt% LA:GA acid mixture with and with a corrosion inhibitor after six hours and ten days of particle suspension at room temperature.

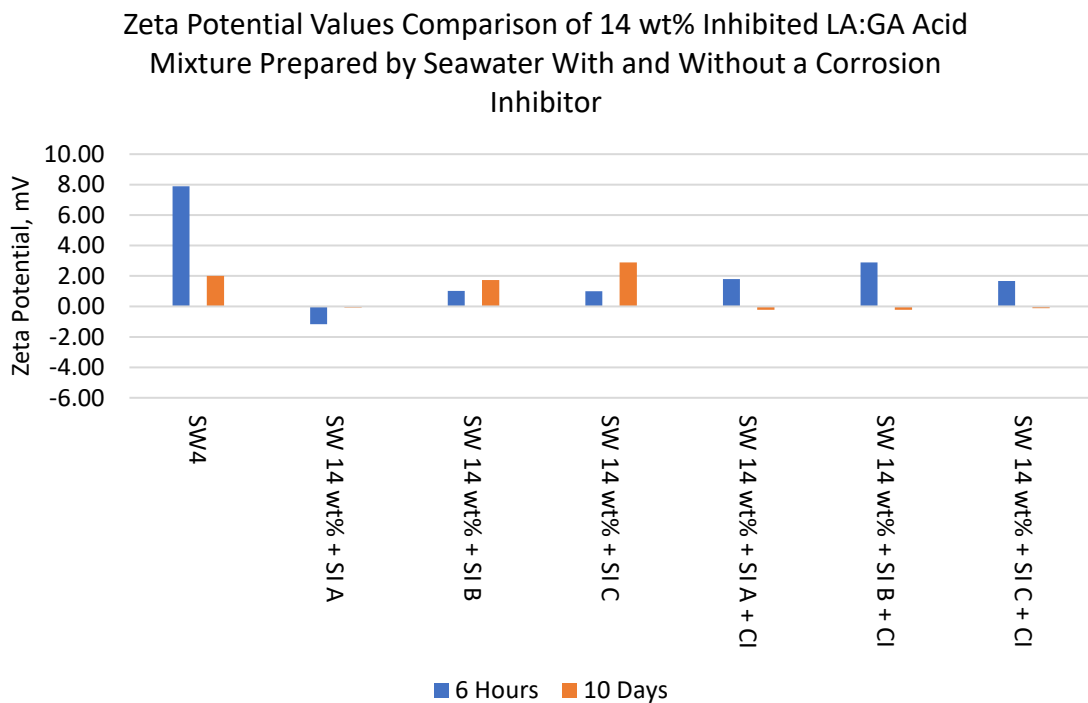


Figure 6.11 Zeta potential values comparison of 14 wt% inhibited LA:GA acid mixture prepared by seawater with and without a corrosion inhibitor.

CHAPTER 7

COREFLOOD TEST: RESULTS AND DISCUSSION

This chapter discusses and evaluates the different LA:GA acid mixtures' abilities to stimulate a carbonate formation by mimicking an acidizing treatment through a coreflood apparatus. A coreflood apparatus can simulate an acidizing treatment by pumping different fluids through a saturated core that is under reservoir conditions of pressure and temperature. The main goals of conducting this test were to prove the LA:GA acid mixtures' ability to dissolve calcium carbonate without any by-product precipitation and to identify the optimum acid concentration and application temperature that would give the minimum pore volume needed to achieve breakthrough. Accordingly, nine tests were performed by pumping different acid mixtures, applying different test temperatures, and utilizing different injecting rates. Table 7.1 summarizes the tests performed with the coreflood apparatus.

The injected acid's ability to create dominant wormholes is the key to a successful carbonate matrix acidizing treatment. When the acid is injected, large pores consume most of the acid and start to get larger than the smaller pores do. As more acid is pumped, these large pores receive more acid and grow in length until wormholes are formed. Dominant wormholes are one of several different possible wormhole patterns that can occur due to acid dissolution. These patterns, shown in Figure 7.1, include face dissolution, conical wormholes, dominant wormholes, ramified wormholes, and uniform dissolution (Economides and Boney 2000; Akanni and Nasr-El-Din 2016). Formation of these patterns is highly dependent on the injection rate, reaction kinetics, flow geometry, formation heterogeneity, and fluid loss rate (Fredd and Fogler 1998; Economides and Boney 2000; Akanni and Nasr-El-Din 2016; Pandey et al. 2018).

Table 7.1 Coreflood Tests Along with Pore Volumes Needed to Breakthrough The Tested Cores.

Parameter	1	2	3	4	5	6	7	8	9
Por Volume (cm ³)	8.12	6.21	5.96	5.95	6.33	6.54	6.04	6.40	6.39
Porosity (%)	13.71	12.13	11.62	11.33	12.17	12.79	11.84	12.50	12.46
Initial Permeability (md)	3.01	3.50	5.00	3.70	4.12	3.40	7.20	1.54	3.02
Injected Rate (cm ³ /min)	1	4	3	2	3	3	3	3	3
Dilution water	DW	DW	DW	DW	DW	DW	DW	DW	SW
Total Acid Concentration of 1:1 molar ratio of LA & GA (wt%)	20	20	20	20	14	27	20	20	20
Temperature (°F)	200	200	200	200	200	200	300	150	200
Pore Volume to BT (cm ³)	Face	3.60	3.45	1.54	4.82	2.14	4.01	4.22	5.48
Final Permeability (md)	Dissolution					> 1000 md			

In matrix acidizing, the main goal is to lower the skin effect and to increase or restore production. Manipulating acid dissolution patterns is a critical step toward developing dominant wormholes. These wormholes are essential to increase the permeability of the near-wellbore zone. In fact, in many cases, matrix acidizing cannot be very beneficial without this optimum connection between formation and wellbore.

7.1 Injection Rate Effects

The optimum injection rate can lead to the creation of dominant wormholes as the acid is consumed at the tip of the evolving flow channel and penetrates the channel (Al-Duailej et al. 2013). At low injection rates, a high volume of the acid would be spent on the rock surface, and a face dissolution or a conical wormhole would occur. At a very high injection rate, a ramified wormhole can occur, which consists of many small branches, due to the acid being forced inside small pores (Fredd and Fogler 1998; Al-Duailej et al. 2013; Akanni and Nasr-El-Din 2016). A 20 wt% of the two-acid LA:GA mixture was tested at 200°F using different injection rates of 1, 2, 3,

and 4 cm³/min to investigate the sensitivity of the two-organic acid mixture's injection rate on carbonate formations.

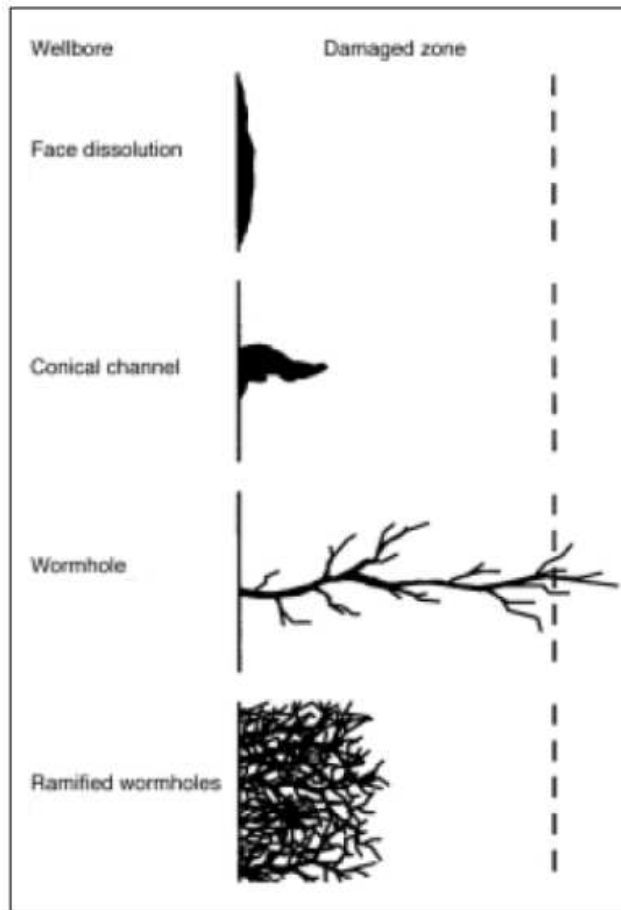


Figure 7.1 Schematic of common dissolution patterns. Maintaining the optimum injection rate can lead to dominant wormhole pattern (From Economides and Boney 2000).

First, the LA:GA acid mixture was tested at 1 cm³/min where a face dissolution was anticipated due to the low injection rate and the lower reactivity of the LA:GA acid mixture at 200°F. The solubility tests illustrated that the acid reactivity was a function of temperature and total acid concentration. Injecting the acid at 1 cm³/min showed a significant pressure increase at the inlet face of the core, which extended for several pore volumes without achieving breakthrough in the core. This increase in the pressure was contributed to the acid mixture reaction with calcium

carbonate and the release of CO₂ gas. The failure of achieving a breakthrough was attributed to the face dissolution pattern that occurred due to the acid mixture being spent on the core inlet. The test was stopped in the middle of running the acid treatment due to the steady increase in the pressure drop across the core after injection of more than 10 PV. The core was removed from the core holder, and face dissolution was observed on the inlet face, as can be seen in Figure 7.2.



Figure 7.2 Test 1 core inlet face before and after treatment showing face dissolution due to low injection rate.

Based on the previous results, the injection rate was increased to 2, 3, and 4 cm³/min at 200°F. Figures 7.3 to 7.5 show the pressure drop profiles along with the regained pore volume amounts to breakthrough the cores. As can be seen in the pressure drop profiles, the pressure drops increased significantly with acid injection due to the acid reaction on the inlet face and due to the mixture viscosity. During the reaction, the pressure drops kept increasing until a complete penetration of the core was achieved. Once reaching a breakthrough, the pressures started to decrease and level off around five psi differential.

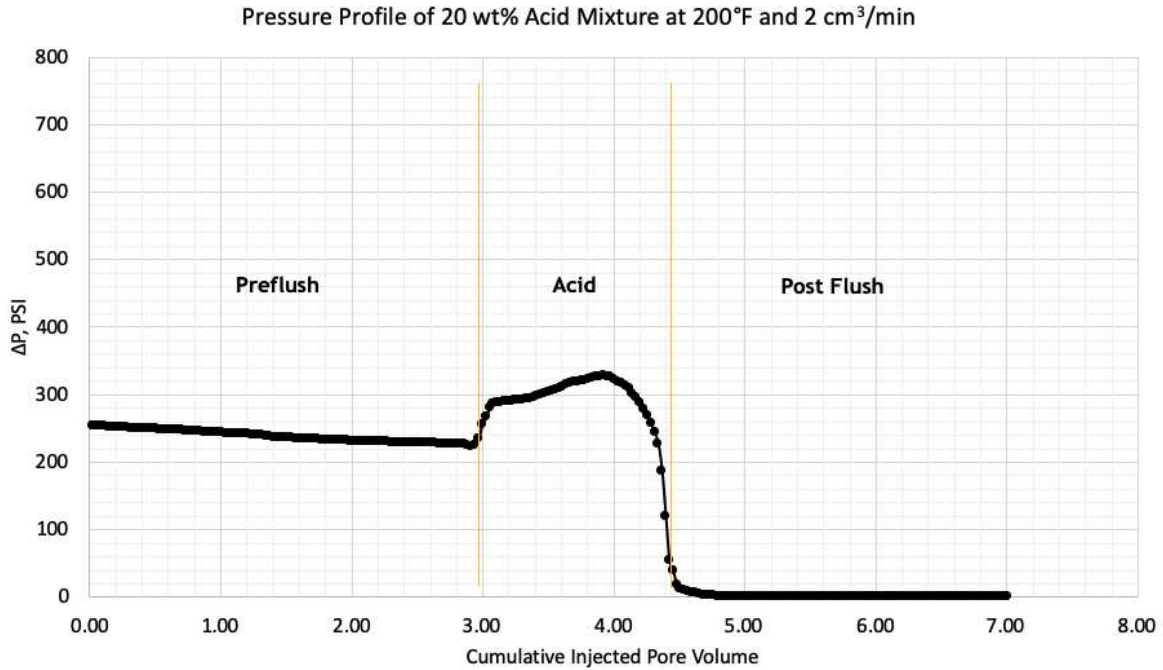


Figure 7.3 Pressure drop across a tested core at 200°F using 2 cm³/min of 20 wt% (1:1) LA:GA acid mixture.

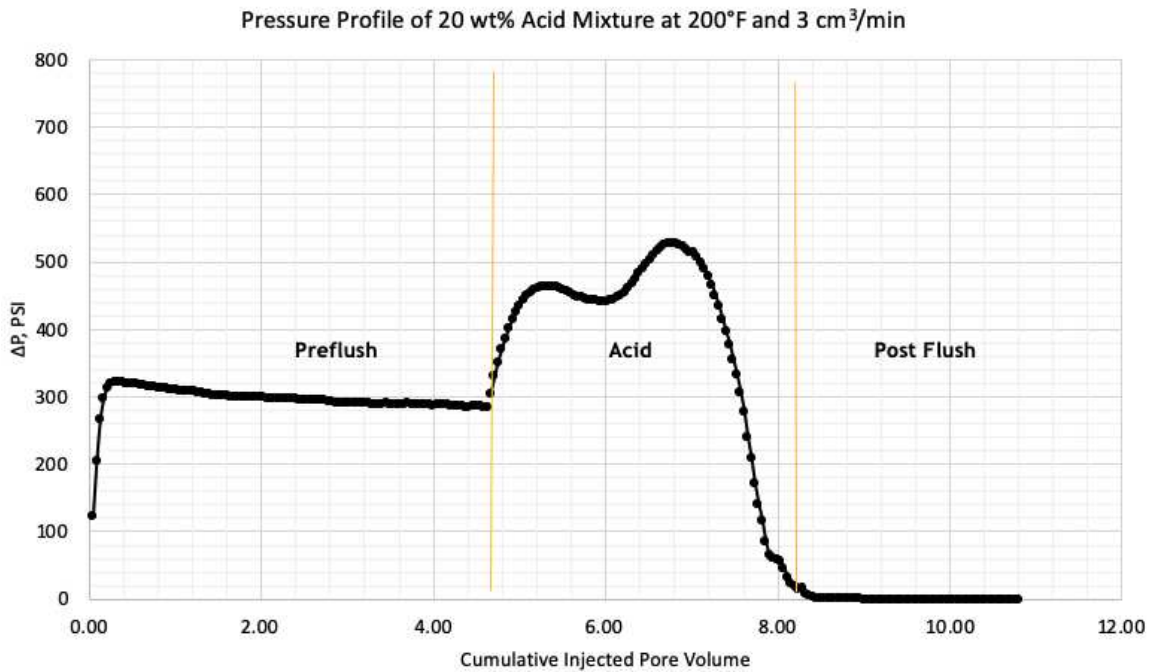


Figure 7.4 Pressure drop across a tested core at 200°F using 3 cm³/min of 20 wt% (1:1) LA:GA acid mixture.

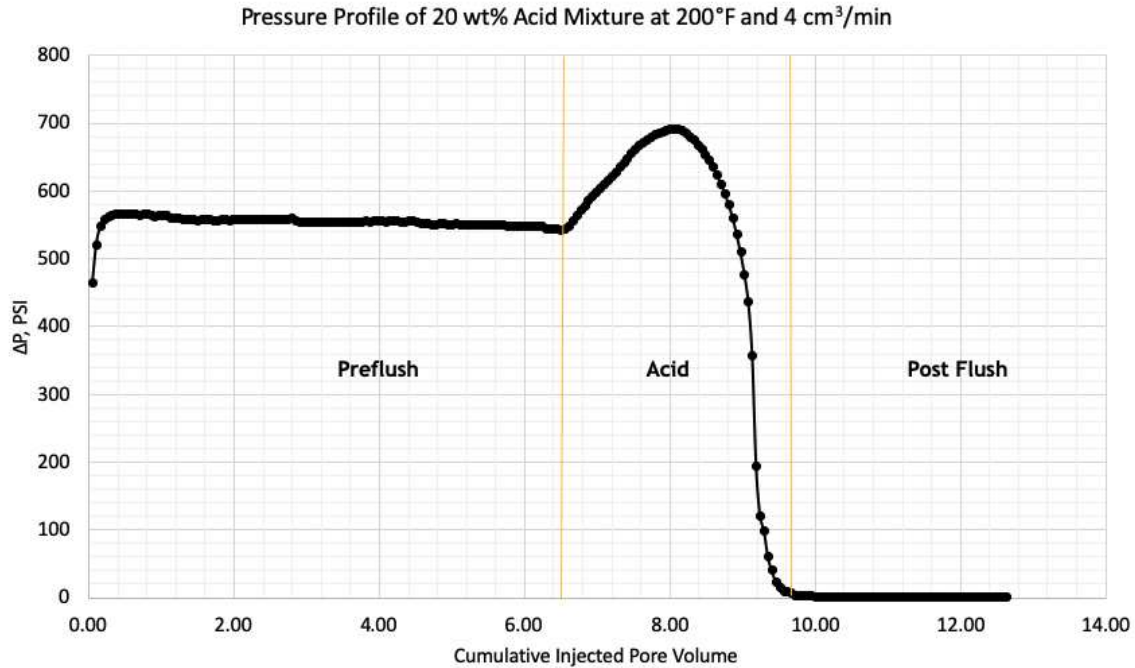


Figure 7.5 Pressure drop across a tested core at 200°F using 4 cm³/min of 20 wt% (1:1) LA:GA acid mixture.

The minimum pore volumes needed to breakthrough the tested cores at 2, 3, and 4 cm³/min were 1.54, 3.45, and 3.60 PV, respectively. The increase in flow rates resulted in higher pore volumes needed to breakthrough as more small branches would be created instead of one dominant wormhole with a few small branches. Many wormholes and branches can cause a ramified dissolution pattern. Based on these results, the optimum injection rate for the tested mineralogy at the mentioned conditions would be 2 cm³/min.

7.2 Total Acid Concentration Effects

The total acid mixture concentration was also manipulated to investigate its effect on stimulating the limestone core. Dissolving the core's matrix material and generating a wormhole depends on the acid reactivity, which is a function of acid concentration and application temperature. An increase in the total acid mixture concentration would increase the acid mixture's reactivity and dissolving capacity on the core's matrix. As mentioned before, the lactic acid-

carbonate dissolution rate is higher than the gluconic acid-carbonate dissolution rate. Thus, an increase in the total acid mixture concentration resulted in an increase in the number of moles of lactic acid in solution since the acid mixture was in a 1:1 acid molar ratio. Therefore, the increase in the total acid mixture concentration was reflected in the required pore volumes to breakthrough the tested cores.

The two-acid LA:GA mixture was prepared at 14, 20, and 27 wt% and tested using 3 cm³/min of injection rate at 200°F. The results showed that more pore volumes were needed to breakthrough the tested core at low acid strength due to lower reactivity. Low reactivity affects the required time to generate a wormhole and to dissolve the matrix materials. At higher acid strength, fewer pore volumes were needed to breakthrough due to the higher dissolving capability of the acid, which was shown before in the acid solubility test section (Section 4.1.3). Figures 7.6 to 7.8 show the pressure drops across the tested cores with 14, 20, and 27 wt% acid mixtures at 200°F, respectively.

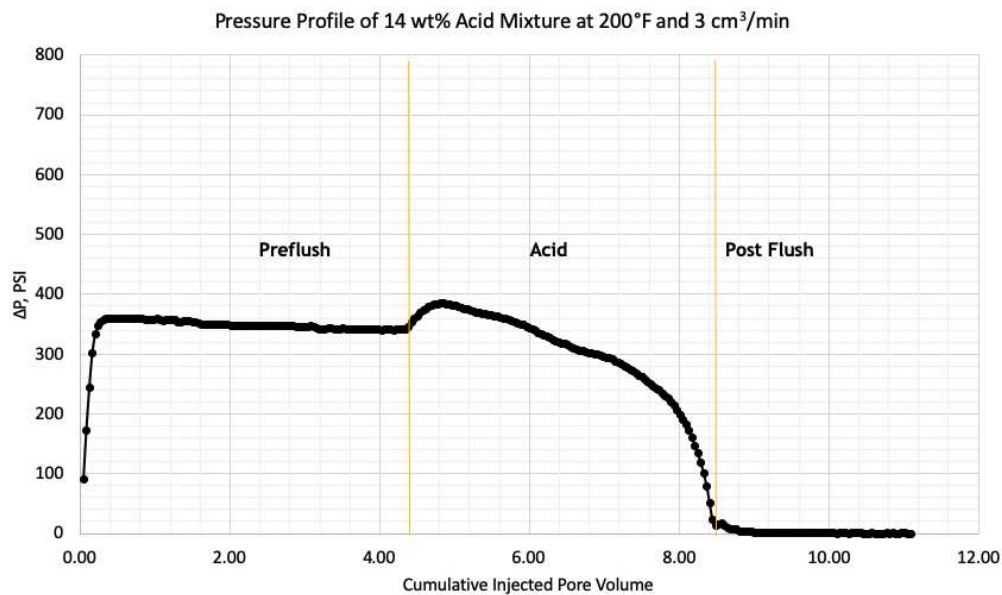


Figure 7.6 Pressure drop across a tested core at 200°F using 3 cm³/min of 14 wt% (1:1) LA:GA acid mixture.

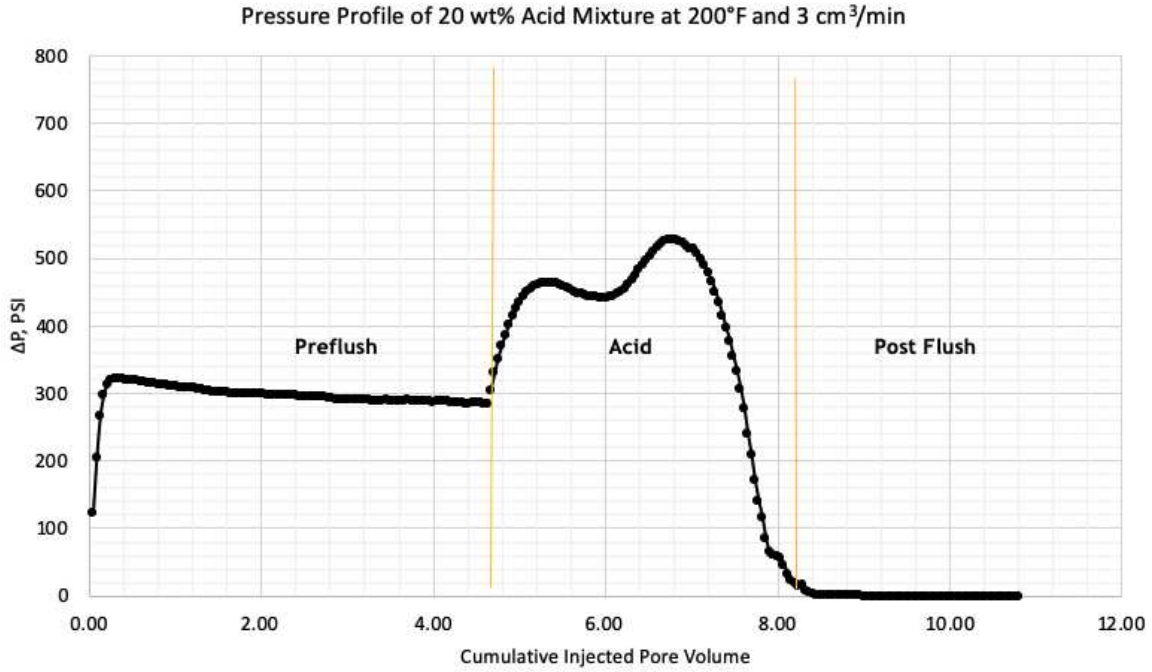


Figure 7.7 Pressure drop across a tested core at 200°F using 3 cm³/min of 20 wt% (1:1) LA:GA acid mixture.

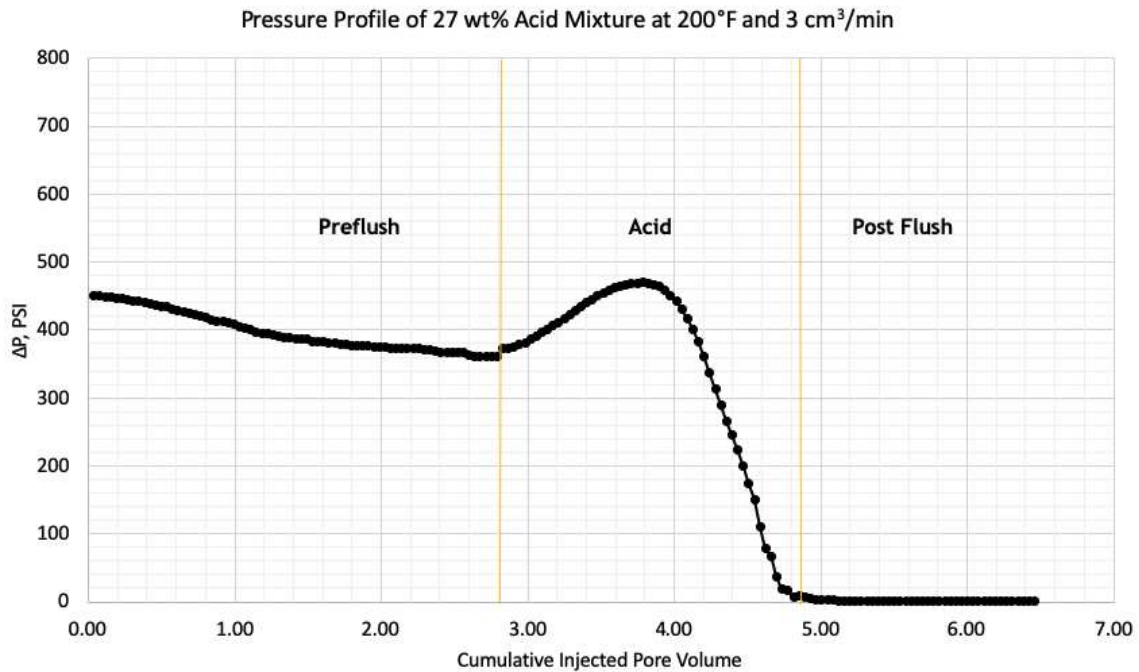


Figure 7.8 Pressure drop across a tested core at 200°F using 3 cm³/min of 27 wt% (1:1) LA:GA acid mixture.

7.3 Test Temperature Effects

The acid solubility test showed that the acid mixture could dissolve more crushed calcite when the temperature increased. This increase in dissolving capacity was attributed to the increase in the acid mixture reactivity due to higher enhanced ion mobility in the solution that would be reflected in an increase in calcium ion diffusion rates and the acid's diffusivity. For example, the lactic acid diffusion coefficient at 80°F is $8.289 \times 10^{-6} \text{ cm}^2/\text{s}$ while it is $4.11 \times 10^{-5} \text{ cm}^2/\text{s}$ at 250°F, which indicates faster flux of the acid passes through each unit of cross-section per unit of time from one region to another.

In low temperature applications, the LA:GA acid mixture would dissolve fewer matrix materials than at high temperatures. However, exceeding the optimum application temperature would result in high dissolving power, which would cause more acid consumption than needed. This behavior was clearly illustrated through the coreflood test, where a 20 wt% LA:GA acid mixture was tested at $3 \text{ cm}^3/\text{min}$ at low and high test temperatures. At low temperature (150°F), the acid mixture was able to create a small wormhole after consuming a large volume of the acid mixture. At a higher temperature (300°F), the acid mixture consumed a large volume of the core matrix to generate a large wormhole due to a higher matrix dissolving ability. However, at the optimum temperature (200°F), less volume was needed to penetrate the core completely. Figures 7.9 to 7.11 show the pressure drop profiles for the coreflood tests at 150, 200, and 300°F, respectively.

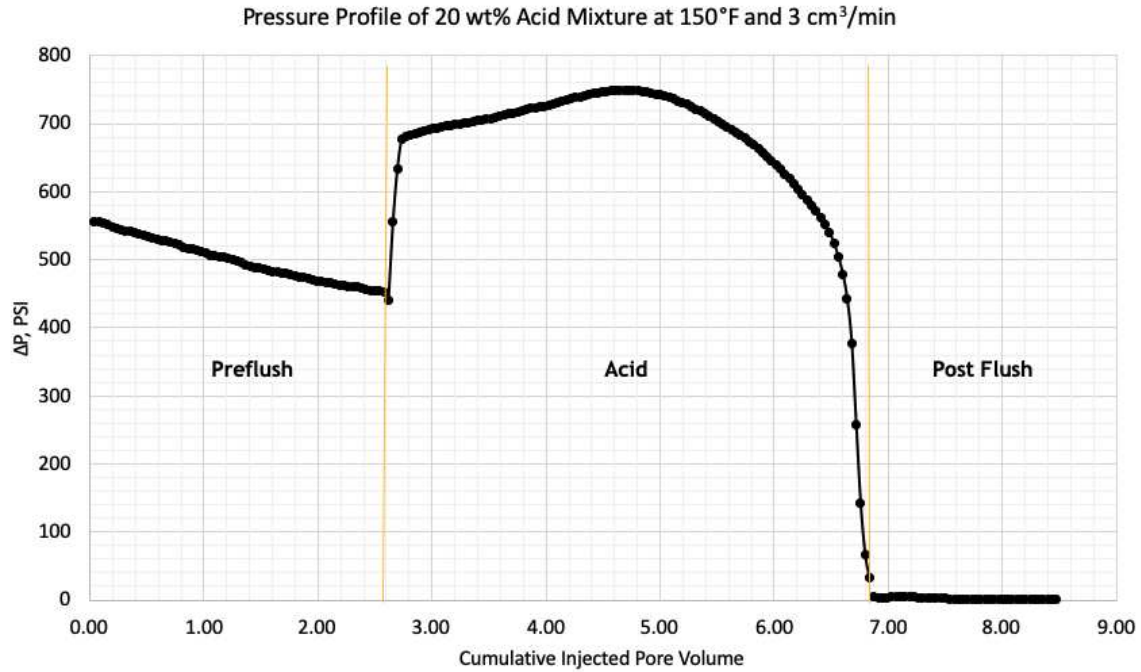


Figure 7.9 Pressure drop across a tested core at 150°F using 3 cm³/min of 20 wt% (1:1) LA:GA acid mixture.

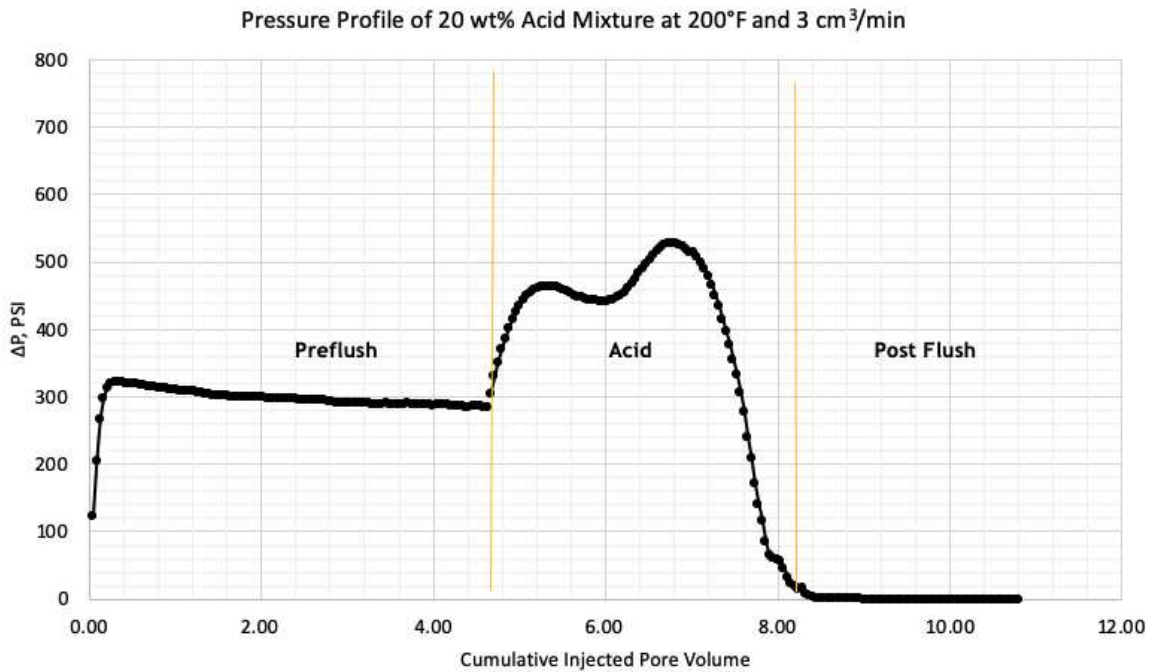


Figure 7.10 Pressure drop across a tested core at 200°F using 3 cm³/min of 20 wt% (1:1) LA:GA acid mixture.

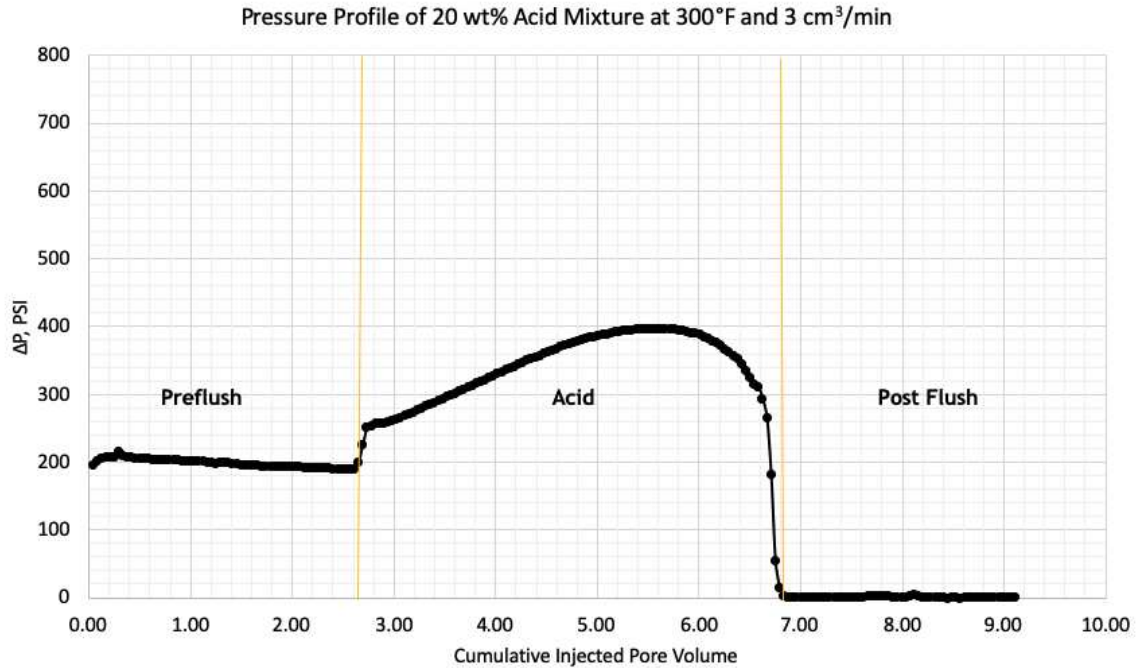


Figure 7.11 Pressure drop across a tested core at 300°F using 3 cm³/min of 20 wt% (1:1) LA:GA acid mixture.

As can be seen from Figures 7.9 and 7.11, 4.22 and 4.01 PV were needed to breakthrough the cores tested at 150 and 300°F, respectively, due to the change in the acid reactivity. The results showed that the minimum pore volume needed to breakthrough was obtained at 200°F as 3.45 PV was needed. At 300°F, the acid mixture became highly reactive and would dissolve more matrix materials, which caused large wormholes with too many small branches. At 150°F, more time was required for the acid mixture to breakthrough due to slower reactivity of the acids at low temperatures. Figure 7.12 shows the inlet faces of cores tested at 200 and 300°F, where the difference in the primary propagated wormhole size can be seen.

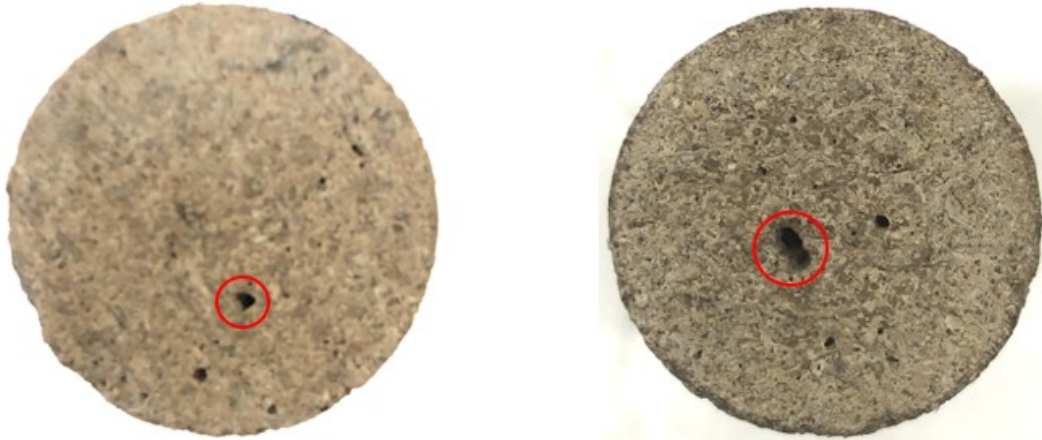


Figure 7.12 The inlet faces of cores tested at 200°F (left) and 300°F (right), where it can be seen the difference in the main propagated wormhole size.

7.4 Seawater Usage Effects

A final test was run by preparing the acid mixture using seawater that contained 4,000 ppm of sulfate with a scale inhibitor. The objective of this test was to determine the seawater ions effect in dissolving the matrix materials and in generating a wormhole in the tested core. The test was run using a 20 wt% acid mixture prepared by seawater using an injection rate of 3 cm³/min at 200°F. The results, illustrated in Figure 7.13, showed that a breakthrough would be obtained with 5.48 pore volumes.

The increase in the needed pore volume to breakthrough, compared to the one prepared with deionized water, is explained by the effect of seawater ions on the calcium diffusion rate from the matrix. This was also reflected by the less dissolving capability shown in the acid solubility test section. The lower solubility occurred due to the adverse effects of the different salts included in the synthetic seawater such as sodium chloride, calcium chloride, magnesium chloride, and sodium sulfate. Al-Khaldi et al. (2003) mentioned that organic acid reactions with calcite is thermodynamically limited by the presence of different ions in solution. This limitation can reduce the calcium ion concentration gradient, which would lower the acid dissolution rate. Nevertheless,

collected fluid effluent samples from the coreflood test using the acid mixture prepared by seawater did not show any precipitation from the calcium sulfate compound.

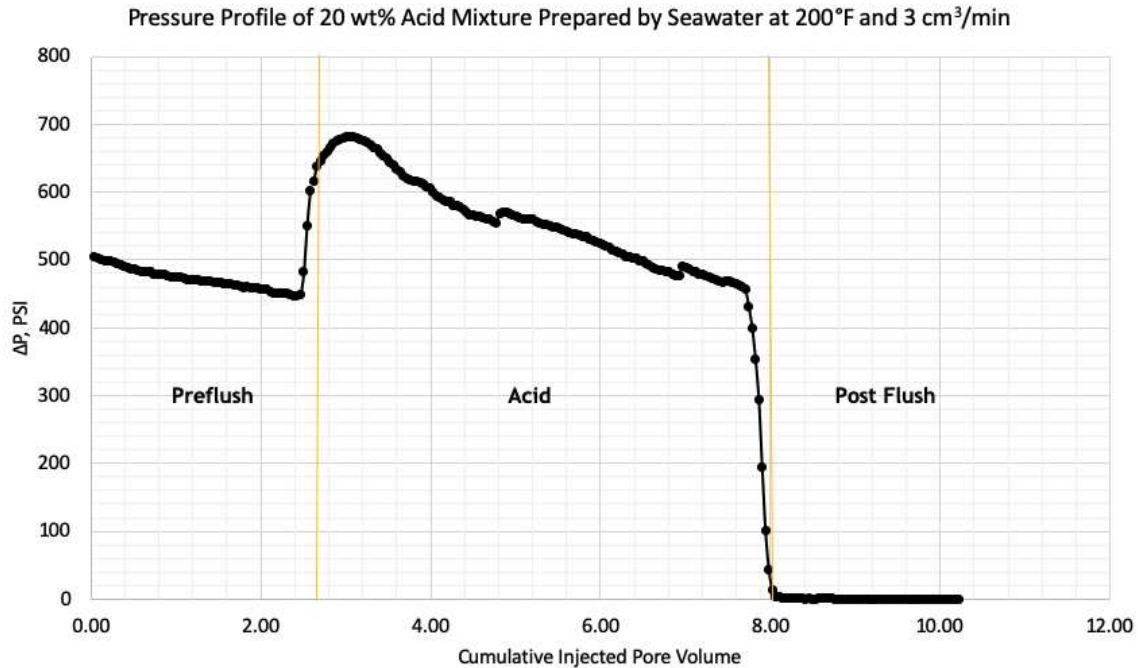


Figure 7.13 Pressure drop across a tested core at 200°F using 3 cm³/min of 20 wt% (1:1) LA:GA acid mixture prepared by seawater.

This test outlined the behavior of the acid mixture when prepared by seawater to stimulate carbonate formations. The risk of calcium sulfate precipitation was minimized by utilizing an appropriate scale inhibitor that would chelate 80% of sulfate ions in solution when seawater with up to 6,000 ppm was used. Additionally, more acid mixture volume was needed to penetrate the core and to generate the desired wormhole.

7.5 CT Scans of a Core Flood by a 20 wt% Acid Mixture

CT scans were performed on different cores to examine the generated wormhole inside the tested cores. Figures 7.14 and 7.15 show CT scans of a low permeability Indiana limestone core before and after being treated with 20 wt% acid mixture using 3 cm³/min at 200°F. As can be seen,

one single dominant wormhole was generated with small branches evolving around it. The CT scan results of the core before and after the test showed that there was not any major structural destruction of the core other than the generated wormhole and the spread branches. These results prove that the tested acid mixture can bypass formation damage within the wellbore area and promote hydrocarbon flow from the treated formation toward the wellbore.

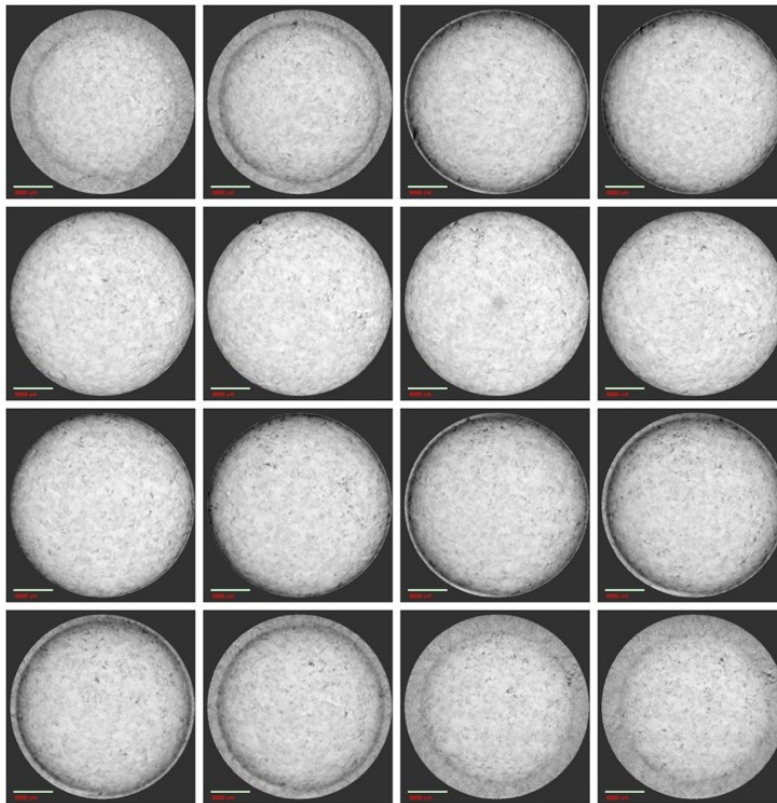


Figure 7.14 CT scans of a low permeability Indiana Limestone core before being treated with 20 wt% acid mixture using 3 cm³/min at 200°F. Each scan is approximately 1/4'' into the core moving from the injection end to the other side, top left to bottom right.

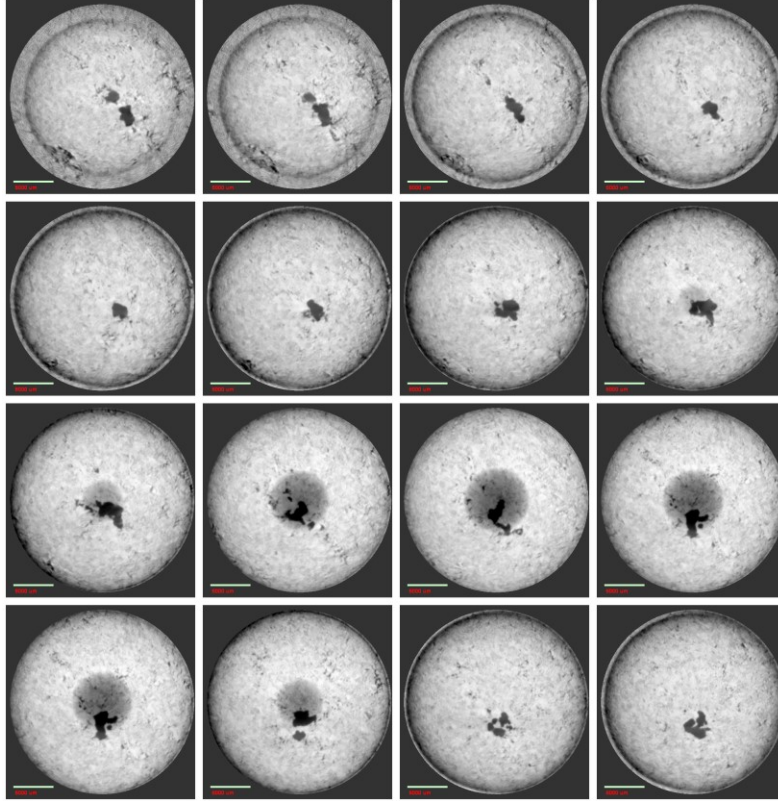


Figure 7.15 CT scans of a low permeability Indiana Limestone core treated with 20 wt% acid mixture using $3 \text{ cm}^3/\text{min}$ at 200°F . Each scan is approximately $1/4''$ into the core moving from the injection end to the other side, top left to bottom right.

CHAPTER 8

FIELD IMPLICATIONS: APPLICATION AND DISCUSSION

This chapter discusses and illustrates the application and benefits of implementing the lactic and gluconic acid mixture in oil and gas acidizing operations. Although this mixture was intended to be applied in matrix acidizing treatment, a brief discussion about acid fracturing is also included in this chapter to show the applicability of the mixture for acid fracturing treatments. At the end of the chapter, a comparison between HCl and the acid mixture is provided to illustrate the benefits and drawbacks of both acids in terms of acid reactivity, formation damage, additives used, and corrosion consequences.

8.1 Application

In carbonate formations, hydraulic fracturing, acid fracturing, and matrix acidizing are the most commonly used techniques to improve a well's productivity. However, matrix acidizing is the most effective technique in terms of treatment cost if it can lower the skin factor to -2 or -3 (Thomas and Morgenthaler 2000). Skin factor reduction can be easily noticed in the IPR curve for any well, where matrix acidizing can reduce the well's skin factor and shift the inflow curve to the right. This shift would increase the well's productivity with a lower bottom hole pressure (Economides and Boney 2000). The following two sections highlight the two commonly used techniques involving the pumping of acids, which are matrix acidizing and acid fracturing.

8.1.1 Matrix Acidizing Wormhole Sensitivity to Different Parameters

Matrix acidizing is the process of injecting a dissolver that is pumped below the fracturing pressure to remove and bypass formation damage. The main goal of matrix acidizing is to recover

or to enhance the treated formation permeability. Matrix acidizing is characterized by a high reaction rate between the injected acid and the treated formation, which allows the acid to penetrate through large pores to generate a nonuniform pathway. As the reaction proceeds, the wall of the pathway gets more extended, and the tip of the pathway gets longer than existing natural fractures. Accordingly, the new pathway becomes dominant for hydrocarbon flow toward the wellbore (Thomas and Morgenthaler 2000; Akanni and Nasr-El-Din 2016). This process is identified as the generation of dominant wormholes and is the main feature of any acid-stimulated formation.

Lund et al. (1973b; 1975) measured the kinetics of HCl reaction with carbonate and dolomite and found that the reaction rate (r_{HCl}) is a function of the reaction rate constant (E_f), acid concentration (C_{HCl}), and the magnitude of the reaction (α). The reaction rate is shown in Equation 8.1:

$$-r_{\text{HCl}} = E_f C_{\text{HCl}}^\alpha \quad (8.1)$$

$$E_f = f(\text{formation, temperature}) \quad (8.2)$$

The main difference between a mineral acid (i.e. HCl) and weak acids is the dissociation extent. HCl dissociates completely in water to produce hydrogen ions that attack the treated formation. Weak acids cannot reach a complete dissociation stage, which makes them weaker than HCl during the same hydrogen ions attack. Therefore, Equation 8.1 can be modified to be suitable for weak acids by adding the dissociation constant of weak acids (K_d). Equation 8.3 shows the reaction rate of weak acids:

$$-r_{\text{weak acid}} = E_f K_d^{\alpha/2} C_{\text{Weak acid}}^{\alpha/2} \quad (8.3)$$

Different studies have been performed to relate the different parameters in the acid reaction toward the critical pore size area that can serve as the initiation of the wormhole. These parameters include injection rate, acid concentration, formation permeability, formation type, and formation temperature. One of the most known derivations to find the critical pore size area was developed by Wang (1993) and Wang et al. (1993). Equation 8.4 shows the final result of the mentioned studies:

$$A_T = 0.93[D_a k]^{2/3} \quad (8.4)$$

In Equation 8.4, A_T is the critical pore size area, $D_a = E_f C_o^{m-1}/u$, and k is the formation permeability. Based on this, A_T is a function of acid concentration (C_o), formation temperature (empirical in E_f), and injection rate (u). Since these three factors have a direct effect on A_T , then the required pore volume to breakthrough is also manipulated by these factors. In the field scale, pore volumes needed to breakthrough are represented by acid volume pumped in the wellbore.

Two parameters can be controlled to drive the acid reaction toward the optimum conditions and include total acid concentration and injection rate. Total acid concentration can be constrained with acid stock expenses, and regulation and environmental rules. In acid fracturing operations, the formation temperature can be controlled by injecting a viscous pad that can initiate the fracture and cool down the formation. However, in matrix acidizing, a preflush fluid can be injected to serve the same purpose.

In this research, coreflood testing was done with different injection rates, test temperatures, and total acid concentrations. These variations were performed to illustrate the effect of these parameters on the required pore volumes to breakthrough the tested cores. The consumed pore

volume amount is related to the acid mixture volume needed to be pumped during matrix acidizing operations in the field.

The coreflood results showed that the acid reactivity is a function of total acid concentration and formation temperature. This is in agreement with Equation 8.3 that shows the acid reactivity increases as the total acid concentration and temperature increase. However, exceeding the optimum acid reactivity would lead to more matrix solubility, which would be reflected in a ramified dissolution pattern. In this case, extra acid results in producing inefficient large wormholes. This behavior is also shown in Equation 8.4 that shows that the wormhole cross-sectional area increases as total acid concentration and formation temperature increase.

Figures 8.1 and 8.2 show the temperature and total acid concentration effects on the required pore volumes (PV) to breakthrough. As can be seen in Figure 8.1, at low temperature, 4.22 PV were needed to breakthrough due to the low reactivity of the acid mixture with the core. At high temperature, the acid mixture consumed a large volume of the acid mixture to generate a large wormhole due to a higher matrix dissolving ability. However, at the optimum temperature of 200°F, less volume was needed to penetrate the core completely.

According to the coreflood results and Equation 8.4, the change in temperature would have a direct impact on the needed pore volume to breakthrough. Based on that, the injection rate should be modified to adjust to this change in acid reactivity. An increase in temperature should result in a corresponding increase in the optimum injection rate. This trend implies that in field operations deep formations should be acidized at a higher rate comparing to shallow formations to correspond to the associated temperature changes. This behavior is also noticeable in reported HCl experiments on dolomite cores, as can be seen in Figure 8.3 (Hill and Schechter 2000). As the temperature increased, the optimum injection rate increased.

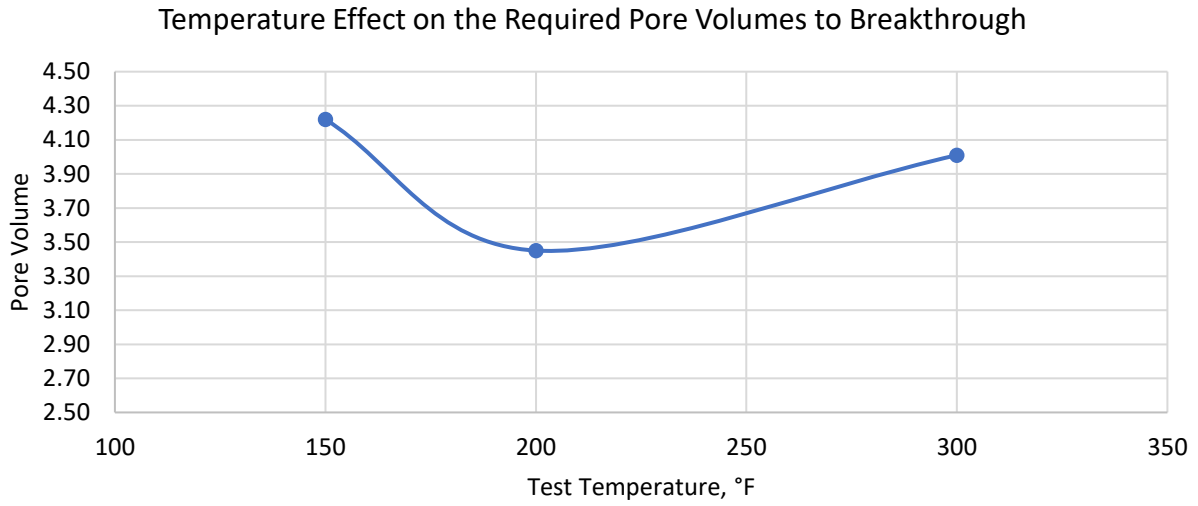


Figure 8.1 Temperature effect on the required pore volumes to breakthrough using a flow rate of 3 cm³/min and a total LA:GA acid concentration of 20 wt%.

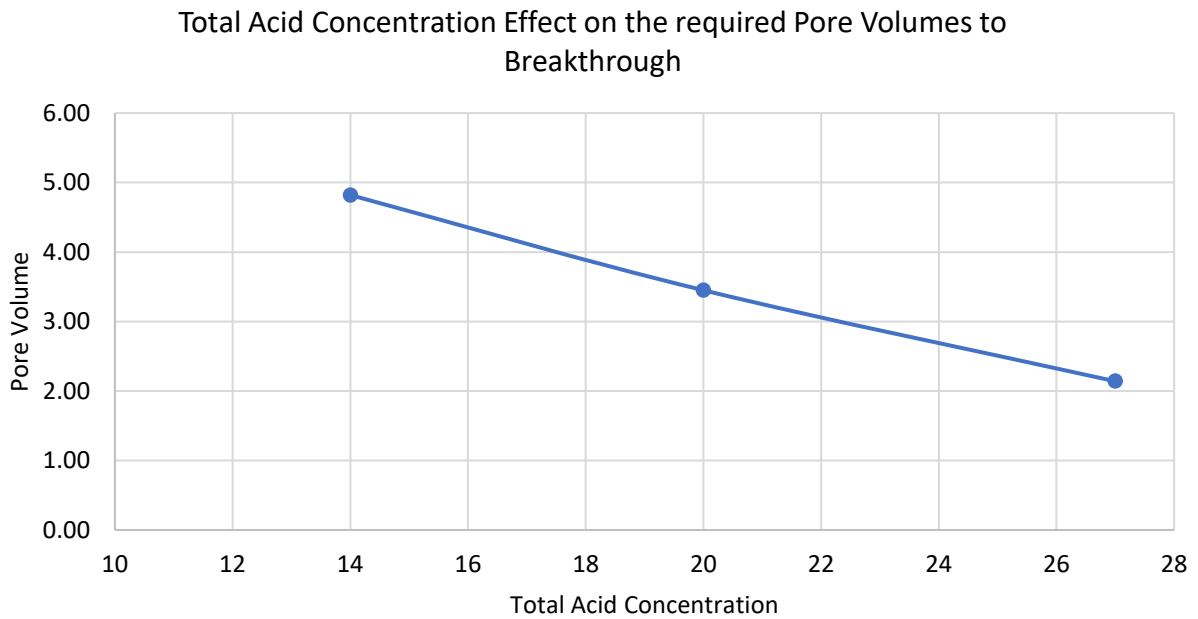


Figure 8.2 Total LA:GA acid concentration effect on the required pore volumes to breakthrough using a flow rate 3 cm³/min and a temperature of 200°F.

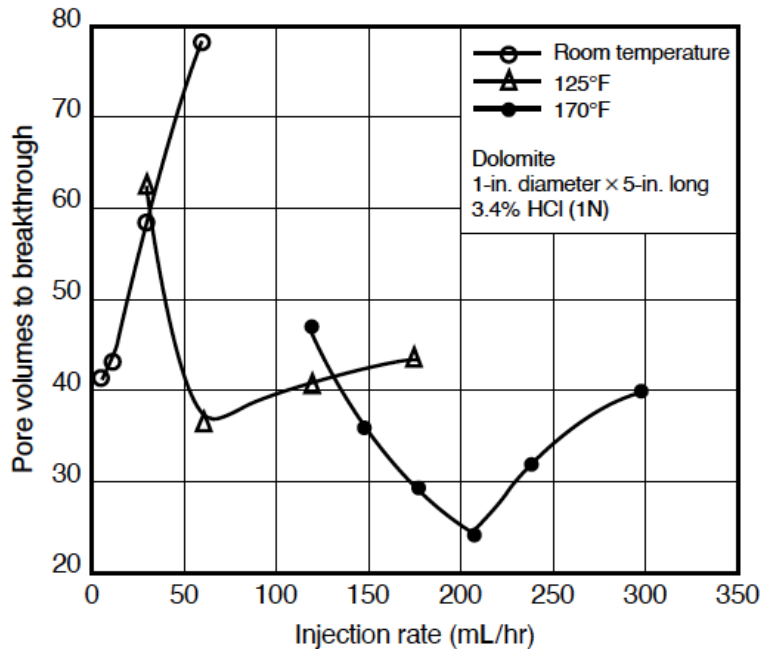


Figure 8.3 Dolomite cores treated with 3.4% HCl using different injection rates and test temperatures. This figure illustrates the effect of test temperature on the optimum injection rate to break through the tested cores (From Hill and Schechter 2000).

Fluid loss is a critical factor for the extension of wormholes; thereby, it is related to the applied injection rate. At a low injection rate, the acid is not forced enough through the formation pores to initiate wormholes and therefore low fluid loss results. At a moderate injection rate, slightly more fluid loss is anticipated, which causes the initiation of wormholes with more acid being forced toward the wormhole tip. However, at a high injection rate, more fluid loss is anticipated, which would result in slow wormhole growth due to less acid being forced to the tip (Hill and Schechter 2000; Thomas and Morgenthaler 2000; Akanni and Nasr-El-Din 2016). Figure 8.4 shows the injection rate effect on the required pore volumes to breakthrough performed in this research.

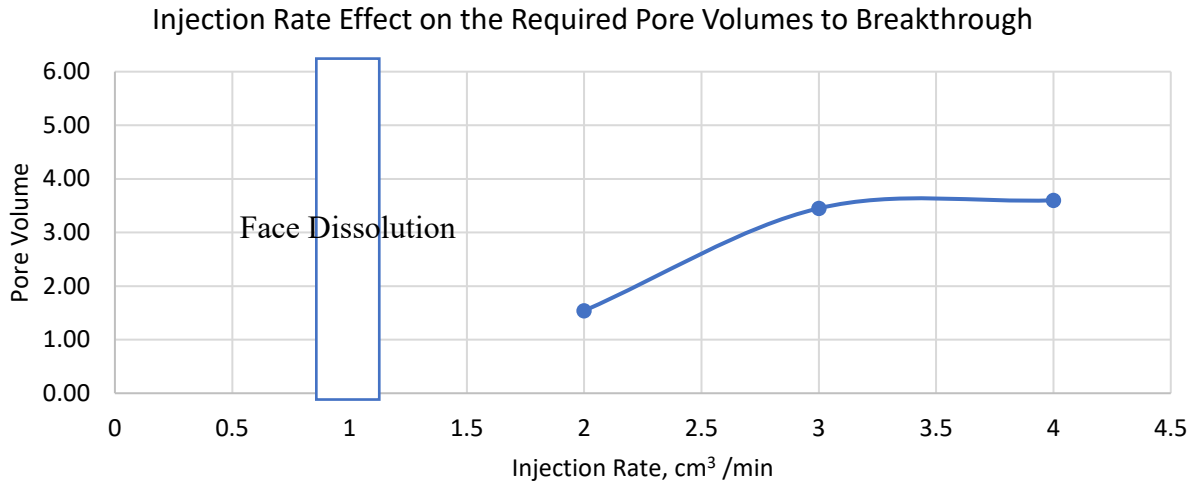


Figure 8.4 Injection rate effect on the required pore volumes to breakthrough using an acid mixture of 20 wt% at 200°F.

Equation 8.4 showed that the acid injection rate manipulates the wormhole cross-sectional area. A low injection rate would cause a large wormhole cross-sectional area that would turn to face dissolution. This was illustrated in the results of this research when limestone core was coreflooded using 1 cm³/min and a face dissolution occurred. A high injection rate would generate small and multiple wormholes that would cause excessive fluid loss. Figure 8.5 shows the inlet and the side faces of the core that was tested at 4 cm³/min. It can be seen that multiple wormholes were generated, and a ramified dissolution was created that was confirmed by the holes generated on the core's side.

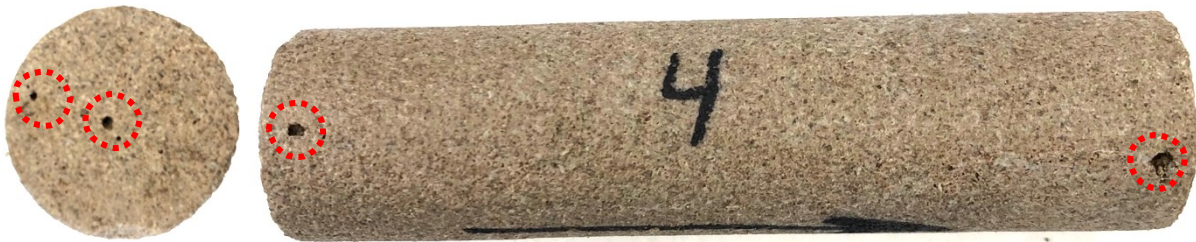


Figure 8.5 The inlet and side faces of a core tested using a high flow rate of 4 cm³/min. Multiple inlet and exit holes (circled in red) indicate that a ramified dissolution pattern was created.

The previous results and discussion show the importance of understanding the target formation for matrix acidizing. Besides the mentioned parameters effect on the needed acid volume, formation mineralogy can impact the final results. Limestone formations are more reactive to mineral and organic acids than dolomite formations. This difference is attributed to the chemical structure of both formations where limestone is CaCO_3 and dolomite is $\text{CaMg}(\text{CO}_3)_2$. More moles of the treated acid are needed to dissolve dolomite comparing to limestone. Accordingly, the lack of proper lab testing can result in spending an unnecessary amount of money and can raise the environmental impact of matrix acidizing.

8.1.2 Acid Fracturing

The first formal application of reservoir stimulation application using acids was developed by injecting inhibited HCl in 1932 by the Pure Oil Company (Elbel and Britt 2000). The term “lifting pressure” was developed in these operations due to exceeding the fracturing pressure, which resulted in the development of a fracture in the treated formation during the acid injection. This behavior was the first introduction of fracturing in reservoir improvement treatments. The main difference between acid fracturing and hydraulic fracturing treatments is the way of developing fracture conductivity. In acid fracturing, an etched fracture with multiple wormholes provides fracture conductivity, while in hydraulic fracturing, proppant placed in the fracture provides fracture conductivity (Thomas and Morgenthaler 2000).

For carbonate and dolomite formations, acid fracturing should be the first option when it comes to choosing between acid fracturing and propped hydraulic fracturing (Thomas and Morgenthaler 2000). In general, acid fracturing advantages are related to the generated conductivity and to the low risk associated with pumping the acid. Operationally, hydraulic fracturing treatments are associated with proppant flow back and screenout challenges that can

compromise the desired conductivity. On the other hand, acid fracturing conductivity is obtained through the etched fracture which can be very high and experiences no proppant flowback. Acid fracturing is mainly a function of the used acid and rock properties, which both derive the reaction kinetics that produce a conductive etched fracture face. Acid fracturing's main disadvantages are fluid loss, reaction rate, emulsion and sludging with oil, unpredicted conductivity, and environmental impacts (Hill and Schechter 2000; Thomas and Morgenthaler 2000).

Successful acid fracturing depends on the etched fractured penetration and conductivity. Higher conductivity is generated when the acid forms deep wormholes. However, many parameters affect the acid fracturing penetration depth and conductivity, such as acid loss, acid viscosity, and acid reaction or spending rate.

Fluid loss is the main limiter of deep acid penetration in an acid fracturing job. The main factors of fluid loss are the formation's permeability and porosity, acid viscosity, the differential pressure between the fracture and reservoir, and the reservoir fluid compressibility. Fluid viscosity is the only parameter that can be altered via the treatment plan, while the other parameters are variable from formation to another. Fluid loss can be manipulated by gelling the acid, which produces a fluid with high viscosity. Different gelling agents have been utilized in this matter, such as guar-based, xanthan biopolymers, acrylamide copolymer, and cellulose-based systems. However, severe plugging can occur along with an inefficient cleanup process.

Viscous pad injection can result in good fluid loss control, which would increase the acid penetration distance. Fluid loss control can be done by opening the fracture with a viscous pad that would insulate the formation by depositing a filter cake barrier. Then, an acid mixture is pumped to etch and to generate the fracture with less acid loss to the formation due to the filter cake barrier. By alternating between an acid and a viscous pad, acid penetration can be deep and can deliver a

conductive fracture. The filter cake barrier from the viscous pad is usually soluble in strong acids, specifically, in HCl, which can hamper filter cake stability. With organic acids or less reactive fluids, the deposited filter cake can provide better fluid loss control (Hill and Schechter 2000; Thomas and Morgenthaler 2000).

Acid penetration depth is also profoundly affected by the rate of acid spending when it reacts with formation. For example, acid penetration from the HCl reaction with limestone is much lower than acid penetration from the same acid reaction with dolomite. This distinction is attributed to the reaction rate difference of HCl between limestone and dolomite, where it is higher with limestone (Elbel and Britt 2000). The acid penetration differences between HCl in limestone and dolomite formations are shown in Figure 8.6.

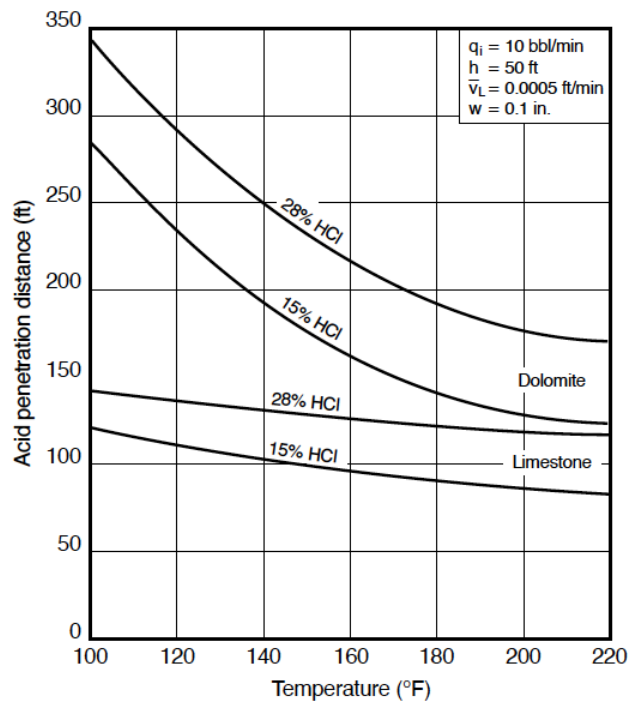


Figure 8.6 The acid penetration differences between HCl in limestone and dolomite formations. This difference also illustrates the effect of acid reactivity on the acid penetration distance, as it is lower in dolomite formations (From Elbel and Britt 2000).

The reaction rate is a critical factor in the depth of acid penetration. In low-to-moderate temperature formations, the reaction rate would not be affected considerably. However, in high temperature formations, the reaction rate would be significantly affected, which would result in an enormous impact on acid penetration. HCl is highly reactive with carbonate, which results in fast spending of the acid within a few feet from the wellbore. Acid retarding agents can be used to retard and to slow down the HCl reaction. The alteration between the viscous pad and acid can also provide a cooling effect on the treated formation, which would also slow down the acid-carbonate reaction (Elbel and Britt 2000; Hill and Schechter 2000; Thomas and Morgenthaler 2000; Akanni and Nasr-El-Din 2016).

Organic acids have been used as an alternative to HCl in acid fracturing due to their slow ionization process in solution. The slow ionization process causes a very slow reaction rate between the organic acids and carbonate, which allow the acid to dissolve more matrix material and penetrate deeper inside the formation. Many studies have been performed on formic and acetic acid reaction behavior with carbonate rock, which overshadowed the use of lactic acid to stimulate carbonate formations (Robert and Crowe 2000; Hall and Dill 1988; Al-Khalidi et al. 2003; Blauch et al. 2003; Buijse et al. 2004; Nasr-El-Din et al. 2007; Elkhatny and Nasr-El-Din 2012).

In this study, the reaction behavior between limestone rocks and lactic acid was shown to be limited by the precipitation of calcium lactate compound, as can be seen in Figure 8.7. However, the addition of gluconic acid to the acid solution chelated calcium ions from bonding with lactate ions to produce calcium lactate. Instead, a new compound was formed that has a high solubility in solution.

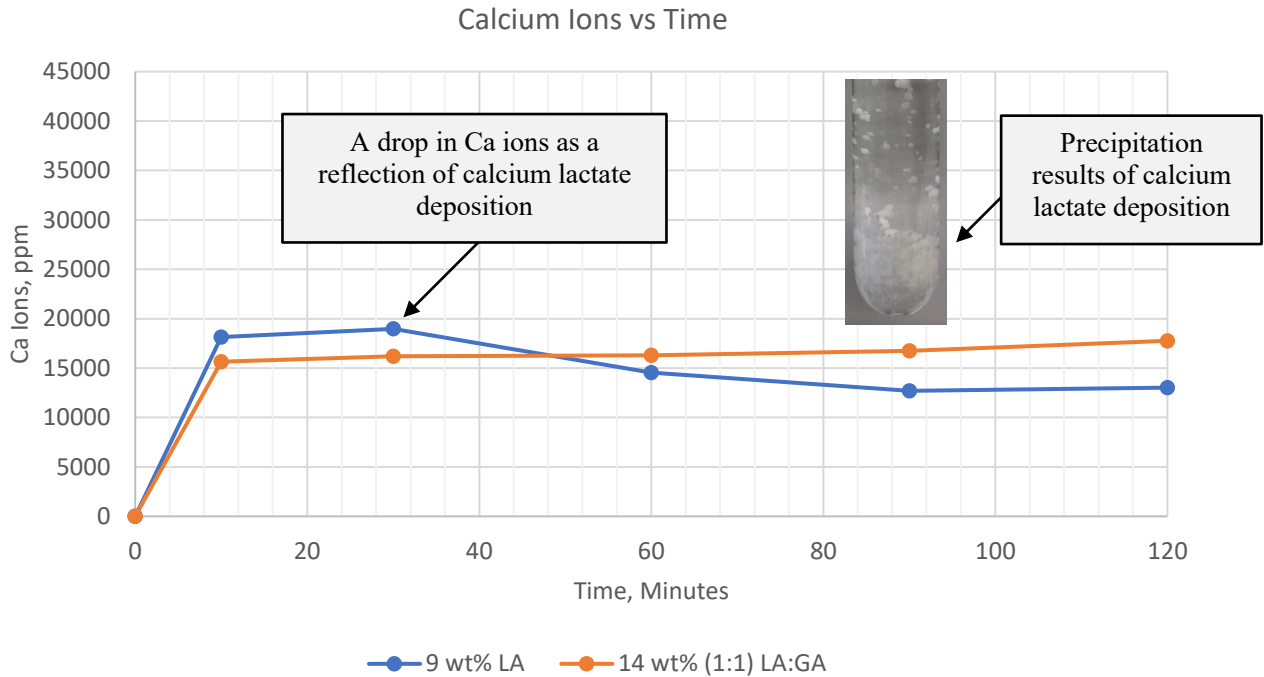


Figure 8.7 Calcium ion concentrations versus time for the reaction of 9 wt% lactic acid and 14 wt% (1:1) of lactic and gluconic acids with crushed core at 70°F and 1,000 psi.

The solubility test also showed that the two-acid LA:GA mixture could dissolve crushed limestone cores without any formation damage risk from reaction product salts deposition. Additionally, the solubility test results showed less dissolving power toward limestone cores comparing to HCl. For example, 15 grams of calcium carbonate would be entirely dissolved in 15 wt% HCl. Half of this amount was dissolved in the 14 wt% LA:GA acid mixture, and 12.6 gram was dissolved in the 27 wt% lactic and gluconic acid mixture. Coreflood results also showed that the two-acid mixture (in any concentration) needs around two pore volumes or more to breakthrough a limestone core. However, 15 wt% HCl usually requires around one pore volume to breakthrough a limestone core within the optimum injection rate, as can be seen in Figure 8.8.

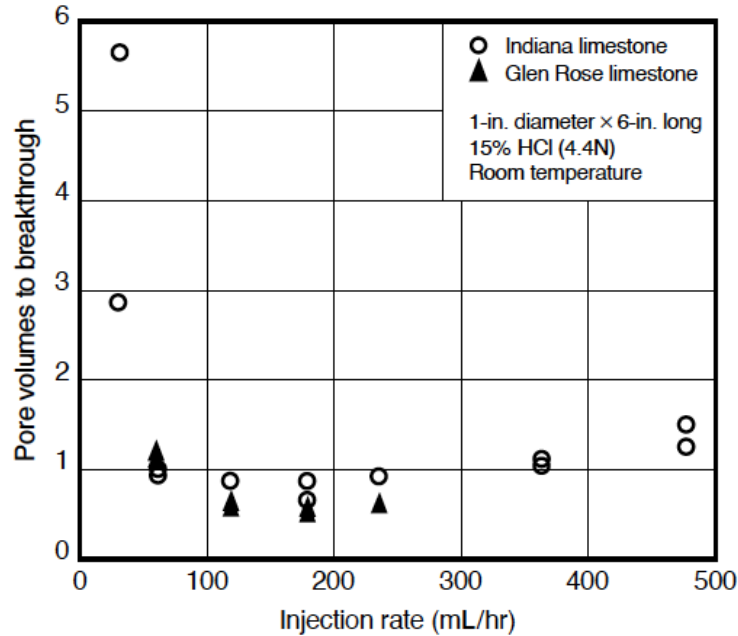


Figure 8.8 Example of different cores treated with 15% HCl. The figure shows that 15% HCl usually needs one pore volume or less to breakthrough a limestone core (From Wang et al. 1993).

In summary, the two-acid mixture has a viscosity that is comparable to water’s viscosity, which makes it unsuitable for effective acid fracturing. Low viscosity fluids can induce high leak-off rates which would limit the acid penetration distance. Based on this, a gelling agent for organic acids is needed to increase the mixture viscosity (Elbel and Britt 2000). The solubility and coreflood tests showed that the acid mixture can dissolve crushed limestone core and provide a conductive non-uniform wormhole.

CT scanning was done on different treated cores and showed the generated wormhole, as can be seen in Figure 8.9. Additionally, the reaction rate is much slower than the HCl reaction rate with carbonate, which put the two-acid mixture in a better position to provide a deep fracture with a low acid spending rate.

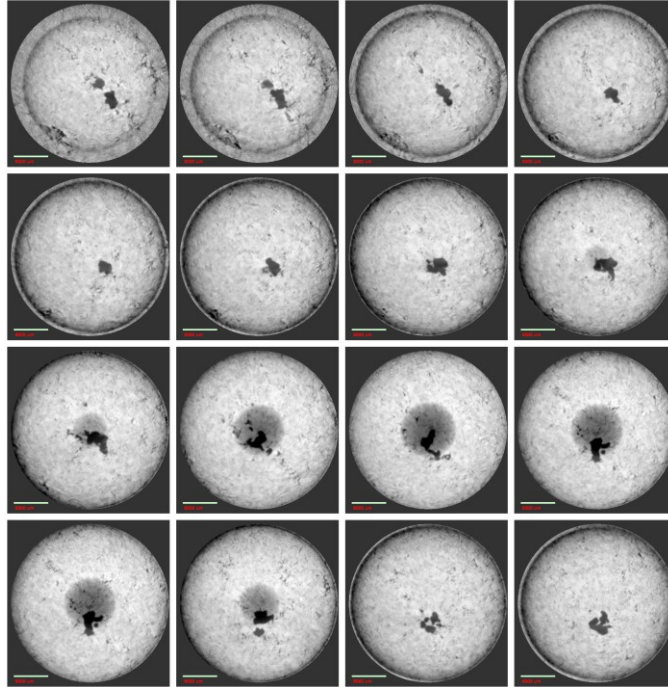


Figure 8.9 CT scans of a low permeability Indiana Limestone core treated with 20 wt% LA:GA acid mixture using 3 cm³/min at 200°F. Each scan is approximately 1/4" into the core moving from the injection end to the other side, top left to bottom right.

8.2 Hydrochloric Acid and Organic Acid Mixture in Acidizing Operations

This section illustrates the main highlights of HCl and organic acid (lactic and gluconic acid mixture) solutions as acid treatment agents. These highlights are shown by comparing HCl solutions with the proposed LA:GA acid mixture in terms of acid reactivity, acid corrosiveness, emulsion and sludging tendency, additives, wettability, and price of the acid per unit volume.

8.2.1 Acid Reactivity

Three steps control the acid-formation reaction. The first one is the transport of the bulk solution to the formation surface. The second one is the surface reaction between the acid and the formation. The final step is the product of the reaction transport away from the surface reaction. The slowest step determines the overall reaction behavior. Since the HCl dissolution rate with carbonate is significantly high, the surface reaction step is much faster than the acid transport to

the formation step. Based on that, the transport of acid to the formation is the slowest step and therefore determines the overall reaction (Thomas and Morgenthaler 2000). To overcome this issue, a high injection rate of HCl is needed, which ultimately can fracture the formation. In matrix acidizing, fracturing pressure can undermine the objectives of the treatment and can cause excessive loss of the acidizing fluid (Blauch et al. 2003; Nasr-El-Din et al. 2007; Chang et al. 2008; Akanni and Nasr-El-Din, 2016).

On the other hand, lactic and gluconic acid reactions with carbonates are much slower than the HCl reaction, which makes the acid transport to the formation the fastest step. Thus, the surface reaction between the acid mixture and the formation is the slowest step and determines the overall reaction behavior. Therefore, a low injection rate is sufficient to keep the reaction of the two-organic acid in the desired behavior window. Controlling the acid reaction would sequentially produce deep acid penetration by generating conductive wormholes (Buijse et al. 2004; Nasr-El-Din et al. 2007; Chang et al. 2008; Akanni and Nasr-El-Din, 2016).

The difference in the reaction behavior between HCl and the two-acid mixture is governed by the dissociation constant. Mineral acids, such as HCl, dissociate completely in water while organic acids do not. During the organic acid dissociation process (Equation 8.5), the dissociated state (A^-) and the undissociated state (HA) coexist within the solution due to the instability state from the conjugate base (A^-) (Al-Harbi et al. 2012; 2013).



There have been different studies and research conducted to understand the reasons behind the incomplete dissociation of organic acids. Buijse et al. (2004) mentioned that as the solution pH increases, more H^+ is generated, which shifts Equation 8.5 to the right. However, during the acid

and rock reaction, CO₂ gas is generated and kept in solution due to reservoir pressure being higher than 1,000 psi. Carbon dioxide enhances the reaction's reversal, which would keep the pH in the range of 4 to 6. At these values, organic acids are not completely dissociated. Additionally, carbon dioxide buffers the acid solution through the generation of carbonic acid which then buffers the solution pH to nearly 4.5 (Buijse et al. 2004; Chang et al. 2008; William et al. 1979). Dissolved CO₂ can generate carbonic acid through Equations 8.6 to 8.8.



8.2.2 Acid Corrosiveness

The complete dissociation of HCl solution in water provides a very strong impact on the formation and steel tubulars. At low and high temperatures, HCl solutions need to be accompanied by different corrosion inhibitors to deal with its corrosiveness. At a temperature above 200°F, a corrosion inhibitor intensifier is required to boost the performance of the corrosion inhibitor (Al-Mutairi et al. 2005). These corrosion inhibitor intensifiers can be limited in use due to environmental and stability issues (do Carmo Marques and Mainier 1994; Fredd and Fogler 1998).

Many studies have been performed to evaluate the corrosiveness of HCl toward low carbon steel-based tubulars and chromium-based tubulars (do Carmo Marques and Mainier 1994; Fredd and Fogler 1998; Al-Mutairi et al. 2005; De Wolf et al. 2017; Ng et al. 2018). In both kinds of tubulars, HCl shows high corrosion and pitting ratings. In this research, neat 15 wt% HCl was tested at 300°F to show its corrosiveness on an N-80 steel coupon. Due to the test vessel limitation,

the test was run for 3 hours using a nitrogen pressure of 1,000 to 1,200 psi. The results showed 0.56 lb/ft² per 3 hours of testing, which is 0.19 lb/ft² per hour.

Organic acids are less corrosive than HCl due to their low dissociation behavior in water. Accordingly, a neat 14 wt% (around the same concentration of the 15 wt% HCl) mixture of lactic and gluconic acid was tested at the same temperature for 4 hours and using a nitrogen pressure of 1,000 to 1,200 psi. The results showed 0.29 lb/ft² per 4 hours of testing, which would be 0.073 lb/ft² per hour. When a 27 wt% (doubling the strength) mixture of lactic and gluconic acid was tested at the same test conditions, a corrosion rate of 0.13 lb/ft² per hour was found.

This significant difference in corrosion rating illustrates the advantage of organic acids over HCl in terms of acid corrosion. Besides that, a loading of 5 gpt of an organic acid suitable corrosion inhibitor was enough to minimize the corrosion rates to low values at 300°F. As mentioned before, at this temperature, HCl solutions cannot be used unless a high loading of corrosion inhibitor and carrion inhibitor intensifiers are used. Figure 8.10 shows the referenced corrosion tests for HCl and the acid mixture.

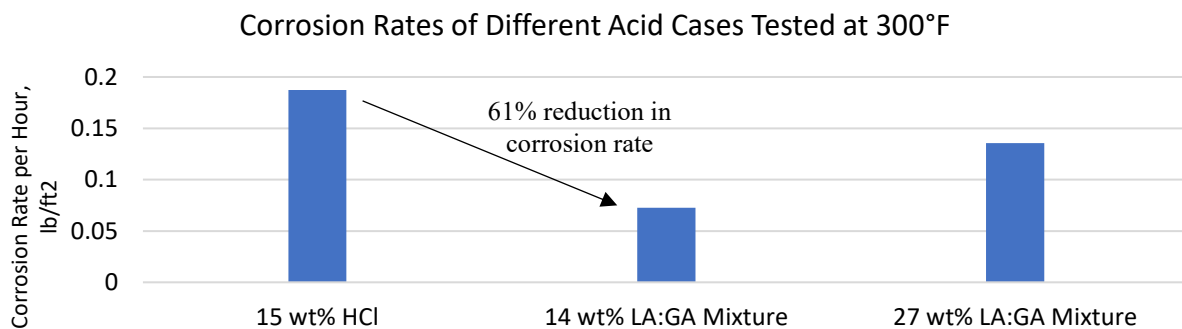


Figure 8.10 Corrosion rates per hour of 15 wt% HCl solution, 14 wt% LA:GA acid mixture, and 27 wt% LA:GA acid mixture. The tests were run at 300°F. The 14 wt% LA:GA acid mixture provides an 61% reduction in corrosion rate over the 15 wt% HCl solution.

8.2.3 Emulsion and Sludging Tendency

One of the main challenges during acidizing operations is preventing emulsion and sludging deposition due to oil and acid contact. A common practice is to inject a pre-flush fluid before the acid treatment to prevent acid-oil contact. However, the risk of emulsion and sludging is still present; specifically, in heavy oil reservoirs (Wong et al. 1996). Asphaltene existence in oil is the main cause of sludging deposition. A disruption in the asphaltene composition by acid contact can precipitate a heavy sludge due to the dissolution of resins and neutralization of asphaltene (Moore et al. 1965; Wong et al. 1996). Moreover, oil with polar compounds such as resin can form a stable emulsion (Bobra 1990; Fingas et al. 1993).

Two main factors manipulate the emulsion and sludging tendency. The first one is the type and strength of the acid used. The second one is the presence of ferric ions in solution. Asphaltene sludge occurs due to H^+ interaction with resin and asphaltene composition (Wong et al. 1996). HCl strong dissociation produces a large number of protons that can disrupt oil with resin and asphaltene.

On the other hand, organic acids have less sludging and emulsion tendency due to their low dissociation behavior (Wong et al. 1996; Buijse et al. 2004; Almubarak et al. 2015). Additionally, HCl is associated with high corrosion risk that can dissolve considerable amounts of ferric ions in solution. Accordingly, anti-sludge, demulsifier, and iron control agents are added to a HCl solution recipe to alleviate the emulsion and sludging tendency (Almubarak et al. 2015).

8.2.4 Additives and Wettability

Any acidizing fluid requires multiple additives to control the treatment side effects such as corrosion, sludging, emulsion, wettability alteration, and iron control. In this study, the solubility test results showed that lactic acid by itself could impose the risk of calcium lactate precipitation

when it is used at high initial concentration. However, the addition of gluconic acid (can be considered as an additive) prevented any reaction product precipitation, as can be seen in the ICP analysis that is shown in Figure 8.11.

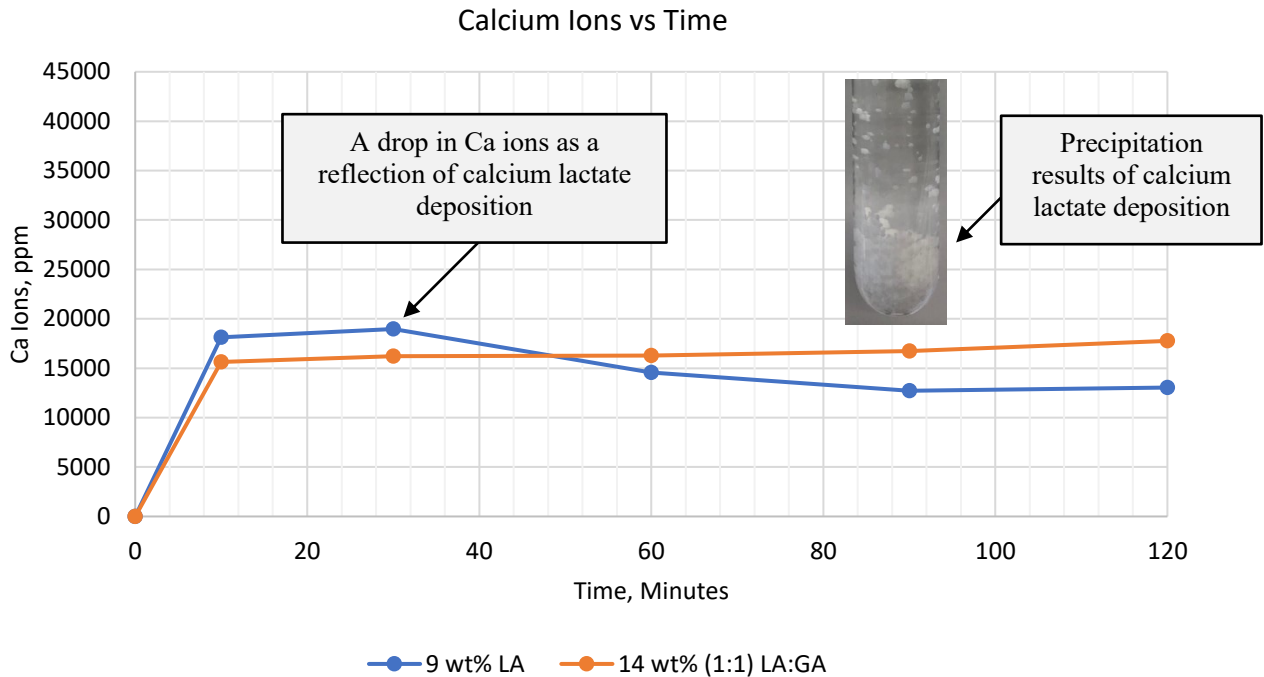


Figure 8.11 Calcium ion concentrations versus time for the reaction of 9 wt% lactic acid and 14 wt% (1:1) of lactic and gluconic acids with crushed core at 70°F and 1,000 psi.

Additionally, the corrosion test results showed that the acid mixture could cause a corrosion rate that is above the acceptable limit. Moreover, iron lactate can precipitate due to the high level of iron ions in the solution that was associated with the acid mixture corrosion, as can be seen in the ICP results shown in Figure 8.12. An adequate corrosion inhibitor was the appropriate additive to lower the corrosion rating and to prevent iron lactate precipitation.

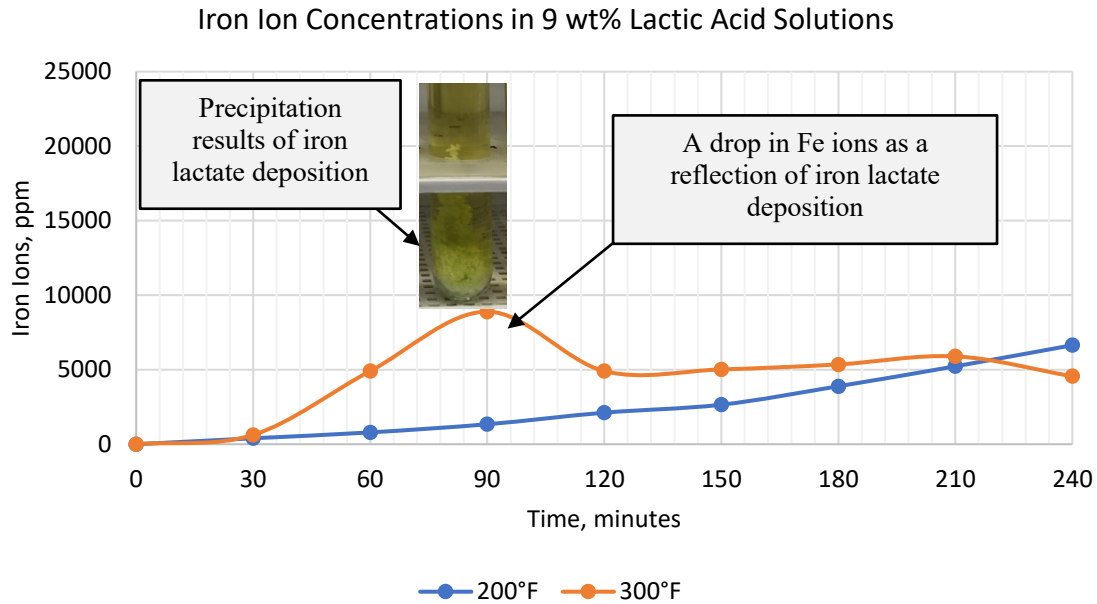


Figure 8.12 Iron ion concentrations in solution for 9 wt% lactic acid solution that was tested at 200 and 300°F at 1,000 psi for 4 hours.

A scale inhibitor was also added to the two-acid mixture solution when seawater was used to prepare the mixture. The scale inhibitor was essential to reduce sulfate ions consumption by calcium sulfate precipitation. Three scale inhibitors were tested at concentrations of 5 and 10 ppm, where both concentrations performed similarly when tested for 14 wt% and 27 wt% of the two-acid LA:GA mixture. Additionally, the three scale inhibitors performed equally when sulfate ion concentration was 6,000 ppm and below.

The zeta potential tests showed that these additives could alter the initial limestone rock wettability significantly and differently if coupled with long soaking time, as can be seen in Figure 8.13. However, the added additives were compatible with the two-acid LA:GA mixture when it was live and spent as no precipitation was noticed. To address the wettability alteration caused by the additives, a mutual solvent should be added to the two-acid mixture that can keep the formation wettability in the desired direction.

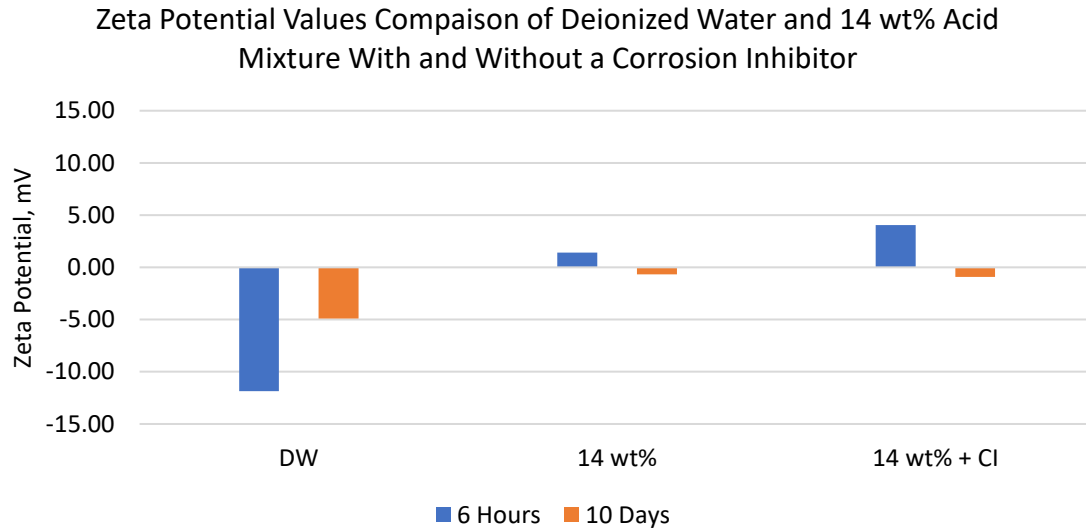


Figure 8.13 Zeta potential values of deionized water (DW) and 14 wt% acid mixture with and with a corrosion inhibitor after 6 hours and 10 days of particles suspension at room temperature.

A mutual solvent is an additive that is usually used in acidizing treatments to water wet the contacted formation. It is commonly used during the preflush stage to reduce the interfacial tension and to facilitate sweeping oil away from the treated zone (Robert and Rossen 2000). A mutual solvent can also reduce the adsorption of the used additives with the formation layer (Hall 1975). Accordingly, a mutual solvent is recommended to be included during the acid treatment and the post flush stage to increase the acid attack and to enhance the formation's favorable wettability (Robert and Rossen 2000).

The additives used in this research showed an alteration toward the suspended carbonate zeta potential, which can result in unfavorable final rock wettability. The addition of mutual solvent in the main acid treatment can help in reducing the interfacial tension between the spent acid and the formation. Thus, it can lower the risk of trapping the spent acid and its additives inside the treated formation pores. Additionally, the mutual solvent would reduce the adsorption of the inhibitor on the rock surface. Based on this, a 10 vol% of ethylene glycol monobutyl ether

(EGMBE) additive is recommended to be coupled with the acid mixture tested in this research. EGMBE mutual solvent showed an effective performance when used in acidizing treatment for the mentioned purpose (Crowe and Minor 1985).

An HCl solution for acidizing operations is always coupled with multiple additives to address different challenges, specifically in high temperature applications. Anti-sludge, demulsifier, and iron control agents are added to the HCl solution recipe to alleviate the emulsion and sludging tendency. Corrosion inhibitors and corrosion inhibitor intensifiers are essential additives to include in HCl solutions to protect the treated well's tubulars and to reduce iron ions in solution. In specific conditions, a gelling agent and a retarder are included in the HCl solution to lower its reactivity with the treated formation. Consequently, a mutual solvent is added to the recipe to keep the stimulated formation wettability in the water wet state.

8.2.5 Economical Analysis

Acidizing operation costs includes different factors, and among them are the acid base cost and the additives package costs. HCl gained its fame for acidizing operations due to its cheap price that increases the gap between operation cost and production gain. The cheap price of HCl comes from the fact that HCl is a waste result of many chemical activities. The process of producing HCl makes it hard to find an alternative in terms of chemical cost (Ameri et al. 2016). On the other hand, organic acid, including lactic and gluconic acids, base costs are usually almost twice the HCl cost. Nonetheless, the total additives package of HCl solutions cost more than those for organic acids. For example, Van Domelen and Jennings (1995) reported that an organic system would cost less than an HCl system by a factor of 0.77 due to the high cost of the corrosion inhibition package of HCl (including a corrosion inhibitor and a corrosion inhibitor intensifier).

Overall, HCl solutions are much harder to inhibit and require excessive amounts of costly inhibition additives to be applicable in high temperature applications (Van Domelen and Jennings 1995; Ameri et al. 2016; De Wolf et al. 2017; Ng et al. 2018). Additionally, acidizing with HCl solutions in high temperature formations would require high volumes of acid solution to overcome the rapid spending rate that would undermine the treatment goal (Sayed et al. 2018).

Besides the operational costs, after production factors should be taken into consideration. Corrosion protection and maintenance costs the US industries around \$170 billion a year, and the oil industry is responsible for a substantial portion from this amount (Brondel et al. 1994). HCl related damage can cause high cost in term of maintenance and replacement of corroded and affected tubulars. Although, HCl solutions causes costly considerations, its cheap price can balance that. However, an acidizing plan should ultimately use an acidizing fluid that is attractive technically and economically. The use of organic acids can be justified by the short return in investment. Lactic and gluconic acids are generally more expensive than HCl but the short return in investment by the fast production gain compensates for the operation cost. The two-acid LA:GA mixture system can safeguard the success of the treatment more than an HCl solution; specifically, in high temperature applications.

Table 8.1 shows a comparison between the two-acid system and other HCl-based acidizing systems. A 27 wt% acid strength was chosen for the two-acid system as it showed the most optimum results in solubility and coreflood tests. HCl-based acid systems were chosen to be a neat acid, an emulsified acid, or a gelled acid. The variation between the three systems ensured a wide range of applications and options for HCl usage in acidizing operations.

In Table 8.1, the cost factors were estimated based on past acidizing treatment cases that have been done with organic acids such as formic and acetic acids. In the industry, there is a lack

of lactic and gluconic acid usage data and a lack of lactic and gluconic acid costs due to the low utilization. Therefore, the acid base costs were taken from the MilliporeSigma Corporate website to be consistent in the comparison.

Table 8.1 Economical Comparison Between Different Kind of Acids. The Main Acid is Based on Lactic and Gluconic Acids While the Other Three are Based on HCl.

Parameter	27 wt% LA:GA	28 wt% HCl	28 wt% emulsified acid	15 wt% gelled acid
Base cost	\$32/liter for LA \$11/liter for GA	\$20/liter	\$20/liter	\$11/liter
	1.00	0.93	0.93	0.51
Extra volume	0.00	0.25	0.00	0.00
Corrosion inhibitor	0.25	1.00	0.50	1.00
Corrosion inhibitor intensifier	0.00	1.00	0.50	1.00
Extra additive	Minimum	Anti-sludge Demulsifier	Anti-sludge Demulsifier Diesel	Anti-sludge Demulsifier Gelling agent
Maintenance	low	high	moderate	moderate

The reaction behavior between HCl and carbonate is acid transport limited due to the high spending rate of the acid on the acid and rock interference (Thomas and Morgenthaler 2000; Sayed et al. 2018). This limitation is high when a neat HCl solution is used, which requires an excessive volume of the acid to satisfy the reaction limitation. The use of diesel and gelling agents with HCl can eliminate this problem. Still, these technologies are associated with costly additives to create the emulsion and to increase the acid viscosity (Blauch et al. 2003).

In terms of corrosion protection and inhibition, many researchers show the high corrosiveness of HCl, which can ultimately increase the maintenance and replacement cost (Brondel et al. 1994; De Wolf et al. 2017; Ng et al. 2018). Controlling corrosion in a neat HCl system would require high loading of costly corrosion inhibitors and intensifiers. These expensive inhibitors can be loaded in lower concentration when emulsified, and gelled acids are in use due to emulsion and viscosity enhancement, respectively (Van Domelen and Jennings 1995). The utilization of the two-acid system would ensure the minimum loading of a corrosion inhibitor additive. This research showed that an appropriate corrosion inhibitor could sustain the harsh conditions in high temperature applications without any need for a corrosion inhibitor intensifier.

8.3 Research Contribution

This research was conducted to investigate the performance of lactic and gluconic acid mixtures on carbonate acidizing operations using four main tests. These tests are solubility, corrosion, wettability, and coreflood tests. The main drawback of lactic acid is the production of calcium lactate salt after the acid-carbonate reaction. Accordingly, a base study was established to illustrate this drawback where calcium lactate precipitation was found in solution when a 9 wt% lactic acid was reacted with crushed limestone core.

Mixing gluconic acid with lactic acid produced another compound that has a high solubility in solution. Therefore, damage from reaction product deposition was eliminated as the solubility test results did not show any precipitation when the test was done at 70, 200, and 300°F using a total acid concentration of 10, 14, 20, 27, and 33 wt%. Consequently, increasing lactate ion concentrations did not produce calcium lactate precipitation due to lactate ion chelation with gluconate ions. The solubility tests also showed good solubility of the acid mixture that was a function of total acid concentration and temperature.

This research also showed that the two-acid LA:GA mixture could perform optimally when the molar ratio between the two acids is 1:1. Further analysis showed that increasing lactic acid molarity over gluconic acid could produce calcium lactate precipitation due to high lactate ion concentration comparing to gluconate ion concentration.

The conducted tests showed this mixture's potential to be utilized in acidizing operations using seawater with a sulfate concentration of 6,000 ppm or less. The risk of calcium sulfate precipitation was found to be high when the acid solution's equilibrium was reached. The acid mixture prepared by seawater and reacted with crushed limestone core showed calcium sulfate precipitation after a few days of conducting the test. However, the addition of a scale inhibitor lowered the calcium sulfate precipitation by 80% due to sulfate ion chelation.

This research also showed the corrosivity of lactic and gluconic acids by themselves and the corrosivity of their mixture at different concentrations and temperatures. Lactic acid, by itself, was found to be less corrosive than HCl. However, it caused corrosion rates that were above the acceptable limits in the industry when tested at 200 and 300°F. Additionally, iron lactate precipitation was found to be a by-product of the high corrosion rates caused by lactic acid. On the other hand, gluconic acid was found to be less corrosive than lactic acid. The two-acid mixture showed moderate corrosion rates at low concentration and high corrosion rates at high concentration with iron lactate precipitation. However, a 5 gpt of an organic acid-based corrosion inhibitor was sufficient to maintain an extremely low corrosion rate of the acid mixture at any concentration for the range of tested temperatures.

The zeta potential study done in this research showed the importance of following the common practice of including a mutual solvent in the fluids used for all acidizing treatment stages. Lactic and gluconic acid molecules altered the zeta potential values of the suspended limestone

particles. The additives used caused different alterations on the final zeta potential values. The prepared seawater ions showed significantly different alteration behavior when the conditioning time was changed to between a few hours and ten days.

This research also showed the capability of the two-acid mixture to stimulate a limestone formation by simulating the treatment using the coreflood test. The coreflood test showed that the needed pore volume to breakthrough was a function of temperature, injection rate, and total acid concentration. The results also showed that a dominant wormhole pattern could be generated in limestone cores without any need to use a high injection rate even in a high temperature environment. The weak dissociation of organic acid advances a lactic and gluconic acid mixture over HCl in term of acidizing deep into a limestone formation. HCl regularly needs an extremely high injection rate to avoid face dissolution and to generate a dominant wormhole pattern.

CHAPTER 9

CONCLUSIONS AND RECOMMENDATIONS

This chapter summarizes the main findings of this research and states recommendations for further studies.

9.1 Conclusions

This research was performed to investigate the performance of lactic and gluconic acid mixtures in matrix acidizing operations. A matrix acidizing fluid should be reactive with the treated formation to generate wormholes, should not impose any formation damage risk, should keep steel tubulars protected from any corrosion, and should not change the formation's wettability. Based on that, four tests were performed to examine lactic acid's potential as a matrix acidizing fluid. The first test was the solubility test, which helped to investigate the two-acid LA:GA mixture dissolving capacity with calcium carbonate and potential formation damage. The second test was the corrosion evaluation test that illustrated the corrosivity of the two-acid mixture toward low carbon steel coupons. The third test was the zeta potential study where the surface charge of the treated calcium carbonate particles were measured to show the effect of the two-acid LA:GA mixture on carbonate rock wettability. The fourth test was the coreflood simulation, which examined the ability of the two-acid mixture to generate a dominant wormhole in the limestone core. The coreflood test also showed the effect of different parameters on the generated wormholes. Based on the performed tests, the following conclusions can be drawn:

1. Lactic acid (LA), as a standalone acidizing fluid, can react with calcium carbonate and dissolve a considerable volume. However, dissolved lactate ions in solution can

complex with calcium ions in solution to produce calcium lactate precipitation when the salt solubility is exceeded as ICP and XRD analyses confirmed. Calcium lactate precipitation occurred even when a 9 wt% lactic acid was used to dissolve calcium carbonate. Previous studies reported that calcium lactate would not precipitate at such concentration.

2. The risk of by-product precipitation from lactic acid in acidizing treatment was eliminated by the addition of gluconic acid (GA) to the acidizing formula. Gluconic acid dissociates in water to add extra strength to acid dissolution by hydrogen protons and to dissolve gluconate ions in solution. Gluconate ions bond with lactate ions by sharing a calcium ion. This new bond produces a highly soluble compound called calcium lactate gluconate.
3. The solubility test showed that a 1:1 molar ratio between lactic and gluconic acids was the optimum ratio between lactate and gluconate ions. Increasing lactic acid molarity caused calcium lactate precipitation due to high lactate and calcium ion concentrations in solution.
4. The two-acid LA:GA mixture at a 1:1 molar ratio showed a dissolving capacity that was highly dependent on the total acid concentration and test temperature. Increasing the total acid concentration increased the hydrogen attack process due to the high amount of dissociated hydrogen from the lactic and gluconic acids. Increasing the test temperature enhanced the mobility of the ions in solution, which increased the acid dissolving capacity.
5. A solubility ratio between 37% and 100% was achieved when the total LA:GA acid concentration and the test temperature were manipulated. Based on this, matrix

acidizing and acid fracturing treatments can be conducted using this mixture without imposing the risk of limited acid penetration due to high acid reactivity. The use of HCl in high temperature applications is associated with a high reaction rate that causes a low acid penetration.

6. When the total LA:GA acid mixture concentration was increased up to 33 wt%, which is associated with high lactate ion concentration in solution, calcium lactate did not precipitate when the molar ratio between lactic and gluconic acid was still at 1:1. This ratio ensured the availability of sufficient gluconate ion concentration to chelate lactate ions.
7. Preparing the two-acid LA:GA mixture with seawater showed the risk of calcium sulfate precipitation when the two-acid mixture reacted with calcium carbonate. ICP analysis showed that calcium sulfate precipitates would deposit after reaching an equilibrium state between the sulfate and calcium ions in solution. Hence, the two-acid LA:GA mixture required a long time to reach equilibrium compared to the HCl solution.
8. The use of a scale inhibitor showed useful chelation of sulfate ions when the seawater contained 6,000 ppm of sulfate or less. Fourteen wt% and 27 wt% of LA:GA mixture prepared with the seawater of 6,000 ppm of sulfate or less contained 80% of the initial free sulfate ion concentration after ten days of acid-carbonate reaction. When the sulfate ions increased to 12,000 ppm, the tested scale inhibitors were able to keep 50% of the initial free sulfate ions in solution.
9. Lactic acid, by itself, can cause severe corrosion in low carbon steel. Corrosion damage is severe when the temperature is around 300°F, and iron lactate can

precipitate due to high concentrations of iron and lactate ions. Lactic acid corrosion damage showed a high dependency on temperature. Gluconic acid was found to be less corrosive than lactic acid at any temperature. The mixture of 4.5 wt% lactic acid and 9.5 wt% gluconic acid showed a corrosion rate less than the one calculated for the 9 wt% lactic acid alone. However, increasing the LA:GA mixture concentration to 27 wt% (9 wt% lactic acid and 18 wt% gluconic acid) caused a severe corrosion rate that was comparable to the rate obtained with the 9 wt% lactic acid alone. A 15 wt% HCl showed the highest amount of corrosion among all the tested acid solutions.

10. A loading of 5 gpt of an organic corrosion inhibitor was enough to keep the corrosion rate of the LA:GA mixture at any concentration below the acceptable limit at 200 and 300°F for 4 hours. The LA:GA mixture at 27 wt% and 300°F showed stability and a compatibility state with the corrosion inhibitor tested for 12 hours as no fluid separation was noticeable. The corrosion rate was also below the acceptable limit.
11. The zeta potential study showed the importance of following the common practice of including a mutual solvent in the fluids used for all acidizing treatment stages. Lactic and gluconic acid molecules altered the zeta potential values of the suspended limestone particles. The additives caused different alterations on the final zeta potential values. The prepared seawater ions showed significantly different alteration behavior when the conditioning time was changed between a few hours to ten days.

12. The coreflood tests showed the risk of obtaining face dissolution when a low injection rate was used to stimulate a limestone core using the LA:GA mixture. However, a slight increase in the injection rate was sufficient to generate a wormhole in the tested cores. The minimum required pore volume to reach a breakthrough using the two-acid mixture was found to be dependent on the resulting dissolution pattern. A ramified dissolution consumes a large amount of the acid mixture to breakthrough due to multiple branches within the tested core. On the other hand, a dominant wormhole consumes the optimum amount of the acid mixture to breakthrough.
13. Total acid concentration, test temperature, and injection rate had a substantial effect on the resulting dissolution pattern and the required pore volumes to breakthrough. The optimum LA:GA acid concentration was found to be 27 wt% as 2.14 PV was needed to breakthrough. 4.82 and 3.45 PV's were needed to breakthrough when the total acid concentration was 14 wt% and 20 wt%, respectively, when the injection rate was 3 cm³/min at 200°F.
14. The optimum application temperature was found to be around 200°F, as 3.45 PV was needed to breakthrough the tested Indiana limestone core. 4.22 and 4.01 PV's were needed to breakthrough when the test was run at 150 and 300°F, respectively, using an injection rate of 3 cm³/min and a total LA:GA acid concentration of 20 wt%.
15. The optimum injection rate was found to be around 2 cm³/min as 1.54 PV was needed to breakthrough the tested Indiana limestone core. 3.45 and 3.60 PV's were

needed to breakthrough for injection rates of 3 and 4 cm³/min, respectively, using a test temperature of 200°F and a total LA:GA acid concentration of 20 wt%.

It should be noted that the listed conclusions are based on the materials used to evaluate the LA:GA mixture. For example, the solubility test and the coreflood test were conducted using Pink Desert and Indiana limestone cores, respectively. A complete change in the subject material will likely affect the final results. However, even so, these conclusions can be used as a guideline to evaluate lactic and gluconic acid mixtures for matrix acidizing carbonate formations.

9.2 Recommendations

Based on the stated conclusions and the limitations of the experiments, the following recommendations can be followed to expand this research work:

1. In this research, limestone cores were used to conduct the solubility and coreflood tests. Another investigation is needed to evaluate the performance of the two-acid LA:GA mixture with dolomitic formations. Dolomite dissolution requires higher amounts of acid moles comparing to limestone dissolution. Therefore, a decrease in the acid dissolving capacity for dolomite particles is anticipated and an increase in the minimum pore volume to breakthrough a dolomite core is anticipated as well.
2. Investigate the performance of lactic and gluconic acid mixtures when they are coupled with hydrofluoric acid to stimulate sandstone formations. Organic acids can replace HCl in mud acid formulas for HCl sensitive cases. The two-acid mixture should be able to remove drilling fluid damages and carbonate contents within sandstone formations.
3. Study the potential of implementing the LA:GA mixture for acid fracturing treatments. One of the main parameters that distinguishes an acid fracturing fluid

from a matrix treatment fluid is the fluid's viscosity. A low viscosity fluid can impose a high leak-off rate. Thus, a suitable gelling agent is needed to be coupled with the two-acid mixture to make it comparable with other acid fracturing fluids.

4. Evaluate the idea of combining lactic acid with HCl to produce a HCl/lactic acid mixture that can reduce HCl drawbacks and the cost of lactic acid. This mixture can provide the strength and retardation characteristics of HCl and lactic acids respectively. This mixture has been tested to remove manganese tetraoxide-based filter cake in a concentration of 1 wt% HCl and 4 wt% lactic acid and showed a good removal efficacy (Al Moajil and Nasr-El-Din 2014).
5. Study the performance of the two-acid LA:GA mixture using a fracture conductivity test. This test can investigate the effect of different closure stresses on the resulted fracture conductivity using limestone and dolomite cores. Additionally, the test could show the ability of the generated etches and fracture swarms to withstand high closure stress.

REFERENCES

- Abdel-Rahman, M. A. and Sonomotoa, K. 2016. Opportunities to Overcome the Current Limitations and Challenges for Efficient Microbial Production of Optically Pure Lactic Acid. *Journal of Biotechnology* **236**: 176-192. <http://dx.doi.org/10.1016/j.jbiotec.2016.08.008>
- Abdel-Rahman, M. A., Tashiroc, Y., and Sonomotoa, K. 2011. Lactic Acid Production From Lignocellulose-Derived Sugars Using Lactic Acid Bacteria: Overview and Limits. *Journal of Biotechnology* **156**, Issue 4: 286-301. <https://doi.org/10.1016/j.jbiotec.2011.06.017>.
- Ahmed, A., Mohamed, M., Salaheldin, E. et al. 2017. Development of New Seawater-Based Formulation to Stimulate Sandstone Formations. Presented at the SPE Kingdom of Saudi Arabia Annual Technical Symposium and Exhibition, Dammam, Saudi Arabia, 24–27 April 2017. SPE-188004-MS. <http://doi:10.2118/188004-MS>
- Akanni, O. O. and Nasr-El-Din, H. A. 2016. Modeling of Wormhole Propagation During Matrix Acidizing of Carbonate Reservoirs by Organic Acids and Chelating Agents. Presented at the SPE Annual Technical Conference and Exhibition, Dubai, UAE, 26-28 September. SPE-181348-MS. <http://doi:10.2118/181348-MS>.
- Al Moajil, A.M. and Nasr-El-Din, H.A. 2014. Removal of Manganese Tetraoxide Filter Cake Using a Combination of HCl and Organic Acid. *J Can Pet Technol* **53** (2): 122-130. SPE-165551-PA. <http://dx.doi.org/10.2118/165551-PA>.
- Al-Duailej, Y.K., Kwak, H.T., Caliskan, S. et al. 2013. Wormhole Characterization Using NMR. Presented at the International Petroleum Technology Conference, Beijing, China, 26–28 March. IPTC-17063-MS. <http://dx.doi.org/10.2523/17063-MS>.
- Al-Harbi, B.G., Al-Dahlan, M.N. and Al-Khaldi, M.H. 2012. Aluminum and Iron Precipitation during Sandstone Acidizing using Organic-HF Acids. Presented at the SPE Formation Damage Control Conference, Lafayette, Louisiana, 10-11 February. SPE-151781-MS. <https://doi.org/10.2118/151781-MS>.
- Al-Harbi, B.G., A-Dahlan, M.N., Al-Khaldi, M.H. et al. 2013. Evaluation of Organic-Hydrofluoric Acid Mixtures for Sandstone Acidizing. Presented at the International Petroleum Conference, Beijing, China, 26–28 March. IPTC-16967-MS. <http://dx.doi.org/10.2523/16967-MS>.
- Al-Khaldi, M.H., Al-Juhani, A., Al-Mutairi, S.H. et al. 2011. New Insights Into the Removal of Calcium Sulfate Scale. Presented at the SPE European Formation Damage Conference, Noordwijk, The Netherlands, 7- 10 June. SPE-144158-MS. <http://doi:10.2118/144158-MS>.

- Al-Khaldi, M.H., Nasr-El-Din, H.A., Blauch, M.E. et al. 2003. New Findings on Damage Potential, Geochemical Reaction Mechanisms, and Production Enhancement Applications for Citric Acid. Presented at the SPE European Formation Damage Conference, The Hague, The Netherlands, 13-14 May. SPE-82218-MS. <http://dx.doi.org/10.2118/82218-MS>.
- Al-Mutairi, S. H., Nasr-El-Din, H. A., Al-Muntasheri, G. A. et al. 2005. Corrosion Control During Acid Fracturing of Deep Gas Wells: Lab Studies and Field Cases. Presented at the SPE International Symposium on Oilfield Corrosion, Aberdeen, 13 May. SPE-94639-MS. <https://doi.org/10.2118/94639-MS>.
- Alarifi, S. A., Mahmoud, M. A., and Kamal, M. S. 2018. Interactions of DTPA Chelating Agent With Sandstone Rocks During EOR: Rock Surface Charge Study. *Fuel* **232**: 684-692. <https://doi.org/10.1016/j.fuel.2018.06.003>.
- Almubarak, T., Alkhaldi, M., Almubarak, M. et al. 2015. Investigation of Acid-Induced Emulsion and Asphaltene Precipitation in Low Permeability Carbonate Reservoirs. Presented at the SPE Saudi Arabia Section Annual Technical Symposium and Exhibition, Al-Khobar, 21-23 April. SPE-178034-MS. <http://dx.doi.org/10.2118/178034-MS>
- Ameri, A., Nick, H. M., Ilangoan, N. et al. 2016. A Comparative Study on the Performance of Acid Systems for High Temperature Matrix Stimulation. Presented at the Abu Dhabi International Petroleum Exhibition and Conference, Abu Dhabi, UAE, 7-10 November. SPE-183399-MS. <http://dx.doi.org.ezproxy.library.tamu.edu/10.2118/183399-MS>.
- Arensman, D.G. and Nasr-El-Din, H.A. 2013. Effectiveness of Calcium Sulfate Scale Inhibitors in Spent Hydrochloric Acid/Seawater System. *Journal of Petroleum & Environmental Biotechnology* **4** (159). <http://doi:10.4172/2157-7463.1000159>.
- Bin Merdhah, A. 2010. Inhibition of Calcium Sulfate and Strontium Sulfate Scale in Waterflood. *SPE Prod & Oper* **24** (4): 545–552. SPE-141168-PA. <http://doi.org/10.2118/141168-PA>.
- Blauch, M.E., Cheng, A., Rispler, K. et al. 2003. Novel Carbonate Well Production Enhancement Application for Encapsulated Acid Technology: First-Use Case History. Presented at the SPE Annual Technical Conference and Exhibition, Denver, Colorado, 5–8 October. SPE-84131-MS. <http://doi:10.2118/84131-MS>.
- Bobra, M. 1990. A Study of the Formation of Water-in-Oil Emulsions. Proc., Arctic and Marine Oil Spill Program Technical Seminar, Edmonton, Canada.
- Brondel, D., Edwards, R., Hayman, A. et al. 1994. Corrosion in the Oil Industry. *Oilfield Review* **6** (2): 4–18.
- Buckley, J. S., Liu, Y., and Monsterleet, S. 1998. Mechanisms of Wetting Alteration by Crude Oils. *SPE Journal* **3** (1): 54–61. SPE-37230-PA. <http://dx.doi.org/10.2118/37230-PA>.

- Buijse, M., Boer, P., Breukel, B., and Burgos, G. 2004. Organic Acids in Carbonate Acidizing. *SPE Production & Operations* 19 (3): 128-134. SPE-82211-PA. <http://dx.doi.org/10.2118/82211-PA>.
- Chang, F.F., Nasr-El-Din, H.A., Lindvig, T. et al. 2008. Matrix Acidizing of Carbonate Reservoirs Using Organic Acids and Mixture of HCl and Organic Acids. Presented at the SPE Annual Technical Conference and Exhibition, Denver, Colorado, 21-24 September. SPE-116601-MS. <https://doi.org/10.2118/116601-MS>.
- Chen, T., Neville, A., and Yuan, M. 2004. Effect of PPCA and DETPMP Inhibitor Blends on CaCO₃ Scale Formation. Presented at the International Symposium on Oilfield Scale, Aberdeen, 26–27 May. SPE-87442-MS. <http://doi:10.2118/87442-MS>.
- Crowe, C.W. and Minor, S.S. 1985. Effect of Acid Corrosion Inhibitors on Matrix Stimulation Results. *JPet Technol* 37 (10): 1853–1860. SPE-11119-PA. <http://dx.doi.org/10.2118/11119-PA>.
- de Wolf, C. A., Nasr-El-Din, H. A., Bouwman, A. et al. 2017. Corrosion Rates of Cr- and Ni-Based Alloys With Organic Acids and Chelating Agents Used in Stimulation of Deep Wells. *SPE Prod & Oper* 32 (2): 208–217. SPE-152716-PA. <https://doi.org/10.2118/152716-PA>.
- do Carmo Marques, L. C., and Mainier, F. B. 1994. Corrosion Problems Associated With the Use of Copper-Based Corrosion Inhibitor Intensifier in Acid Stimulation Treatments. *SPE Advanced Technology Series* 2 (1): 58–62. SPE-23634-PA. <https://doi.org/10.2118/23634-PA>.
- Economides, M. J. and Boney, C. 2000. Reservoir Stimulation in Petroleum Production. In *Reservoir Stimulation*, third ed, Economides, M. J. and Nolte, K. G., Chap. 1, pp 1-30. New York: Wiley.
- Elbel, J. and Britt, L. 2000. Fracture Treatment Design. In *Reservoir Stimulation*, third ed, Economides, M. J. and Nolte, K. G., Chap. 10, pp 1-50. New York: Wiley.
- Elkatatny, S. and Nasr-El-Din, H. A. 2012. Removal Efficiency of Water-based Drill-in Fluid Filter Cake Using Polylactic Acid. Presented at the EAGE Annual Conference & Exhibition, Copenhagen, Denmark, 4-7 June. SPE-154192-MS. <http://doi:10.2118/154192-MS>.
- Fan, C., Kan, A.T., Fu, G. et al. 2010. Quantitative Evaluation of Calcium Sulfate Precipitation Kinetics in the Presence and Absence of Scale Inhibitors. *SPE J.* 15: 977–988. <http://dx.doi.org/10.2118/121563-PA>
- Fann. 2017. Drill Pipe Corrosion Coupons. *Product Information*, 2007. <http://www.fann.com/public1/pubsdata/Brochures/Drill%20Pipe%20Corrosion%20Coupon.pdf> (accessed 24 November 2017).

- Fingas, M., Fieldhouse, B., Bobra, M. et al. 1993. The Physics and Chemistry of Emulsions. *Proc.*, Proceedings of the Workshop on Emulsions, Marine Spill Response Corporation, Washington, DC, p.7.
- Fredd, C.N. and Fogler, H.S. 1998. The Kinetics of Calcite Dissolution in Acetic Acid Solutions. *Chem Eng Sci* **53** (22): 3863–3874. [http://dx.doi.org/10.1016/S0009-2509\(98\)00192-4](http://dx.doi.org/10.1016/S0009-2509(98)00192-4).
- Frenier, W. W. and Ziauddin, M. 2008. *Formation, Removal and Inhibition of Inorganic Scale in the Oilfield Environment*. Richardson, Texas: Society of Petroleum Engineers.
- Gerstner, G. and Ladenburg, G. J. 2002. Calcium Lactate Gluconate – The Innovative Solution for Extra Calcium. *Innovations in Food Technology*. Vol (**16**): 2-3.
- Hall, B. E. and Dill, W. R. 1988. Iron Control Additives for Limestone and Sandstone Acidizing of Sweet and Sour Wells. Presented at the SPE Formation Damage Control Symposium, Bakersfield, California, USA, 8–9 February. SPE-17157-MS. <http://dx.doi.org/10.2118/17157-MS>.
- Hall, B.E. 1975. The Effect of Mutual Solvent Adsorption in Sandstone Acidizing. *J Pet Technol* **27** (12): 1439–1442. SPE- 5377-PA. <http://dx.doi.org/10.2118/5377-PA>.
- Hawkins, M. F. Jr. 1956. A Note on the Skin Effect. *J Pet Technol* 8 (12): 65–66. SPE-732-G. <https://doi.org/10.2118/732-G>.
- He, J., Mohamed, I.M., and Nasr-El-Din, H.A. 2011. Mixing Hydrochloric Acid and Seawater for Matrix Acidizing: Is it a Good Practice? Presented at the SPE European Formation Damage Conference, Noordwijk, The Netherlands, 7–10 June 2011. SPE-143855-MS. <http://dx.doi.org/10.2118/143855-MS>
- Hill, A. D. and Schechter, R. S. 2000. Fundamentals of Acid Stimulation. In *Reservoir Stimulation*, third ed, Economides, M. J. and Nolte, K. G., Chap. 16, pp 1-28. New York: Wiley.
- Holten, C. H., Müller, A., Reh binder, A. et al. 1971. *Lactic Acid; Properties and Chemistry of Lactic Acid and Derivates*. Weinheim, Germany: Verlag Chemie
- Hunter, R. J 1981. *Zeta Potential in Colloid Science: Principles and Application*; Academic Press: New York.
- Khaleel, O., Teklu, T. W., Alameri, W. et al. 2019. Wettability Alteration of Carbonate Reservoir Cores-Laboratory Evaluation Using Complementary Techniques. *SPE Res Eval & Eng* **22** (3): 911 – 922. SPE-194483-PA. <http://doi:10.2118/194483-PA>.
- Komesu, A., de Oliveira, J. A. R. Martins, L. H. et al. 2017. Lactic Acid Production to Purification: A Review. *BioRes* **12**(2): 4364-4383. DOI: 10.15376/biores.12.2.Komesu
- Kubantseva, N. and R. W. Hartel. 2002. Solubility of Calcium Lactate in Aqueous Solution. *Food Rev. Int.* (**18**):135–149.

- Legens, C., Toulhoat, H., and Cuiec, L. 1999. Wettability Change Related to Adsorption of Organic Acids on Calcite: Experimental and Ab Initio Computational Studies. *SPE J.* **4** (4): 328–333. <http://dx.doi.org/10.2118/57721-PA>.
- Lund, K., Fogler, H. S., McCune, C. C. et al. 1973a. Kinetic Rate Expressions for Reactions of Selected Minerals with HCl and Hf Mixtures. Presented at the SPE Oilfield Chemistry Symposium, Denver, Colorado, 24-25 May. SPE-4348-MS. <https://doi.org/10.2118/4348-MS>.
- Lund, K., Fogler, H.S., and McCune, C.C. 1973b. Acidization—I: The Dissolution of Dolomite in Hydrochloric Acid. *Chem. Eng. Sci.* **28** (3): 681–700. [http://dx.doi.org/10.1016/0009-2509\(77\)80003-1](http://dx.doi.org/10.1016/0009-2509(77)80003-1).
- Lund, K., Fogler, H.S., McCune, C.C. et al. 1975. Acidization—II. The Dissolution of Calcite in Hydrochloric Acid. *Chem. Eng. Sci.* **30** (8):825–835. [http://dx.doi.org/10.1016/0009-2509\(75\)80047-9](http://dx.doi.org/10.1016/0009-2509(75)80047-9).
- Mahani, H., Keya, A. L., Berg, S. et al. 2015. The Effect of Salinity, Rock Type and pH on the Electrokinetics of Carbonate-Brine Interface and Surface Complexation Modeling. Presented at the Reservoir Characterization and Simulation Conference and Exhibition, Abu Dhabi, UAE. 14-16 September. SPE-175568-MS. <http://doi:10.2118/175568-MS>
- Mahmoud, M. A., Nasr-El-Din, H. A., de Wolf, C. A. et al. 2011. Evaluation of a New Environmentally Friendly Chelating Agent for High-Temperature Applications. *SPE J.* **16** (3): 559–574. SPE-127923-PA. <http://dx.doi.org/10.2118/127923-PA>.
- Martinez, F. A., Balicunas, E. M., Salgado, J. M. et al. 2013. Lactic Acid Properties, Applications and Production: A Review. *Trends in Food Science & Technology* **30**: 70-83.
- Moore, E. W., Crowe, C. W., and Hendrickson, A. R. 1965. Formation, Effect and Prevention of Asphaltene Sludges During Stimulation Treatments. *JPT* **17** (09): 1-023. <https://doi:10.2118/1163-PA>.
- Nasr-El-Din, H. A., Al-Mutairi, S., Al-Malki, B. et al. 2002. Stimulation of Deep Gas Wells Using HCl/Formic Acid System: Lab Studies and Field Application. Presented at the Canadian International Petroleum Conference, Calgary, Alberta, Canada, 11-13 June. PETSOC-2002-289. <http://dx.doi.org/10.2118/2002-289>.
- Nasr-El-Din, H. A., Driweesh, S. M., and Muntasheri, G. A. 2003. Field Application of HCl-Formic Acid System to Acid Fracture Deep Gas Wells Completed with Super Cr-13 Tubing in Saudi Arabia. Presented at the SPE International Improved Oil Recovery Conference in Asia Pacific, Kuala Lumpur, Malaysia, 20-21 October. SPE-84925-MS. <http://dx.doi.org/10.2118/84925-MS>.

- Nasr-El-Din, H.A., Al-Zahrani, A.A., Garzon, F.O. et al. 2007. Acid Fracturing of Gas Wells Using an Acid Precursor in the Form of Solid Beads: Lessons Learned from First Field Application. Presented at the SPE Annual Technical Conference and Exhibition, Anaheim, California, USA, 11–14 November 2007. SPE 110895-MS. <http://dx.doi.org/10.2118/110895-MS>.
- Nasr-El-Din, H.A., Al-Zahrani, A., Garzon, F.O. et al. 2009. Acid Fracturing of Gas Wells by Use of an Acid Precursor in the Form of Solid Beads: Lessons learned From First Field Application. *SPE Production & Operations*: May 320–335. SPE-110895-PA. <https://doi.org/10.2118/110895-PA>.
- Nathan, C. C. 1973. *Corrosion Inhibitors*, Houston, Texas, USA: NACE.
- Ng, J. H., Almubarak, T., and Nasr-El-Din, H. A. 2018. Low-Carbon-Steel Corrosion at High Temperatures by Aminopolycarboxylic Acids. *SPE Production & Operations*: February 131-144. SPE- 188007-PA. <https://doi.org/10.2118/188007-PA>.
- Pandey, J. S., Nazari, N., Thomsen, K. et al. 2018. A Novel Equipment-Friendly and Environment-Friendly Well Stimulation Fluid for Carbonate Reservoirs: Better Wormholes and Lower Corrosion at Reservoir Conditions. Presented at the SPE International Conference and Exhibition on Formation Damage Control, Lafayette, Louisiana, USA, 7-9 February 2018. SPE-189496-MS. <http://doi:10.2118/189496-MS>
- Panias, D., Taxiarchou, M., Paspaliaris, A. et al. 1996. Mechanisms of Dissolution of Iron Oxides in Aqueous Oxalic Acid Solutions. *Hydrometallurgy* **42** (2): 257–265. [https://doi.org/10.1016/0304-386X\(95\)00104-O](https://doi.org/10.1016/0304-386X(95)00104-O).
- Petrowiki. 2015. Fluid Flow With Formation Damage, 29 June 2015, https://petrowiki.org/Fluid_flow_with_formation_damage (accessed 13 June 2019).
- Phadungath, C., and Metzger, L.E. 2011. Effect of Sodium Gluconate on the Solubility of Calcium Lactate (in English). *Journal of Dairy Science* **94**(10): 4843–4849.
- Pierre, A., Lamarche, J., Mercier, R. et al. 1990. Calcium as Potential Determining Ion in Aqueous Calcite Suspensions. *J. Dispers. Sci. Technol.* **11**(6), 611–635. <https://doi.org/10.1080/01932699008943286>.
- Plummer, L.N., Wigley, T.M., and Parkhurst, D.L. 1978. The Kinetics of Calcite Dissolution in CO₂ Water Systems at 5°C to 60°C and 0.0 to 1.0 atm. CO₂; *J. American Science*, Vol. **278**, No. 2, pp. 179-216.

- Rabie, A.I., Saber, M.R., and Nasr-El-Din, H.A. 2015. A New Environmentally Friendly Acid System for HP/HT Carbonate Acidizing with Enhanced Product Solubility. Presented at the 2015 SPE International Symposium on Oilfield Chemistry, The woodland, Texas, 13-15 April 2015. SPE-173751-MS. <http://dx.doi.org/10.2118/173751-MS>.
- Rabie, A.I., Shedd, D.C., and Nasr-El-Din, H.A. 2014. Measuring the Reaction Rate of Lactic Acid with Calcite and Dolomite Using the Rotating Disk Apparatus. *SPE J.* **19** (6): 1192–1202. SPE-140167-PA. <http://dx.doi.org/10.2118/140167-PA>.
- Ramachandran, S., Fontanille, P., Pandey, A. et al. Al. 2006. Gluconic Acid: Properties, Applications and Microbial Production. *Food Technol. Biotechnol* **44**(2):185–195.
- Robert, J. A., and Rossen, W. R. 2000. Fluid Placement and Pumping Strategy. In *Reservoir Stimulation*, third ed, Economides, M. J. and Nolte, K. G., Chap. 19, pp 1-25. New York: Wiley.
- Robert, J.A., and Crowe, C.W. 2000. Carbonate Acidizing Design. In *Reservoir Stimulation*, third ed, Economides, M. J. and Nolte, K. G., Chap. 17, pp 1-15. New York: Wiley.
- Rozenfel'd, I. L. 1981. *Corrosion Inhibitors*. New York, USA: McGraw-Hill.
- Rueda, E. H., Grassi, R. L., and Blesa, M. A. 1985. Adsorption and Dissolution in the System Goethite/Aqueous EDTA. *J. Colloid and Interface Science* **106** (1): 243–246. [https://doi.org/10.1016/0021-9797\(85\)90401-1](https://doi.org/10.1016/0021-9797(85)90401-1).
- Saneifar, M., Fahes, M. M., Lewis-Hosein, R. et al. 2010. The Effect of Spent Acid on Carbonate Rock Wettability. Presented at the Trainidad and Tobago Energy Resources Conference, Trainidad, Spain, 1 January 2010. SPE-133166-MS. <http://doi:10.2118/133166-MS>
- Sayed, M., Cairns, A.J., Aldakkan, B.S. et al. 2018. A Low-Viscosity Retarded Acid System for Stimulation of High- Temperature Deep Wells. Presented at the Offshore Technology Conference, Houston, Texas, USA, March. <https://doi.org/10.4043/28838-MS>.
- Shehata, A. and Nasr-el-Din, H. 2015. Zeta Potential Measurements: Impact of Salinity on Sandstone Minerals. Presented at the SPE International Symposium on Oilfield Chemistry, Woodlands, Texas, USA, 13–15 April. SPE-173763-MS. <http://dx.doi.org/10.2118/173763-MS>.
- Sjöberg, E.L., and Rickard, D. 1984. Temperature Dependence of Calcite Dissolution Kinetics Between 1 and 62°C at pH 2.7 to 8.4 in Aqueous Solutions; *Geochemica et Cosmochemica Acta*, Vol. **48**, No. 3, pp. 485-493.
- Smith, C. F., Dollarhide, F. E., and Byth, N. J. 1978. Acid Corrosion Inhibitors - Are We Getting What We Need? *J Pet Technol* **30** (5): 737-746. SPE-5644-PA. <http://dx.doi.org/5610.2118/5644-PA>.

- Strand, S., Austad, T., Puntervold, T. et al. 2008. Smart Water for Oil Recovery From Fractured Limestone: A Preliminary Study. *Energy Fuels* **22**(5): 3126–3133. <https://doi.org/10.1021/ef800062n>.
- Tansam, G.F., Kindstedt, P.S., and Hughes, J.M. 2014. Powder X-Ray Diffraction Can Differentiate Between Enantiomeric Variant of Calcium Lactate Pentahydrate Crystal in Cheese. *Journal of Dairy Science* **97** (12): 7354–7362.
- Taqvi, S. and Bassioni, G. 2019. Understanding Wettability Through Zeta Potential Measurements In *Wettability and Interfacial Phenomena*, Rita Khanna, Chapter 3. London: IntechOpen.
- Thomas, R.L., and Morgenthaler, L.N. 2000. Introduction to Matrix Treatments. In *Reservoir Stimulation*, third ed, Economides, M. J. and Nolte, K. G., Chap. 13, pp 1-38. New York: Wiley.
- Van Domelen, M. and Jennings, A. 1995. Alternate Acid Blends for HPHT Applications. Presented at the SPE Offshore Europe, Aberdeen, United Kingdom, 5-8 September. SPE-30419-MS. <http://dx.doi.org/10.2118/30419-MS>.
- Van Everdingen, A. F. and Hurst, W. 1949. The Application of Laplace Transformation to Flow Problems in Reservoirs. *J Pet Technol* **1** (12): 305–324. SPE-949305-G. <https://doi.org/10.2118/949305-G>.
- Wang, Y. 1993 *Existence of an Optimum Rate in Carbonate Acidizing and the Effect of Rock Heterogeneity on Wormholes Patterns*. PhD dissertation, The University of Texas at Austin, Austin, Texas, USA (1993).
- Wang, Y., Hill, A. D., and Schechter, R. S. 1993. The Optimum Injection Rate for Matrix Acidizing of Carbonate Formations. Presented at the SPE Annual Technical Conference and Exhibition, Houston, Texas, 3-6 October. SPE 26578-MS. <http://dx.doi.org/10.2118/26578-MS>.
- Weder, N., Roger, A., and Ralph, K. 2016. Thiourea Derivatives as Potent Inhibitors of Aluminum Corrosion: Atomic- Level Insight into Adsorption and Inhibition Mechanisms. *The Journal of Physical Chemistry C* **120** (3): 1,770–1,777.
- Williams, B. B., Gidley, J. L., and Schechter, R. S. 1979. *Acidizing Fundamentals*, first edition, New York: Henry L. Doherty Memorial Fund of AIME, Society of Petroleum Engineers of AIME.
- Wong, T.C., Hwang, R.J., Beaty, D.W. et al. 1996. Acid Sludge Characterization and Remediation Improve Well Productivity. Presented at the Permian Basin Oil and Gas Recovery Conference, Midland, Texas, 27-29 March. SPE-35193-MS. <https://doi.org/10.2118/35193-MS>.
- Yukselen, Y. and Kaya, A. 2003. Zeta Potential of Kaolinite in the Presence of Alkali, Alkaline Earth and Hydrolyzable Metal Ions. *Water Air Soil Pollution* **145** (1-4): 155-168. <https://doi.org/10.1023/A:1023684213383>.

Zhang, Z., Liu, Y., and Tomson, M. B. 2016. Impact of Fe(III)/Fe(II) on Scale Inhibition. Presented at SPE International Oilfield Scale Conference and Exhibition, Aberdeen, Scotland, UK, 11-12 May. SPE-179905-MS. <https://doi.org/10.2118/179905-MS>.